DELFT UNIVERSITY OF TECHNOLOGY

MS53010 AND MS53035

Effect of mechanical properties of paint on the craquelure propagation within historical paintings modelled as multilayered structures

Author:

Mathijs Lefferts 4483332

Supervisors:

Prof. dr. J. Dik	TU Delft
Dr. A. Vandivere	Mauritshuis
Prof. dr. ir. A.S.J. Suiker	TU Eindhoven

December 6, 2022

1 Abstract

Historical paintings degrade over time due to environmental influences, for example fluctuations in humidity, temperature and sunlight. Nowadays museums try to keep paintings in good state by controlling the environment. However, over time craquelure, cracks in the paint layers, become visible. Theoretical models describe a bilayer system that behaves in the same was as a simplified model of a historical painting, these theoretical model describes three distinctive ways of failure within the system. With the use of this models the effect of the mechanical properties of paint on the craquelure is investigated.

The layered structure of *Girl with a Pearl Earring* is visualised with the help of previously conducted research by Abbie Vandivere and Emilien Leonhardt. Showing that the surface topography of the painting, including paint cracks can be visualised using dedicated microscopic examination. In this thesis a comparison is made between theoretical models of crack formation in historical paintings on the one hand and cracks observed in *Girl with a Pearl Earring* on the other. In order to help this comparison multiple schematic reconstruction are made by Mané Veldhuizen of preparatory and pictorial layers that are found in *Girl with a Pearl Earring*. These are made in the same way Johannes Vermeer would have using historically correct materials. However, these reconstructions are newly made and are not aged.

Tensile tests are conducted on the schematic reconstructions with the use of a Dynamic Mechanical Analyser (DMA). With the use of failure mechanism model the data of the DMA is examined and theoretical multiple types of failure mechanisms are found, thereafter the theoretical results are compared with previously conducted research and topography maps made of *Girl with a Pearl Earring*. The DMA tests have shown that the schematic reconstructions have a Young's Modulus that is 10-100 times lower than is expected from literature research, although the paint becomes stiffer over time. Resulting in the conclusion that mostly failure modes mechanisms 1 and 2 (both finite failure modes, without delamination) are present within the paint layers in the examined areas. X-ray photographs show that failure mode mechanism 3 (infinite failure mode, total delamination) is also present, but mostly in other regions. For a full 2 or 3D reconstruction of the crack propagation more paint samples have to be made and tests on mechanical properties (e.g. on toughness) have to be conducted.

Contents

Nomenclature

α	Moisture profile parameter $[-]$
β	Hygroexpansion coefficient
ΔL	Chance in length $[m]$
ϵ	Strain $[-]$
η	function of the diffusion coefficient
Γ_i	Toughness in layer i $[Jm^{-3}]$
μ	Average $[-, orunitofset]$
$\sigma_i^{\infty}(y)$	Total stress induced by moisture $[MPa]$
σ	stress $[MPa]$
σ_c	Minimum crack channeling stress $[MPa]$
σ_d	Plane-strain delamination stress $[MPa]$
Σ_i	Linear part of moisture induced stress $[MPa]$
σ_i	Uniform part of moisture induced stress $[MPa]$
A	Area $[m^2]$
D	Diffusion coefficient
E	Young's Modulus $[MPa]$
F	Force $[N]$
h_i	Thickness of layer i $[m]$
L	Lenght $[m]$

List of Figures

List of Tables

2 Introduction

The 17th century has been called the 'Golden Age' for the Dutch, during this period the trading commerce flourished bringing wealth to the Netherlands creating a demand for paintings in the art industry. One of the painters who lived in the Netherlands during this period was Johannes Vermeer (1632-1675) who painted among other famous paintings *Girl with a Pearl Earring*, Figure 1, around 1665-1666 [14]. Multiple aspects of this painting have been investigated during these examinations one of which are the dark coloured surroundings around the *Girl* another the types of materials used for the paint. For the surroundings a new technology called the *"camera obscura"* may have influenced Johannes Vermeer recreating the visual effect in a painting although this cannot be proven with certainty [12, 15].

The effect of the *"camera obscura"* focuses the light on the *Girl*, therefore creating a darker surrounding and giving depth to the painting by this unbalanced light distribution. However when observing *Girl with a Pearl Earring* a craquelure pattern can be seen, Figure 1 (with a zoomed in part emphasising the craquelure, photo made with raking light). This pattern consists out of small cracks visible in the pictorial layers, though a crack can extent through multiple layers of the painting and are formed due to stresses in the paint. This reduce the *"camera obscura"* effect considerably [16]. Furthermore, cracks change over time due to fluctuations in (relative) humidity altering the look of a painting when it ages [6], altering the way the painting is perceived over time.

Figure 1: *Girl with a Pearl Earring* by Johannes Vermeer, with in the red square an enlarged view on the pearl earring to show the craquelure pattern in more detail. Photo made by René Gerritsen Art & Research Photography using raking light photography [1]

Over the passed centuries *Girl with a Pearl Earring* has changed due to external effects, for example conservation interventions or the responses of the painting to changes in humidity, heat and sunlight. Distinctive layers within the painting react differently on external influences, as changes of the environmental conditions cause differences in expansion and shrinkage of the paint with internal stresses as a result [1]. All these different effects contribute to changes in the appearance of a painting, for example due to the growth of the surface cracks, loose paint flakes and changes in gloss [1].

This research is part of the project *The Girl in 1665* answering the question "How did the painting look like when *Girl with a Pearl Earring* was recently painted?", which is a project conducted by researchers from different backgrounds. For this study the goal is to make a basis for a visual model showing the propagation of a crack through *Girl with a Pearl Earring* over time.

In order to get more insight into the degradation of *Girl with a Pearl Earring* schematic reconstructions will be tested to find experimental results. A Dynamic Mechanical Analyser is use on the schematic reconstructions, the experimental results are used in the existing models describing failure mechanisms. In order to compare the theoretical results and the observations made on the painting. Topographical models and figures, out of previous research, of *Girl with a Pearl Earring* are used for the observations on the failure mechanisms that are present in the real painting. The research questions are being answered are:

1. What are the mechanical properties of the paint used by Johannes Vermeer?
2. How do the experimental mechanical properties of historical reconstructions of Johannes Vermeer's paint relate to the properties found in literature?
3. How can the found mechanical properties of reconstructed paint samples be fitted in the failure mechanism model?
4. How do the theoretically described craquelure patterns and failure modes relate to the patterns observed in the *Girl with a Pearl Earring*?

In the following chapters a background literature study is shown of craquelure and of *Girl with a Pearl Earring*. Moreover, the used failure mechanism models are described and set apart. This part is followed by the methods and techniques chapter giving an overview on the tests used for finding the mechanical properties of the paint and the techniques used for showing the craquelure pattern of *Girl with a Pearl Earring*. The results chapter gives an overview on the the experimental mechanical properties and on the found craquelure patterns out of topographical research. Followed by the discussion showing the relation between the experimental properties, values found in literature, models and the craquelure pattern of the painting. Lastly, the conclusion gives an overview of all the research questions and an outlook.

3 Literature and background research

3.1 Introduction

In this chapter the build-up of a painting is explained and in particular the build-up of the painting *Girl with a Pearl Earring* can be found. First, the basic build-up of a historical painting is shown and the used paints and pigments are discussed. And a few moments in the history of *Girl with a Pearl Earring* relevant to the propagation of craquelure are described.

Furthermore, the formation process of craquelure and the failure mechanism model are explained in order to answer the research questions "How can the found mechanical properties of reconstructed paint samples be fitted in the failure mechanism model?" and "How do the theoretically described craquelure patterns and failure modes relate to the patterns observed in the *Girl with a Pearl Earring*?".

3.2 Layered build-up of a historical painting

Historical paintings often have a systematic build-up consisting out of multiple layers; an example model of this build-up can be seen in Figure 2 [2, 17]. In this section the paintings are considered to be a multilayer structure, the layered build-up of a painting and the different layers will be shown and their purpose clarified.

The support of most historical paintings are made out of canvas underneath the preparatory and pictorial layers of the painting. To ensure that the binding agent, or pigment, that are used in the following preparatory steps and pictorial layers cannot be absorbed into the canvas or support structure the canvas is first sized and grounded. By applying these two layers the support is protected against adverse effects of the binding agent, meaning that the canvas keeps its integrity and it will be able to give a better substructure for the following paint layers ensuring a more stable support for the paint. Most of the ground layers used in historical paintings are made out of a mixture of animal glue and chalk [18], sometimes mixed together with a coloured pigment to act as a base for the painting. This layer is compatible with both the layers underneath and on top, and this layer functions as a base surface for the paint layers and as reflective layer for light [2, 19].

Next, multiple layers are administered on top of the ground starting with an imprematura, this layer is used to act as both a toned base layer and to seal the pictorial layers from the absorbent effect of the glue in the ground layer. The layers that follow on top are the pictorial layers of the painting and do contain binding agents and pigments. Finally, the last translucent layer which is either a glace or varnish is added. This last layer could be added for two reasons, it acts as a protective layer and secondly the layer could be used to influence the characteristics of the painting, e.g. a matt or glossy effect [2].

An assumption that could be made while (re)viewing a painting is that a painting is a two dimensional artwork. However, paint layers are often not flat and actually have a third dimension, this third dimension is often thoughtfully constructed. Painters, like Johannes Vermeer, often use this three dimensional effect to emphasise and highlight specific parts of a painting [1].

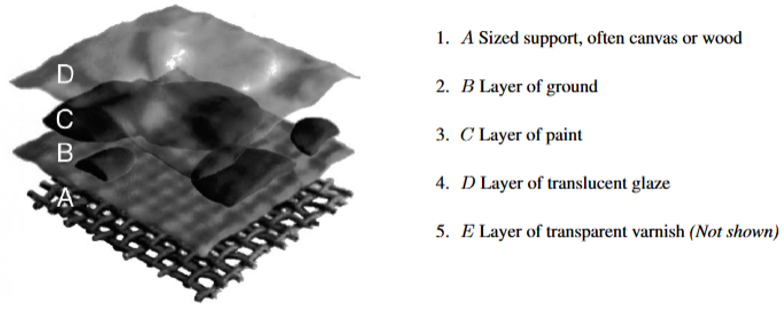

Figure 2: A simple structured layer build-up of painting, shown in the figure as A, B, C, D. REspectively a sized support; layer of ground; layer of paint; layer of translucent glaze (and not shown transparent varnish layer E on top) [2].

Girl with a Pearl Earring painted by Johannes Vermeer has more or less the same build-up as described above, multiple different type of preparatory layers can be found underneath the pictorial layers. Conducted research on cross-sections of the painting has shown that Johannes Vermeer used a simple build-up consisting mostly out of one or a single set of layers underneath the pictorial paint layers [12, 14], a layer build-up that is typical for Vermeer's painting technique [3].

Exemplary for this simple build-up is the headscarf that can be divided into three different sections. From left to right these three sections are: (1) a relative light blue; (2) a transition region in the middle (with both lighter and darker blue); and (3) a darker blue tone on the right side of the headscarf [3], these three parts are shown in Figure 3. In the ground layers underneath the blue headscarf multiple distinctive build-ups can be detected, below the left part (area nr. 1) of the headscarf only a grey ground can be found. However, underneath the darkest part of the headscarf (area nr. 3) a black under layer was applied on top of the ground. This black under layer was only used in the bottom right part of the headscarf, where the shadow can be seen. The more lit and brighter part of the headscarf, the upper left and the middle (area nr. 1 and area nr. 2), are painted directly on top of the grey ground layer. This ground layer can be found underneath the whole painting, accompanied by monochrome paint layers in the following colours: cream, brown or black [3].

Figure 3: Three blue zones in the headscarf, from left to right (1) lighter part on top of a light grey ground. (2) A transition region also on top of grey under paint. (3) A darker blue part on top of black under paint creating a shadow effect [3]

3.3 Paint and Pigment

Mass manufactured paint, for example the collapsible paint tube, made an introduction in the year 1841, enabling painters to focus on painting instead of being both painter and also paint-maker [2]. Research on paint colours out of paintings used prior to this moment is of extra importance as each batch of paint could be slightly different and could have different properties. During the paint making process pigment is ground fully into a stiff paste of small particles, creating an even distribution in the paint mixture without changing the morphology of the particles. Often this grinding of the pigment was done by the painter or an apprentice [2]. However some of the paints used by Vermeer could be both readily and locally bought [12].

Multiple types of binding materials are used in historical paintings such as tempera or encaustic, using egg or wax as binding material, though *Girl with a Pearl Earring* was painted with a linseed oil as binding agent [12]. This binding agent together with the pigments, realising the colours, used make up the paint that is applied on top of the canvas and base layers, as is shown in Figure 2 in layer C.

The most important pigments founds in the *Girl with a Pearl Earring* are [12]:

1. Red pigments: vermillion, red lake, cochineal. Vermillion could be made synthetically in the Netherlands, cochineal is made in Mexico out of crushed insects and was found in the clothing of *Girl with a Pearl Earring*.

2. Yellow and brown pigments; earth pigments, lead-tin yellow, yellow lake, yellow ochre. Lead-tin yellow was available in Delft and was made synthetically. Most of the other earth pigment could have been sourced from many places in Europe.

3. Blue pigments; natural ultramarine and indigo. Ultramarine sourced out of the stone called Lapis Lazuli, found in the region what is now called Afghanistan, used for the headscarf of *Girl with a Pearl Earring*. Indigo was used for a green glaze.

4. Black; charcoal and bone black. Used for both shadow effects and as main component for the base and under layer.

5. White; lead-white. Used on the collar, pearl earring and the eyes, the pigment was also mixed into other colours in order to create lighter shades.

3.3.1 Oil paint

The above mentioned types of colours in the paint that were used by Vermeer all uses a certain oil as binding agent for the grounded natural and synthetically made pigments.

Paints with an oil as binding material use drying oils as basis, these oils dry upon contact with the air and do take a long time to dry. The linseed oil used by Johannes Vermeer was most common oil for paintings in the seventeenth century, other like walnut are found occasionally in historical painting [2, 12]. The properties of the paint change and become more stable over a period of 50 years after this period the properties do not change significantly. This drying process of the oil consists mostly out of crosslinking of the oils, in contrast to binding agents based on solvents that dry due to the evaporation of elements over time

Elements that leave the paint layers during the drying process are often replaced by oxygen. These volatile and heavier compounds leave the paint (lighter oxygen enters the paint), this process results in a mass loss. This process can behave differently within the multiple layers of the paint. The most outer layer where the greatest differences in mass occurs, changes the most resulting in brittle drying cracks [20]. However, long term physical and mechanical changes due to ageing are minor compared to those produced by overcleaning, and exposure to fluctuations in heat or moisture. According to previously conducted research, hydrolysis of a paint film over time will not necessarily cause a paint film to become brittle. A paint film will become stiffer and more brittle when it is heated (at any relative humidity) or treated with a solvent. Both procedures extract materials with a relatively low molecular weight material, by respectively evaporation and extraction [21].

Museums use guidelines in order to create stable environments for the conservation of paintings and other historic artefacts. Before these guidelines, for over long periods of times decisions on the environment in a museum were based on guesses or on minimal evidence [22]. However, now stable climates are created in order to create less fluctuations in the temperature and moisture. For example, the Smithsonian museum has a climate based on $45 \pm 8\%$ RH and $21 \pm 2°$C, values that are within the range of the conservation guidelines, that can differ for types of art and locations around the world.

3.4 Previous Research on *Girl with a Pearl Earring*

Girl with a Pearl Earring, has been thoroughly examined twice before by the Mauritshuis in the last few decades. First in 1994 and later in 2018 during the project called *Girl in the Spotlight*. In this chapter the objectives of these researches will be given and the techniques that were used will be explained. In order to give an overview on the history of the painting and reasons for why the perception of the painting has changed.

3.4.1 Research conducted in 1994

In 1994 *Girl with a Pearl Earring* has been restored in a special restoration procedure that happened in front of the public, during this treatment the painting has been subjected to a technical examination [14]. During this examination the goal was to asses the state of the painting at a specific moment, which is a vital part in both understanding the history of the painting as well as for scheduling possible treatment steps that could be necessary in the future.

Actual structural treatment was not necessary during the 1994 restoration, however, an aesthetic treatment was desirable. The varnish needed to be reapplied and old retouchings demanded to be improved as both had discoloured significantly over time, and the darkened craquelure pattern was visually disturbing and filled with dust. Furthermore, over time small fragments of paint that came loose were removed by conservators during the restoration [23, 24].

The different samples of the painting that were removed came loose due to a phenomenon called cupping. A schematic view of this process is shown in Figure 4. Cupping occurs when multiple layers within the painting act different on changes and fluctuations of the external environment. Creating shrinkage in the lining and causing the cupping process in the paint layers above. In this case, during a relining treatment, with glue-paste, the canvas shrunk causing stresses in the pictorial layers leading to cracks and giving the fragments a characteristic form of a cup [1].

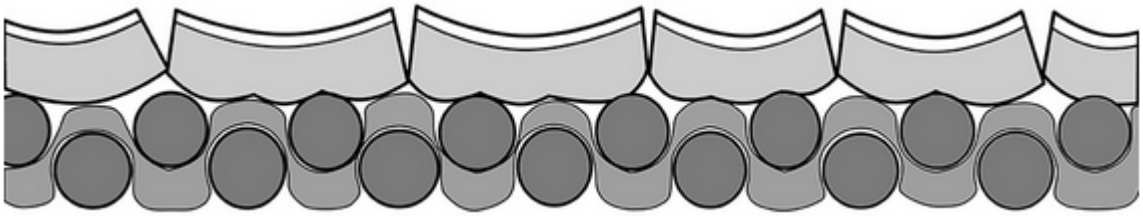

Figure 4: The cupping process leads to cracks and lifting of the paint at the crack edge creating the so-called 'cups'. Cupping occurs whenever the canvas shrinks more and faster than the paint layers. Model made by Moorea Hall-Aquitania [4].

Cross-sections of the painting were looked upon with the use of light microscopy, scanning electron microscopy-energy dispersive X-ray analysis and infrared spectroscopy, other small painting particles were evaluated with, among many more technologies, the use of polarised light microscopy and high-performance liquid chromatography. Enabling the researchers to distinguish different pigments, binding agents and materials added to the painting during previous restorations in the multiple layers of the painting [14].

3.4.2 Research conducted in 2018, project *Girl in the Spotlight*

In the (re)examination of the painting in 2018 most of the 1997 samples were analysed again with new technologies, this time research was not prompted by specific conservation concerns. However, the research was initiated with a goal to find out more about Vermeer's material and techniques in order to answer the following questions [14]:

1. What steps did Vermeer take to create the painting?
2. What can we find out about layers beneath the surface?

3. Which materials did Vermeer use and where did they come from?
4. Which techniques did Vermeer use to create subtle optical effects?
5. What did the painting look like originally, and how has it changed?
6. What is the chemical and physical condition of the painting?

One of the requirements for the examination was that all of the methods employed in this phase of the project had to be non-invasive, meaning that the painting could not be damaged. Therefore, old paint flakes were re-examined with new methods and multiple 3D scanning methods were used. Fore example, the used Hirox RM-2000 3D digital microscope combines optical microscopic imaging with 3D topographic information. These methods could be used to research the topographical state and the craquelure patterns of the painting.

Multiple types of scanning techniques have been used in order to get higher quality pictures of certain parts of the painting and their corresponding topography, visualising individual cracks and topographical features even more. The three used techniques are multi-scale optical coherence tomography, 3D scanning based on fringe-encoded stereo imaging and 3D digital microscopy. Both the multi-scale optical coherence topography and 3D digital microscopy give the data with the highest accuracy and precision [1].

Spectral domain resolution 3D scan is not able to generate a high enough resolution to identify finer cracks in the painting. Multi-scale optical coherence tomography (MS-OCT) and 3D digital microscopy generate the highest accuracy and precision compared to 3d scanning techniques [1]. However, the area that can be scanned with these techniques are very small, limited in speed and therefore less suitable to cover whole paintings. The latter due to the error that arises with the stitching of separate photos.

In Figure 5 six different close-ups of the lips are shown, with different technqiues that ahve been used to visualise the craquelure pattern of the painting [1]. Figures a to f three show different methods that are used to obtain the craquelure pattern, all three are shown in both colour and with a rendered matt white background to increase the visibility of the pattern. The following techniques are shown in the figure sets:

1. a, b; Raking light photograph zoomed in (a) and craquelure pattern traced by hand (b).
2. c, d; Craquelure visualised using colour topography data of the 3D digital microscope (c). On the right side the colour is replaced with a white matte rendered surface (d).
3. e, f; Crack pattern is visualised using the 3D data obtained form high resolution 3D scan (e). Again on the right side the rendered with a matte white background (f).

The data obtained specific from the painting *Girl with a Pearl Earring* document the condition of the painting at a certain time. Offering researchers, or conservators, information on both the history of the painting as well as on the degradation of the materials. Height and topography maps in 3D show the amount of paint that was used by Johannes Vermeer and the arisen craquelure patterns, the way Vermeer painted and used impasto as a technique, rheological properties of the paint and effects of past treatments. For example *the pearl* has been flattened in the past and this gives a moating effect around the impasto of 200 micron deep. The lining procedures out of the past have had less influence on the topography visible on the bottom of the painting (in for example the jacket) where no noticeable moating can be

found. Overall the research conducted by Willemijn Elkhuizen shows that the technology that is available is capable of tracking and creating enlarged photographs of the surface topography of a painting [1].

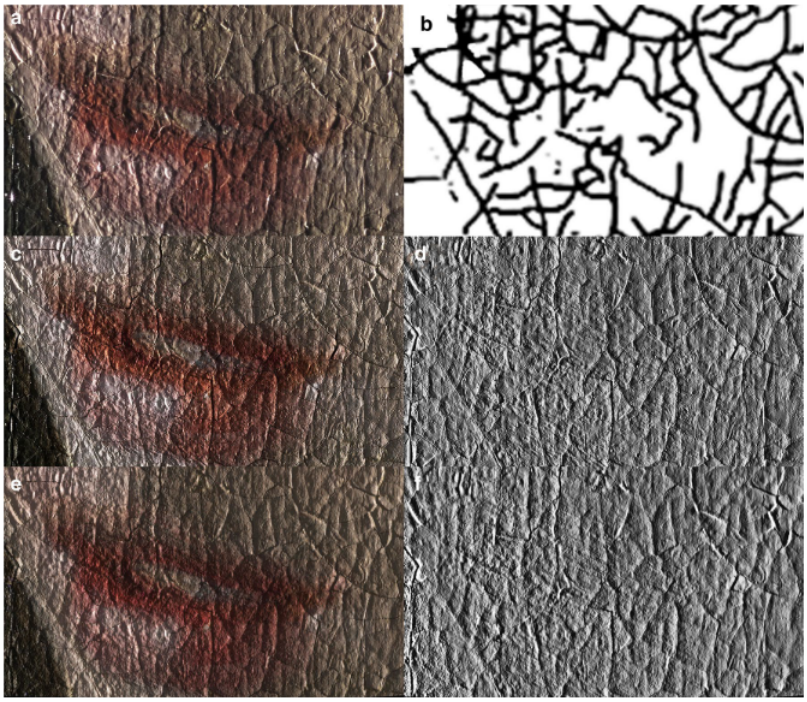

Figure 5: Craquelure pattern visualised. Top row, a, b, show raking light photograph and craquelure pattern traced by hand. c, d are obtained with the use of 3D digital microscopy. Bottom row, e, f, are obtained with the use of High-Resolution 3D scan [1]

3.5 Lining and previous restorations

Protecting or slowing the depreciation down the pictorial paint layers against deterioration is the main reason for paintings to be lined. Elongating the life of a painting by lining has been done since the 19th century [19]. During this process the support of the pictorial layers is being stiffened, therefore enabling the tensile loads to be transferred from the paint layers and onto the newly refurbished more rigged support. Theoretically this lowers the mechanical loads in the paint and lowering the chances of mechanical failure, preserving the picture without major cracks and damages [19].

3.5.1 History of restoration procedures *Girl with a Pearl Earring*

In the history of *Girl with a Pearl Earring* a couple of known treatments and retouches have taken place one of which happened before the painting became part of the Mauritshuis collection in 1903. In 1882 the painting was treated by Van De Heghen, a restorer based in Antwerp. During this restoration the painting was relined using a starch based adhesive paste and furthermore Van De Heghen, probably, consolidated outer layers of the painting with animal glue [1, 14].

In 1915 and 1960 a second and third treatment were required during its stay in the Mauritshuis. First Derix the Wild regenerated the outer varnish layer in 1915, without (re)touching or affecting the older retouches, this varnish

regeneration has been conducted again in 1922 [14]. Jan Cornelis Traas carries a second and more complete restoration out in 1960. The support layer was being lined, secondly a new varnish layer was applied and finally damages to the painting were retouched [1, 14].

Girl with a Pearl Earring has had two different types of lining both of which influenced the pictorial layers. The first one was with an aqueous lining. This water based relining caused the canvas to shrink, due to this shrinkage of the support the paint experienced a load and started to alter from, the cupping progress could be seen. For the second lining procedure the first lining was taken off and a new wax-relining was applied. During this process both heat and pressure were used to apply a new support to the painting. With the pressure some parts, such as the *Earring*, of the painting have been flattened, around these former elevated areas of paint moating can be seen [25].

The lining and retouch processes of 1882, 1915 1960 together with the aqueous adhesives have most probably caused to contract the canvas causing further flaking and cupping of the paint. The forehead of *Girl with a Pearl Earring* is an example where the paint flaked more than in other places, here the Pettenkofer technique has been used in order to stop the flaking process. This technique uses a water-ethanol vapour mixture to flatten the paint flakes onto the layers underneath. Resulting in broader cracks with soft and round edges in comparison to cracks from other regions of the painting [26].

3.6 Cracks

Across the surface of historical painting cracks can be found called craquelure. The amount often depends on age and multiple different causes can be assigned to the craquelure pattern. Fractures in the pictorial layers can be identified as edge fractures as the initiation of the cracks starts at an open surface [17, 27]. These fractures together form a branched network that gives a visible record of the history, visualising stresses and strains applied on the painting over time. Often the formation and propagation of these cracks are dependent on changes in humidity or induced by (photo)chemical changes [1, 7]. However, a crack can also start to form due to external influences such as a lining procedure, especially procedures that use heat and/or pressure can alter the topography of a painting (for example flattening the topography) [1].

Two main types of cracks can be distinguished from each other, drying and age cracks [16, 28]. Drying cracks, also called premature cracks, form a pattern of craquelure that originates during the drying process of the paint layers. These cracks grow and propagate during the drying process in the ductile paint. However, this is not the predominant type of cracks found in *Girl with a Pearl Earring* [14, 16]. The other main type of cracks are age cracks, the pattern of cracks that continue to grow over a long periods of time. In contrast to drying cracks this type of cracks form in aged paint, which is brittle. And compared to the ductile drying cracks these cracks are smaller, have sharp edges and are able to move through more layers in the painting and are often associated with a fine maze of cracks. This second type of cracks, age cracks, originate mostly due to stresses in the paint layers of a painting and due to changes and differences in the mechanical properties of the superimposed paint layers. Often due to fluctuations in humidity and temperature [16].

Paintings are made out of different materials and superimposed layers that react differently to the changes in the environment such as humidity. These different components expand when the moisture content increases and shrink when the content declines, although all elements change at a different rate [17]. This mismatch in moisture response between different layers (ground, paint layers and support layer) is one of the most important reasons for fractures

found in the layers of a painting [28]. The propagation of these fractures within a layered structure is due to the stress transfer between intact layers and fractured layers in the region of arisen cracks.

3.6.1 Basic Mechanics

Girl with a Pearl Earring has been subjected to multiple different external loads over the years during multiple lining procedures and environmental loads, e.g. changes in temperature or humidity. In order to see how the painting reacts to certain changes in relative humidity models are made based on mechanical properties and hygroscopic values of the used paints. In this paragraph a few basic mechanical properties and units are described.

In the basis, uniformly applied external forces (both tensile and compressive) lead to uniformly distributed stresses within an object, the tested sample is said to be under, normal, stress (σ). Which can be calculated as shown in Equation 1 with the use of the applied force (F) and the area (A). Due to the load the length of the test sample can change, with the original length (L) and the change in length (ΔL) the strain (ϵ) can be calculated as shown in Equation 2. Furthermore, the stress and strain depend on each other as described in Hooke's law showing that the ratio between stress and strain is always constant in the linear-elastic regime, this constant is different for each material and is called the Young's modulus (E), Equation 3 [5].

$$\sigma = \frac{load}{area} = \frac{F}{A} \tag{1}$$

$$\epsilon = \frac{change\ in\ length}{original\ length} = \frac{\Delta L}{L} \tag{2}$$

$$E = \frac{\sigma}{\epsilon} \tag{3}$$

Using both the stress and strain a graph can be constructed, where the stress is depicted against the strain. The stress-strain curve can be split up into multiple segments and a few important points can be marked. The first linear part of the curve has a slope equal to the Young's Modulus (E), this is elastic region of the material. Where after the curve bends into a more horizontal direction, respectively the elastic and plastic regime. Figure 6 shows these parts as well as the yielding point, ultimate strength and the fracture point. These three points are found in the beginning, approximately middle (highest stress level, depending of material properties) and at the end of the plastic regime [5].

Within the elastic regime the materials deforms due to the stress, at the moment the stresses are released the sample changes back to its original dimensions. After the yield strength is reached the sample behaves in the plastic regime, meaning that within this range a plastic deformation is achieved. The material changes shape due to the high stresses and part of this strain stays therefore the material does not change back to its original form [5], eventually the materials fails.

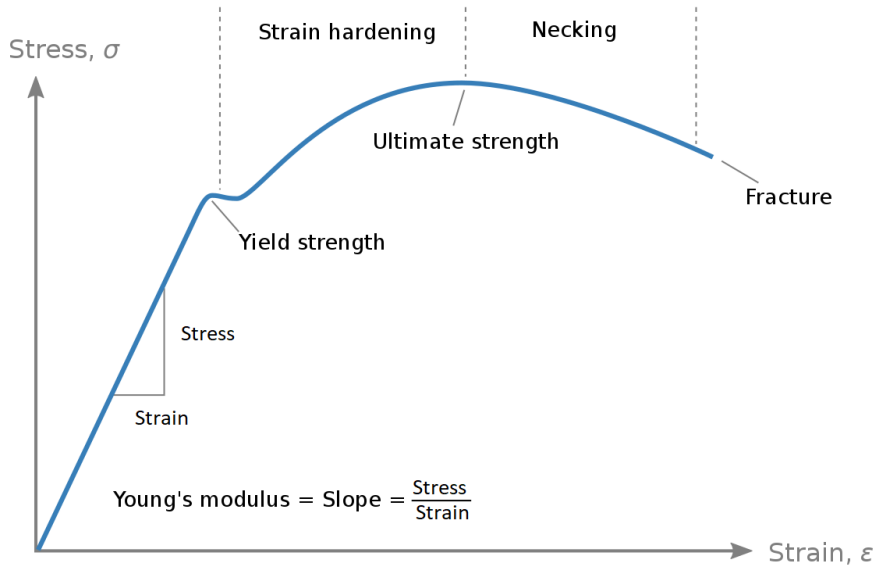

Figure 6: Stress (σ) against strain (ϵ); linear part until the yield point, marking the end of the linear elastic regime. The slope of the graph in the linear part gives the constant "Young's Modulus E". Where after the hardening part starts and necking before fracture, highest achieved stress is called the ultimate strength [5].

The following equations show the hygro-thermal relation to the stress and strain equations shown previously. Temperature gradient (ΔT), is involved as well as the moisture weighting factor (α), the previously shown relations and equations still stand. However, now the strain (ϵ) depends on both the elastic strain (ϵ^e) and hygro-thermal strain (ϵ^{th}). In the case of a total strain that is assumed to be 0, the stress depends on both the Young's Modulus, on the change in moisture weighting factor and temperature, Equation 8.

$$\sigma = E \cdot \epsilon^e \tag{4}$$

$$\epsilon = \epsilon^e + \epsilon^{th} \tag{5}$$

$$\epsilon^{th} = \alpha \cdot \Delta T \tag{6}$$

$$\sigma = E(\epsilon - \epsilon^{th}) = E(\epsilon - \alpha \cdot \Delta T) \tag{7}$$

$$\epsilon = 0 \rightarrow \sigma = -E \cdot \alpha \cdot \Delta T \tag{8}$$

3.7 Introduction Failure Mechanisms

In this chapter a model based on three crack types and propagation mechanisms is described. The research papers that are discussed describe cracks that propagate through a bilayer system, composed out of a coating and a support. Described types of failure mechanisms in the form of fractures and fracture propagation are induced by external effects and facilitated by the dissimilarity of the mechanical properties between two superimposed layers. Furthermore, the research conducted can be applied to the failure mechanisms found in historical paintings and "addresses the behaviour of a brittle crack channelling in a bilayer under a moisture (or temperature) gradient in the thickness direction" [7].

The three different types of cracks that can be distinguished are all three induced by the critical remote stress in a layer that is supported by a second layer. The first of the three mechanisms is a single crack in the depth direction of the pictorial layers down to the support. However, such a crack can deflect under stress from its original direction forming an interfacial crack between two layers, starting a delamination process. This process can be split up into two different types, a stable type with finite delamination and secondly an unstable type that will result in paint flaking. These two types form the second and third type of mechanisms that are described. All three mechanisms are depicted in Figure 7, a shows only a vertical crack down to the support; b depicts a finite horizontal crack (possible in both directions) in between the coating and support; and c shows infinite horizontal crack or delamination [6, 7].

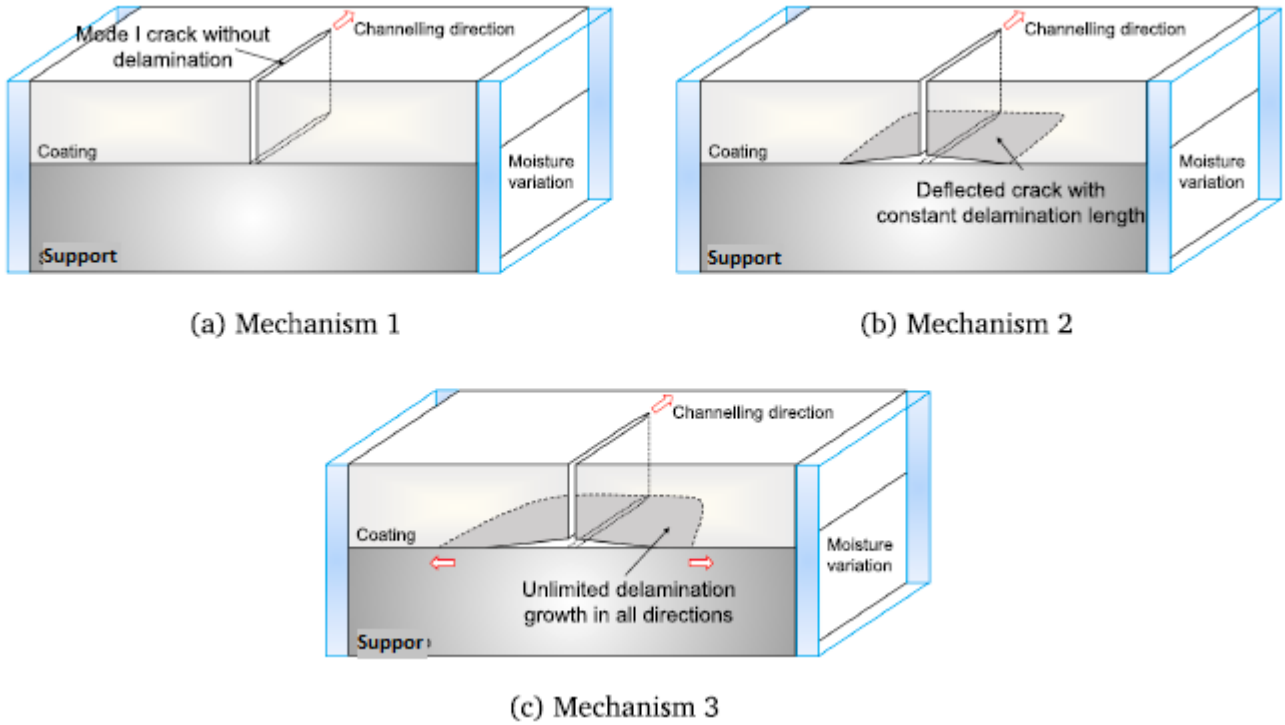

Figure 7: Three different types of cracks that can be found in a bilayer system. (a) Mechanism I: Perpendicular crack on the support (stable); (b) Mechanism II: Vertical crack with horizontal, stable and finite, crack (stable); (c) Mechanism III: Vertical crack with a horizontal infinite propagating crack (unstable, resulting in paint flaking) [6].

In the following part a coating-support system is considered containing a single crack and is subjected to a moisture or temperature gradient. The following assumptions are made; elapsed time is of no influence as the diffusion process is in steady-state [7, 29]. However, as stated this study considers a single crack and historical paintings often have a whole branched network of fractures called craquelure, often with a spacing of around 10 to 50 times the coating thickness between them [16]. Therefore, it has been confirmed with numerical analysis that "the stress field in the coating approaches the value of the remote stress at a distance from the delamination tip of less than six times the coating thickness" and accordingly the cracks may be treated as isolated defects [7].

3.7.1 Cracking in bilayer

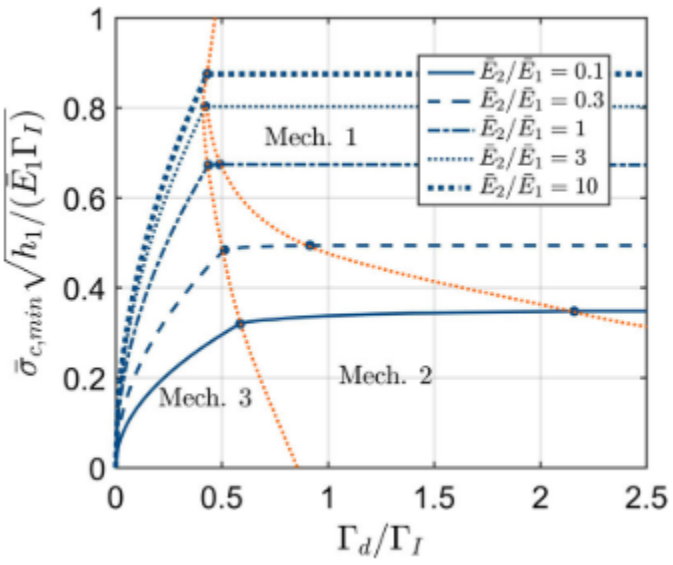

Figure 8: Failure map with 3 types of failure mechanisms, minimum crack channelling stress in the coating is depicted versus the toughness ratio, multiple stiffness ratios are shown. for constant moisture profile [7]

Figure 8 shows a failure mechanism map visualising for where each failure mechanism is active. Here the minimum crack channelling stress is shown as a function of the toughness ratio, this ratio is based on both mode I toughness and the delamination toughness, and multiple stiffness mismatches are shown in the graph. The stiffness mismatches are a result of different mechanical properties of the superimposed layers. Assume that the bilayer system has layers of equal thickness and a constant moisture profile. The three different failure mechanisms can be found in the three distinguishable orange dotted sectors.

Firstly, it can be seen in Figure 8 that mechanism 3 is apparent for every stiffness mismatch at low toughness mismatch ratios. For toughness mismatch ratios higher that 0.5, both mechanisms 1 and 2 can be found for different stiffness mismatches. Along the orange dotted vertical line mechanisms 3 changes into either mechanism 2 for the lower values in stiffness mismatches (0.1 and for a short toughness mismatch range 0.3 and 1). For stiffness ratios higher that 3 mechanism 3 transforms, directly, in mechanism 1 [7]. An important note is that these values and mechanisms are independent of both the hygral expansion and diffusion coefficients, or the mismatches in these values.

3.7.2 Influence of the moisture parameter Alpha on the crack formation

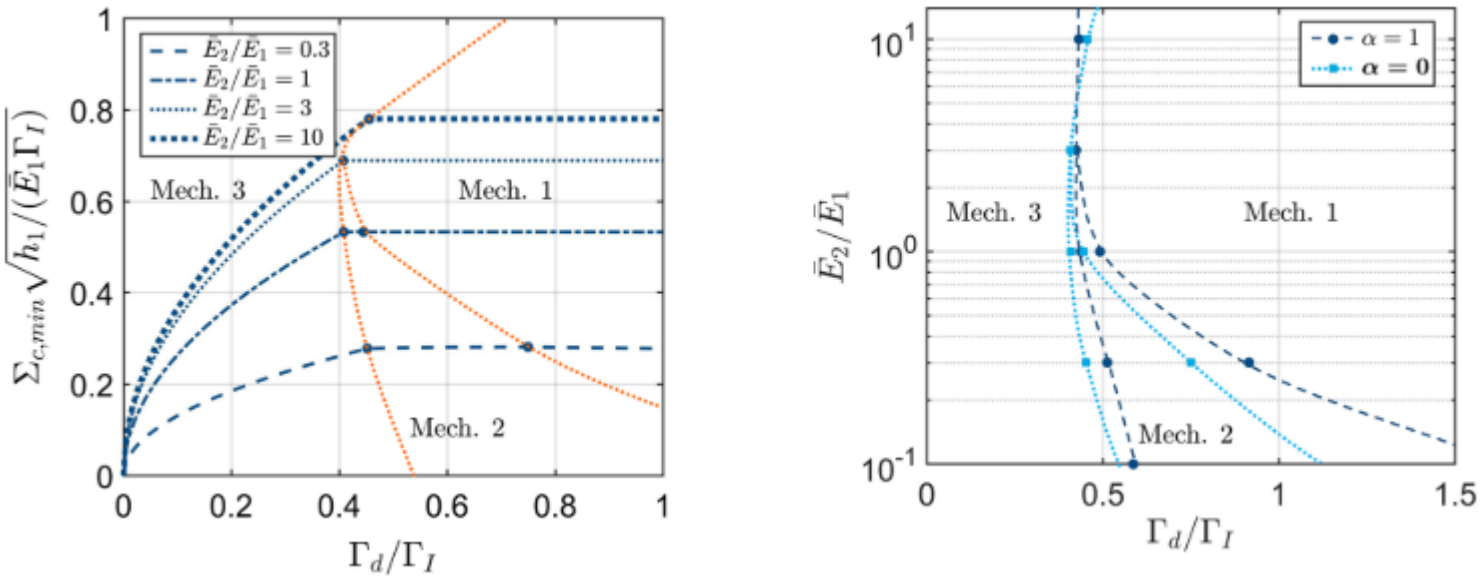

Figure 9: Left: Failure map shows three different types of failure modes for $\Sigma_{c,min}$ (linear part of stress profile) plotted against the toughness ratio at a $\alpha = 0$ value. Areas where failure mechanisms are active are distinguished from each other with the use of orange dotted lines. Right: Failure mechanism map, stiffness mismatch plotted against the toughness ratio. Two different failure mechanisms can be seen visualised in dark and light blue with different moisture parameters (respectively $\alpha = 1$ and $\alpha = 0$. [7]

Figure 9 shows two failure mechanism maps, the left figure shows the failure mechanisms for a equal bilayer system ($h_2/h_1 = 1$). However, contrary to the first failure map (Figure 8), this figure shows a bilayer under influence of a linear moisture profile (instead of constant moisture profile), moisture weighting factor $\alpha = 0$. The minimum crack channelling stress Σ that can be found in the coating layer of the system is plotted against the toughness ratio. For this linear moisture content profile related to a weighting factor $\alpha = 0$, Σ_c is therefor same as $\sigma_c^{\infty,\alpha}$ as shown in the remote channelling stress Equation 9. For multiple different stiffness mismatches the failure mechanisms can be found, depicted with different types of dotted blue lines. The remote channelling stress is shown in Equation 9 and shows how both the linear and uniform stress depend on the moisture weighting factor α [7].

$$\sigma_c^{\infty,\alpha}(y) = \alpha\sigma_c + \Sigma_c(1 + \frac{y}{h\eta_1}) \tag{9}$$

The third failure mechanism map shows the stiffness mismatch plotted against the toughness ratio, on the right side of Figure 9. Both the extreme values of the moisture weighting factor α ($0 \leq \alpha \geq 1$) are shown with blue dotted lines, the differences in the areas where the failure mechanisms are active can be seen. The dark and light blue lines show respectively the boundaries of the failure mechanisms for respectively a linear, $\alpha = 0$ and uniform moisture profile, $\alpha = 1$. Note that for a stiffness mismatch E_2/E_1 equally or bigger than 3 failure mechanisms 2 is not dominant, mechanisms 1 transforms into mechanisms 3 without transition period.

3.8 Conclusion Literature

3.8.1 *Girl with a Pearl Earring*

In the basis a painting is made of multiple layers on top of each other; canvas, glue, ground layers, layers of paint and varnishes. Subsequently, historical paintings can be modelled as multi layer structures. All layers are added with different and often specific purposes, for colours or shadow effect, and to protect the canvas in order to resist paint absorption. A simple build-up consisting out of multiple superimposed layers was used by Johannes Vermeer, and could be found in the painting *Girl with a Pearl Earring*. Using a few layers underneath the pictorial layers, often using these under layers for the creation of shadow effects.

For a period of over 50 years the properties of oil paint change due to the drying process in which the oils crosslink. Oil based paint types, linseed oil is the binding medium, and simple colours that were used by Vermeer change during the drying time. Drying cracks originate during the drying process whenever elements evaporate from the paint layer, lighter elements such as oxygen reenter the material. The material becomes more brittle due to this process and drying cracks can be found. These type of cracks have not been found in *Girl with a Pearl Earring*. And these changes can be seen on the surface of the painting: topography has changed over time due to environmental effects, details have vanished, cracks started growing and colours faded.

Craquelure mapping has been the main focus for some research projects. Multiple types of methods are used in the research conducted by Willemijn Elkhuizen in order to make the craquelure pattern more visible. With the use of raking light and with 3D-microscopy the cracks have been made more visible on photographs. During two mayor research projects the condition of the painting has been monitored, in 1994 and in 2018. However, no real research has been conducted on the mechanical properties of the materials that are present in *Girl with a Pearl Earring*.

3.8.2 Failure mechanisms

Researchers have found relations between the moisture content and two mechanical properties, stiffness and toughness. Multiple equations show how the stresses develop in a test sample under different circumstances. Three different failure mechanisms can be distinguished in a bilayer under hygro-thermal stress consisting out of a brittle coating and a support. An important annotation for this system consisting out of two superimposed layers with the same diffusion coefficient but with variations in the stiffness, toughness and hygroexpansion coefficient. The first two types of failure systems result only in the cracking of the paint, and a third unstable failure type that results in paint flaking.

These three failure mechanisms are shown in multiple failure maps, where different material properties (toughness, stiffness) influence the failure mechanisms that can become active in a material. The failure mechanism maps a are shown in Figure 8 and Figure 9. These are respectively showing the minimum crack channelling stress verses the toughness for linear moisture constant profile ($\alpha = 1$), minimum crack channelling stress verses the toughness for uniform moisture constant profile ($\alpha = 0$) and showing the stiffness mismatch versus the toughness mismatch. All three of the failure maps show that unstable failure mechanism three, infinite delamination (with paint flaking as result), is present for low values in the toughness mismatch (between 0.5 and 1).

Together with the simple layered structure used by Johannes Vermeer and the results of the conducted research on the failure mechanism models it can be concluded that paintings, when simplified, can be modelled as layered structures.

And that theoretically at least 3 different types of craquelure can be found in the layers of a painting. Furthermore, the propagation of craquelure depends on both the mechanical properties and on external influences.

4 Methods and Techniques; painting build-ups, schematic reconstructions, tensile tests and topography

In order to answer the question "What are the mechanical properties of the paint used by Johannes Vermeer?" schematic reconstructions are made and analysed, to obtain experimental values on historical correct reconstructions of paint used by Johannes Vermeer. In this chapter the use of different methods, techniques, computer programs and devices during this research are explained. For the execution of the tensile tests the use of the Dynamic Mechanical Analyser (DMA) and the corresponding computer program are explained. Furthermore, the use of the computer program "MountainsMap" is described for the research on the topography of the painting, in order to find answers for the question "How do the theoretically described craquelure patterns and failure modes relate to the patterns observed in the *Girl with a Pearl Earring*?".

4.1 Layer build-up *Girl with a Pearl Earring*

In previous chapters the layered build-up of paintings has been presented, here the results of more literature research shows the use of these layered structures by Johannes Vermeer. Figure 10 shows both the whole painting and close-ups of multiple different parts out of the headscarf figures $c - f$ show craquelure patterns. For example a visible ground layer underneath the blue surface layer in d, and visible brush strokes in $c - f$. Figure e shows thicker applied blue paint layers in order to create depth and highlights, f shows more details of thicker and wider applied paint. Note that samples 23, 41 and 42 locate the original positions of the numbered samples in the headscarf. Sample location 23 is located in the darkest part whereas samples 41 and 42 are located in a less dark part. And although located close to each other samples 41 and 42 have a different layered build-ups.

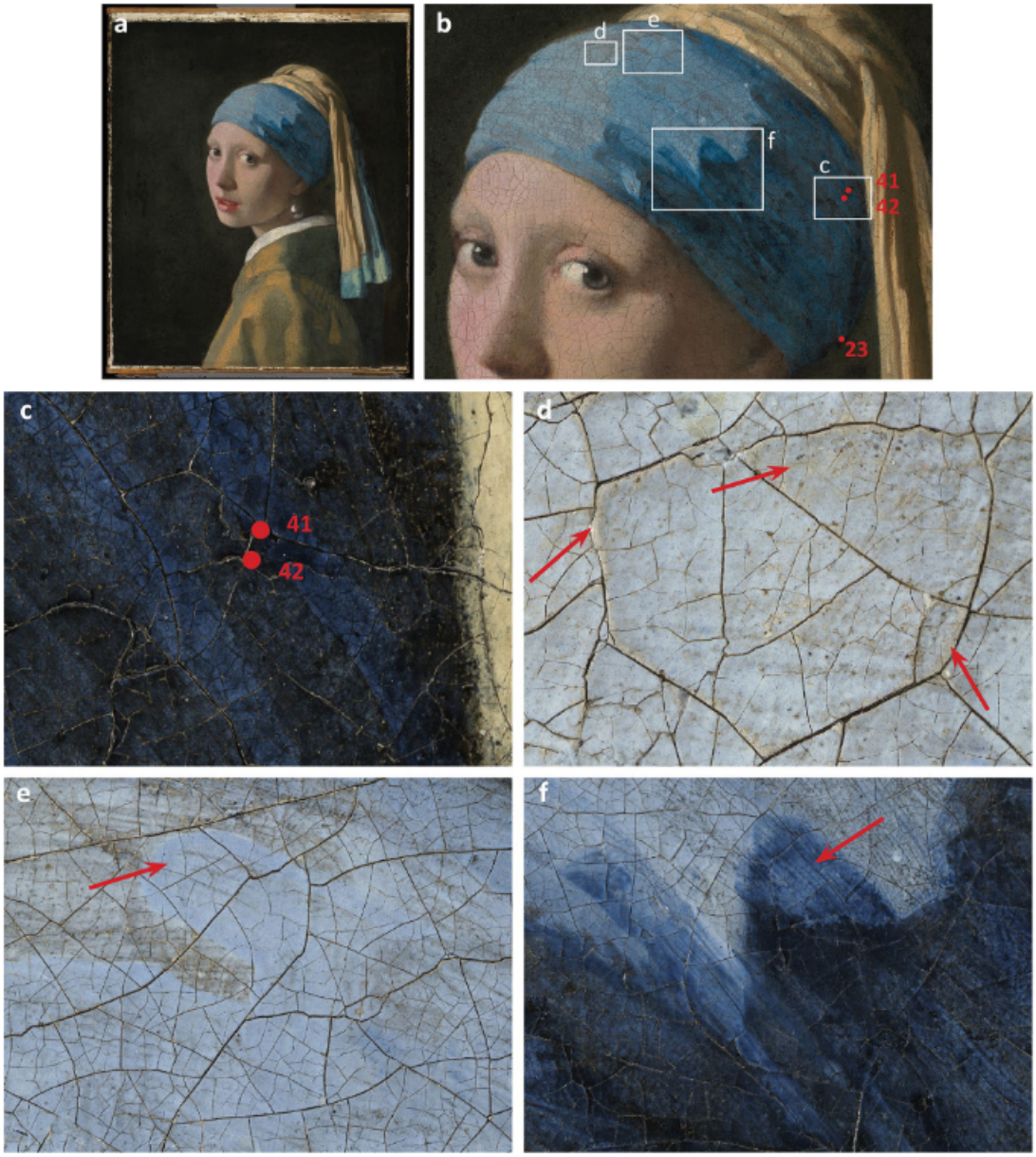

Figure 10: *Girl with a Pearl Earring* (a) with close up of the blue headscarf (b), showing details of thicker applied paint, brushstrokes and details of ground layers (d) underneath blue surface layer ($c - f$). Furthermore, the original locations op samples 23, 41 and 42 are shown (b, c). [3]

.

Samples 23, 41 and 42 are visible in the following figures, the simple build-up that was used by Johannes Vermeer are clearly visualised.Figure 13 shows a cross-section of a sample from the original painting, b shows a light microscope photo of the sample that is obtained out of the location shown in a, here the different layers are the most clear. Cross-sectional photos of the samples 23 and 41 out of a different location are shown in Figure 12 and Figure 11, although in these samples the simple layered structure is less clearly visible. Because the ground layer (layer 1)is missing in these figures, only the pictorial layers are visible. The thick bright blue layer, sample 41, has dimensions in thickness up to

$70\mu m$ as visible in Figure 12. Thicknesses that are found in sample 42 are different where the ground layer 1 shows a thickness up to $50\mu m$ and the two layers on top, layers 2 (thin black under layer) and 3 (thin blue surface layer), have thicknesses around $10\mu m$.

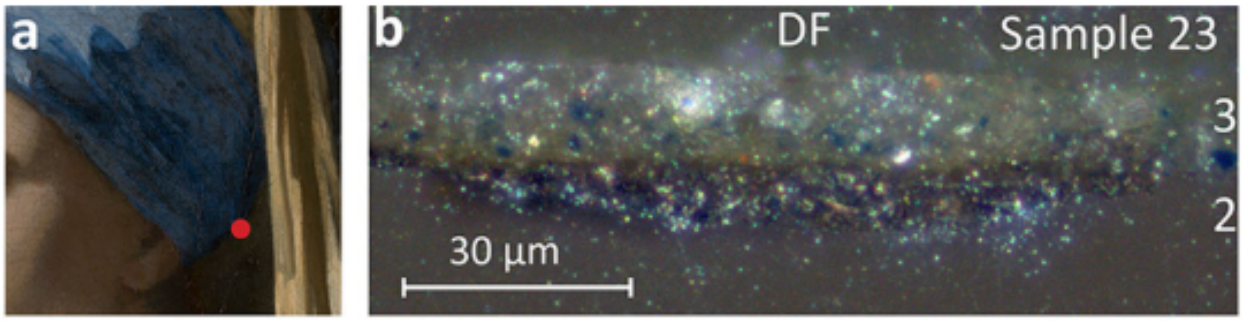

Figure 11: Cross-section of sample 23 from the painting *Girl with a Pearl Earring*, specific original location shown in a with a red dot. b shows a cross-sectional photo obtained with a light microscope (dark field) showing the simple layered structure with layers 2 (black under layer) and 3 (thick blue surface layer), layer 1 (ground layer) is not visible in this photo [3].

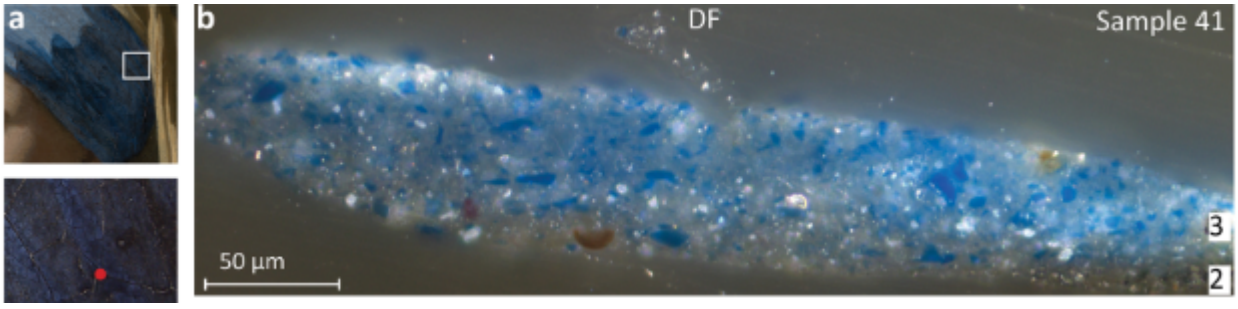

Figure 12: Cross-section of paint sample 41 from the painting *Girl with a Pearl Earring*, a shows the original location of the paint sample with a red dot and white square. b shows a dark field photo obtained with a light microscope showing most of layer 3, the pictorial layer in blue with a thickness or around $70\mu m$. Layer 1 is the ground layer that is not visible in this photo [3].

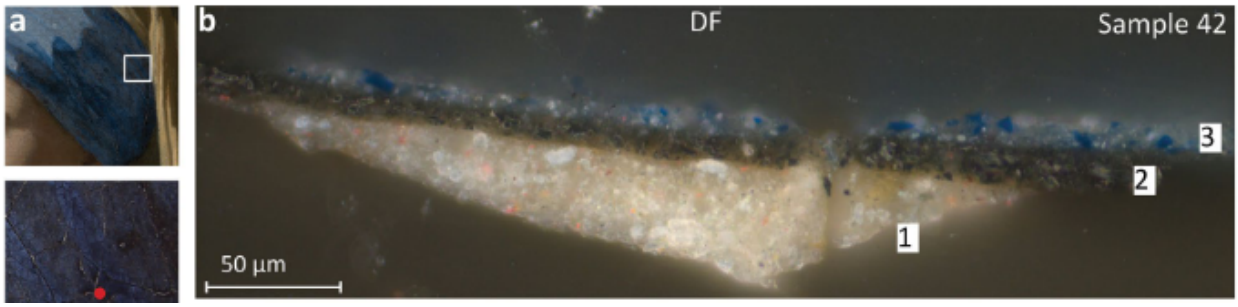

Figure 13: Cross-section of paint sample 42 from the painting *Girl with a Pearl Earring*, a shows the location of the paint sample both with a white square and a red dot. b Shows a light microscope (dark field) photo of the sample. 3 layers are identified, 1 ground $50\mu m$ 2 thin black under layer ($10\mu m$) and 3 thin blue surface layer [3].

4.2 Schematic Reconstructions of Paint Layers

Multiple different schematic reconstructions, single paint layers on a substrate, have been made by Mané van Veldhuizen. The following text, out of the logbook of Mané van Veldhuizen, describes the compositions of the different paint types used for the schematic reconstructions. Mané van Veldhuizen made the paint types in a historically correct way.

1. Ground: made out of chalk; lead white; lamp black; English red and Siena
2. First brown undermodelling made out of Okhra paint 'oxyde de fer jaune naturel inde n33j' with a bit of bone black (47100 Kremer pigmente) and lac dye (35020 Kremer pigmente) (this type of brown is called "middle brown")
3. Black undermodelling made with charcoal black, chalk, alabaster gypsum, potah alum and a tiny bit of brown
4. The cream layer was made with tube lead white Rublev no. 1 series 5, chalk 58000 from Kremer pigmente, red lake Lac 36020 Kremer pigmente, charcoal black and yellow earth n.27 from Okhra. This was mixed 50/50 lead white with chalk and small amounts of yellow earth and bone black.
5. Lips; vermillion, red lake, yellow earth (nr.27), lead white, okhra (nr.33)
6. face paint; vermilion, red lake yellow earth (nr. 27), lead white (more yellow earth and lead white than the paint used for the lips)
7. Blue; Kremer 10550 ultramarine and a tiny bit of Kremer 10540, lead white Multiple blue colours paints sample

The following was found in the logbook:

"To ensure the paint could be used for experiments loose paint strips had to be created. For this process the two supports 'thick melinex' and 'silicone-release melinex' were used. With the help of a draw down bar a layer of a single thickness can be applied on top of both the types of melinex, when dried the paint should release easily from either of the two melinex supports. However after drying the 'thick melinex' would not release the paint and the 'silicone- release melinex' turned out to had two different sides with different properties. The less smooth side of the 'silicone-release melinex' came out best during the peel-test and this was used for the rest of the schematic reconstructions. A second

problem showed up with some of the paints became very streaky and shrunk during the drying process, this happened with the brown paint. Resulting in a thicker layer forming an heterogeneous layer dissimilar that the needed μm, no real solution was found for this problem. Most of the paint layers have been painted in a thicknesses of $100\mu m$, unless stated otherwise (often $50\mu m$)."

4.3 Tensile Test

Tensile tests are tests used for finding mechanical properties as the stiffness and specific values out of the stress-strain curve (e.g. yield stress, ultimate tensile stress). During tensile tests the sample is clamped (vertically) into the stiff machine and a tensile load is set onto the material. Tensile testers have a screw driven or hydraulically operated movable clamp, ensuring a precise change in either the load on the sample or the elongation of the sample. As both the force and the deformation are measured, a stress-strain curve can be made with the use of the found results. The Young's modulus of a material is the property that gives information on the, tensile or compressive, stiffness of a material. By testing samples in a static and uni-axial way both the properties that describe the elastic and the plastic regime of a material can be found [30].

There are two separate ways to conduct a tensile test, by either controlling the applied load and measuring the elongation of the sample. The second way is by controlling the displacement of the clamp and measuring the corresponding load. These two types are respectively called force controlled and displacement controlled. If there is a linear relationship between the stress and strain the results should be the same for the two different types (this is the case in the linear, elastic, part of the curve). However, when the relationship becomes non-linear the results obtained by these two types of tests can be different (in the non-linear (plastic deformation part) of the curve). During displacement controlled tests a change in load can be measured and results in a drop in the load whereas by load controlled tests plastic changes often leads to a horizontal path in a graph as shown in Figure 14 [8].

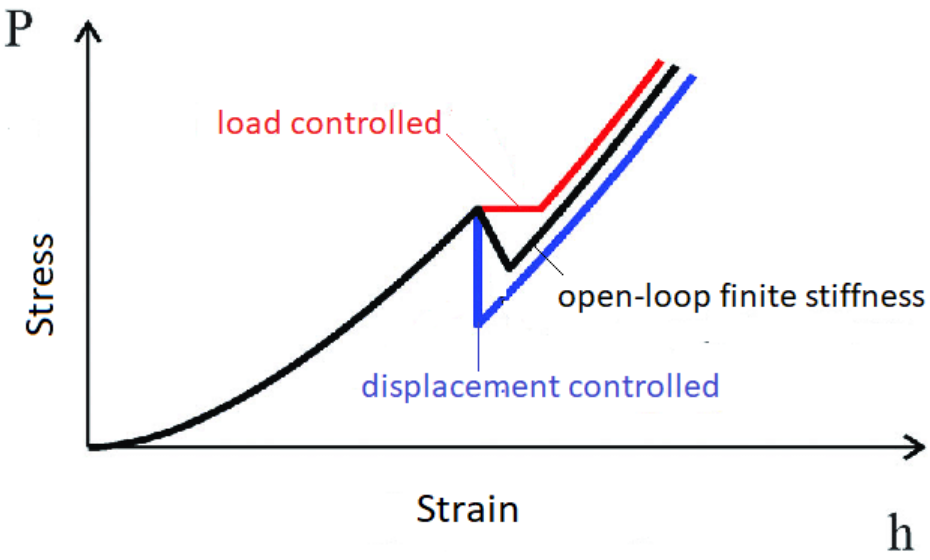

Figure 14: Load controlled vs displacement controlled tensile test results [8].

4.3.1 Dynamic Mechanical Analyser

For the tensile tests the "TA instruments Dynamic Mechanical Analyser Q800" (DMA) is used, most of the specifications of this machine are shown in Figure 15. As can be seen this machine is made for samples that deform or yield under low forces and stresses (minimum force $0.0001N$ and maximum of $18N$). The force and strain resolutions of this machine are respectively $0.00001N$ and $1nm$. Such a high precision test machine is needed for tests on samples that are fragile, brittle or show small ductile deformations. Furthermore, a reproducible force is created by the magnetically driven motors, providing oscillatory and static forces needed for experiments ensuring reproducible results [9].

Maximum Force	18 N
Minimum Force	0.0001 N
Force Resolution	0.00001 N
Strain Resolution	1 nanometer
Modulus Range	10^3 to $3{\times}10^{12}$ PA
Modulus Precision	±1%
TanA Sensitivity	0.0001
TanA Resolution	0.00001
Frequency Range	0.01 to 200 Hz
Dynamic Sample Deformation Range	±0.5 to 10,000 pm
Temperature Range	-150 to 600 °C
Heating Rate	0.1 to 20 °C/min
Cooling Rate	0.1 to 10 °C/min
Isothermal Stability	±0.1 °C
Time/Temperature Superposition	Yes

Figure 15: Specifications of the TA Dynamic Mechanical Analyser Q800 obtained from brochure of the DMA [9]

The tension clamps that are used inside the DMA are made for films, fibers and materials with a low stiffness modulus. The rectangular shape of the clamps eliminates twisting of the sample, and are fastened with screws (using a torque wrench the screws can be fastened with a specific preset load). This clamping mechanism consists out of two separate clamps, an upper and lower clamp. The upper clamp is fixed in place whereas the lower clamp can be moved vertically, and is supported by air bearings. Figure 16 shows a picture of the total clamping mechanism holding a sample with both the upper and lower clamp (nr. 1,3) and the two screws (nr. 2,4) holding the clamps in place.

According to the manual of the DMA TA Q800 the dimensions of the test samples for this machine need to be $5 - 30$ mm in length; up to 8 mm in width; up to 2 mm in thickness in order to fit into the clamps [9]. The paint strips are cut in correct length using a sharp knife, before the schematic reconstructions are loosened from the melinex supports. Finally, all the dimensions of the samples are measured multiple times and with the use of tweezers the strips are inserted into the clamps, as shown in Figure 16.

Before the real tensile tests are conducted a few test experiments are conducted in order to find out the value of the clamping force needed during the tests, as no slip or failure within the clamps due to excessive clamping forces should take place during the tests. When the paint samples are fastened with a force that is too great the sample deforms inside the clamp and this can cause pre-stresses inside the sample interfering with the results.

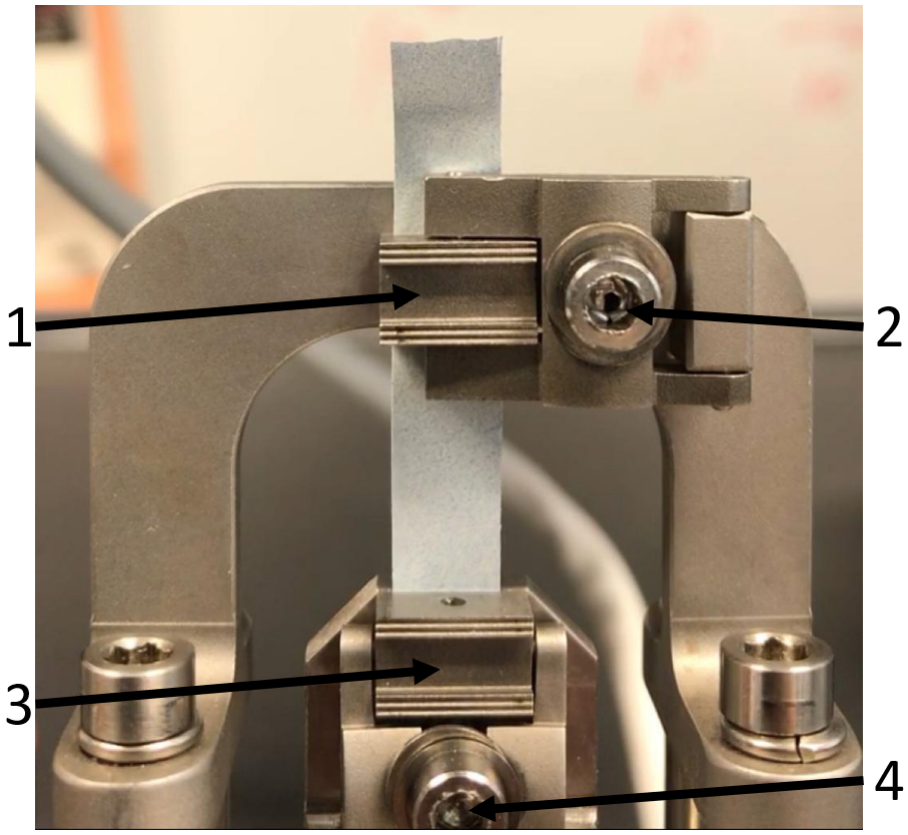

Figure 16: DMA, clamps shown with paint strip clamped in. 4 numbers shown (1) upper clamp (fixed), (2) fastening mechanism upper clamp, (3) lower clamp (floating; movable up and down), (4) fastening mechanism lower clamp. Photo made at TUDelft laboratory.

4.3.2 Dynamic Mechanical Analyser, computer program

At the moment the samples are secured in the clamps, the computer program QSeries -[Q800@Mfg-DMA] (found via the TA instruments explorer program) is used for controlling the DMA. A new 'Experiment' is made and the program asks to adjust multiple settings for the specific experiment. The type of test and the dimensions of the sample have to be filled in. First, under the tab 'Summary' a specific mode can be selected and the type of clamp and samples need the settings "Tension: film". Secondly, under the tab "Procedure" the test information has to be filled in e.g. the type of test and specific information on the process of the test e.g. the preload force, force ramp rate and the upper force limit.

All the dimension, (length, width and thickness) of all the samples are measurements thrice and averages are used in order to eliminate measurement errors. For the actual test multiple types forces have to be chosen that the DMA applies on the test material, the force increments (per unit of time (Newton/min)) and the ultimate maximum force. For the tensile test the goal is to achieve maximum stress, this inserted value for the ultimate force is not significant and can be put on a large number in order to make sure it does not interfere with the actual test, i.e. the DMA should not stop the experiment before the ultimate stresses are found therefore a large ultimate force is used.

4.3.3 Tested Schematic Reconstructions

As discussed earlier the original paint used by Johannes Vermeer have been made on a basis of oil and as seen in the logbook of Mané van Veldhuizen all the reconstructed colours are made out of different types of materials and pigments. Though the colours are a combination of oil, lead white or chalk and specific pigments. Figure 17 with 8 Macro-XRF maps ($b - i$) shows *Girl with a Pearl Earring* visualising the distribution of different material types in the paint layers. Maps b, e and h show very large areas that can be described as lighter (grey or almost white) showing the areas specific materials are present, corresponding to the map.

Figure 17: a Visible light image; $b - i$ eight Ma-XRF maps showing the distribution of specific materials respectivily Pb-L (Lead), Fe (Iron), Pb-M (Lead), Hg (Mercury), K-K (Potassium), Ca-K (Calcium) and Cu (copper) [10].

Note that the elements lead and calcium can be found throughout the whole painting, Lead white is a white colour (with Pb-L and/or Pb-M) both used as a paint type and mixed with other colours. Calcium is found in the chalk that is used in the ground layer and is also found in the darker, shadow, part of the headscarf (h shows Ca-K) [10]. Other maps such as d, f and j show the distribution of respectively iron, mercury and copper. Those materials are only used in specific areas and colours (e.g. skin, lips and background).

Both the colour Lead white and the layer type ground are being tested with the DMA, in order to find out the influence of materials within layers. Furthermore, two different coloured paint found on the *Girl* are being tested, blue (headscarf) and red (lips). Multiple types of blue are tested to compare the differences in mechanical properties of these types, all are found in the headscarf. These different blues are: thin blue and thick blue and also an under layer blue. The second coloured paint that is tested,red, is used on the lips of the *Girl*. Furthermore, multiple types of preparatory layers are tested, Ground, two types of brown and a black under layer. Another reason for these specific colours to be tested is the practical reason that not all colours were painted on the right type of melinex and therefore usable at all. Because of these reasons the following paint types are selected for further research:

1. 'Lead white'

2. Three different types of blue; 'Thin blue layer shadows headscarf', 'Thick blue layer midtones headscarf' and 'Blue under layer midtones headscarf'

3. 'Lips surface'

4. Multiple types of ground; 'Ground' and 'Brown under 1 and 2', 'Black Under'

The obtained schematic reconstructions of paint are fragile and the layer thickness is not always homogeneously spread out, small air pockets and deformations can be seen when inspecting the paint. As a result of these imperfections in the paint tests fail generating usable data. Data can be generated that has a higher reliability by selecting areas that are homogeneously spread out and flat from the schematic reconstructions and using a sharp knife for cutting.

As stated earlier oil paints dry over a long period and the schematic reconstructions are relatively young. Therefore, the schematic reconstructions are stored under relatively stable conditions and most of the tests are executed in a short time consecutive to each other. Creating a time period in which the paint can be considered stable and data sets can be compared against each other. Any trials and testing of material and machinery is done before and separately of the real tests and not in between test sequences [2, 12, 13].

Figure 18: Left: Visible light photograph of *Girl with a Pearl Earring*. Right X-radiography photo of the same painting, visualising the wooden frame, canvas and nails. But, even more important, visualising black dots scattered over the painting. These black dots indicate the places where fragments of paint left the surface of the painting. In the middle a few bigger black spots can be seen, at the bottom an area of smaller dots. [11]

At the right side of Figure 18 the x-radiography photo of *Girl with a Pearl Earring* is shown. Besides the wooden framework, nails and canvas also multiple black holes can be seen. Some of these can also be seen in Figure 17, especially in sub-figures b and e. These black holes represent areas where the radiation of the x-radiography has not reflected back, indicating that the paint does not, or is smaller extent, contain materials that reflect radiation (in case of sub-figures b and e this material is mostly lead). At these places, for some reason, the paint flakes left the surface and the painting has been retouched during an examination. This is often done with newly made paint and materials that do not contain, in this case, lead [11].

4.3.4 Tensile Test Analysis

The results obtained by the DMA are visualised in a graph that can be opened with the use of the program 'TA Universal Analysis 2000'. The graphical output of the test can be examined in detail and the program has multiple options to help calculate slopes, areas underneath the slope of the graph, or find specific points on the lines. To find usable data points the generated output of the DMA is published in a document for each single test, categorised in 12 different signals:

1. Signal 1: Time (min)
2. Signal 2: Temperature (°C)
3. Signal 3: Displacement (μm)
4. Signal 4: Static force (N)
5. Signal 5: Position (mm)

6. Signal 6: Length (mm)
7. Signal 7: Stress (MPa)
8. Signal 8: Strain (%)
9. Signal 9: Stiffness (N/m)
10. Signal 10: Relaxation Modulus (MPa)
11. Signal 11: Freep Compliance (μm^2/N)
12. Signal 12: GCA Pressure (kPa gauge)

Signals numbered 1 and $3-8$ are of interest for further research. For example the stiffness (signal 8) is of interest. However, as this is being calculated at a specific time it has less accuracy. For this reason the stiffness will be calculated separately using multiple data points generated by the DMA, by using the data point 6 (length) and 7 (stress). By using two data points over a period of time the elongation (strain) can be calculated and the differences in stress. Because most of the schematic reconstructions has some minor deformations at the start this type of approach gives better results as multiple data points are taken into account.

For further calculations both the formulas for averages and standard deviations, Equation 10 and Equation 11, are used for verifying and monitoring the reliability of the results.

$$Average(\mu) = \frac{\sum(n_i + n_{(i+1)} + ... + n_{(1+k)})}{k} \tag{10}$$

$$Standarddeviation(\sigma) = \sqrt{\frac{\sum(n_i - \mu)^2}{N}} \tag{11}$$

4.4 Topography

During previous researches data has been created on the topography, for example with the use of Hirox RH-2000 3D digital microscope and Scanning Electron Microscopy. Light microscopy have been used for further analysis on embedded paint samples (nr. 23, 41 and 42 are shown) [1, 10, 12]. The Hirox RH-2000 3D digital microscope was used in combination with a specially made motorised stand, enabling a 500 x 500 mm (XY-direction) area to be examined (200 nm steps). A spatial sampling from 4.4 μm/pixel down to 0.03 μm/pixel was achieved. *Girl with a Pearl Earring* was fully scanned during this process, the results have been used for the detailed figures in this thesis [3]. Figure 19 shows multiple figures of the *Pearl*. Photo a digital micro photograph, note the line and the four (digital added) coloured points, b shows a topographical profile, cross-section along the line through the four coloured points, here the topography is visualised. Both c and d show the same photograph as shown in a, however here the photo is tilted making the topography more visible, e gives more information on the height profile visible in d.

These figures are created with the use of the program MountainsMap, the needed (TDR) data is provided by Abbie Vandivere and Emilien Leonhardt, partly used as shown in Figure 19 and data of other regions are also provided, see the results section for details. With the use of this computer program topography data can be visualised in height maps and graphs showing the height profile. This is of interest for the layered build up of the painting and also for the failure mechanisms that are present. The failure mechanisms do have influence on the topography and thus on the heights

visualised on the cross-sectional height profiles. Potentially linking the theoretical failure mechanism model and the data obtained out of tests to the real painting.

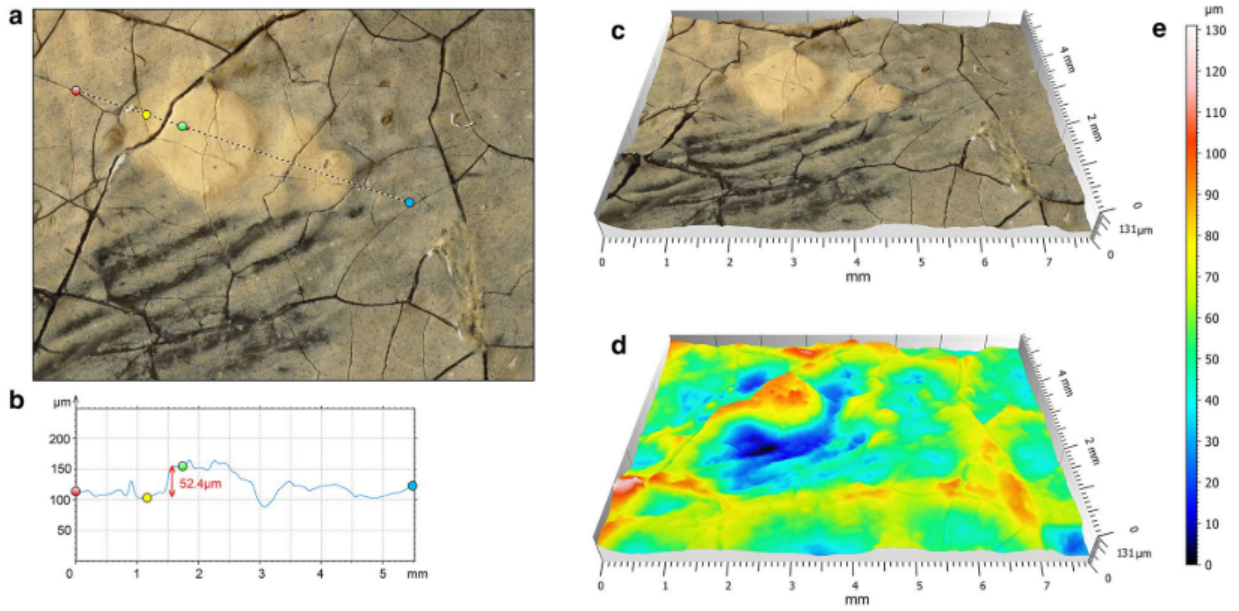

Figure 19: a detailed view of part of painting, micro photographe, height profile of dotted line is shown in b. c shows 3D view on a and d shows the same as c bot giving more detail on topographical view. e scale used in d [12]

5 Results; Tensile tests and Topography

In this chapter the results of the conducted tests are shown, and potential topics of discussion are mentioned. First the DMA test results are presented, see Appendix C for the first set of results of the experiments that were carried out for testing the material. This first set of results is used as guideline for the experiments of which the result are shown here. Furthermore, with the use of the program MountainsMap more topography data has been found shown in the second part of this chapter.

One result of the experimental tests that should be noted is that not all colours could be separated from the melinex base layer compromising the amount of test that could be conducted. Furthermore, the Brown under 1 and Black under layer became streaky after drying and did not form a coherent layer, this can be seen in Figure 20. Making the schematic reconstructions unusable for further testing, for more pictures of unusable reconstructions see Appendix B. Therefore, only the following schematic reconstructions have been tested:

1. 'Lead white'
2. Three different types of blue; 'Thin blue layer shadows headscarf', 'Thick blue layer midtones headscarf' and 'Blue under layer midtones headscarf'
3. 'Lips surface'
4. Two types of ground; 'Ground' and 'Brown under 2'

Figure 20: Two schematic reconstructions of the colours Brown under 1 and Black under that became streaky. When separated from melinex only small fragments came loose , unable to be used for tensile tests.

5.1 Results DMA, tensile tests

All data obtained by the DMA (with exception of the data used for calibration) with the use of the tensile tests are shown in the next figures. All graphs are standard graphical output of the software used by DMA in the laboratory at the TUDelft, for all raw data see Appendix D and subsection D.2. Showing stress strain diagrams visualising the tensile tests, the strain is visualised in percentages on the horizontal axis and vertically the stress in MPa. The strain is visualised as a percentage in order to compare different tests with each other.

Figure 21, shows the data obtained from the lead white sample set. Some results have a horizontal path at the beginning of the curve this is due to the air bearing of the DMA, the sample is clamped in the holders and subsequently the lower clamp rises before going down during the actual test. As a result a horizontal part is added the beginning of the curve, except for a few outliers the maximum stresses are around the 1.0 MPa.

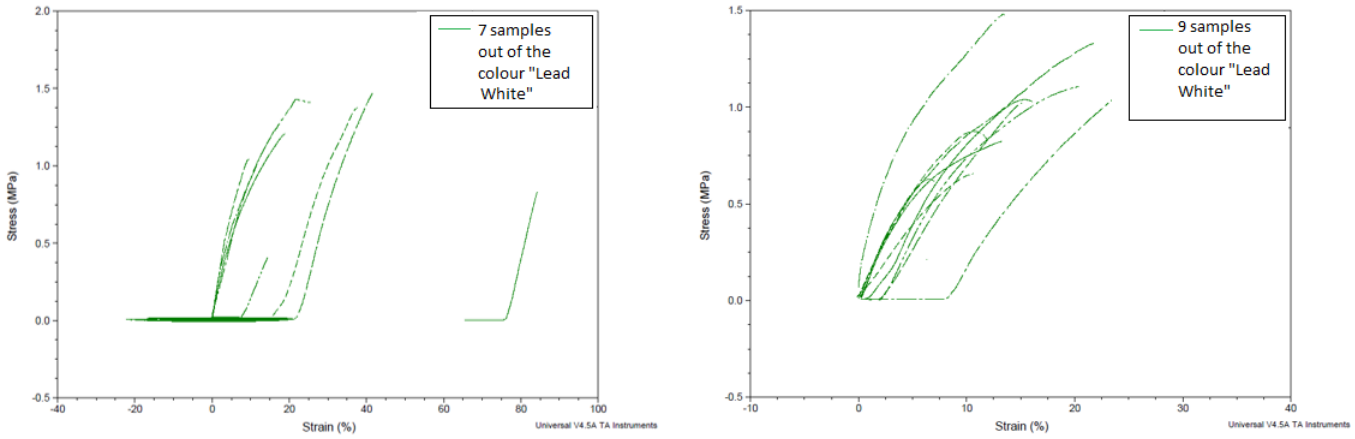

Figure 21: Stress-strain diagram showing all obtained results of the tensile tests on Lead white specimens.

The following three diagrams show the stress strain curves of three types of schematic reconstructions of blue paint, Figure 22 Figure 23 and Figure 24, respectively Blue under layer midtones headscarf, a Thick blue layer midtones and Thin blue layer shadows headscarf. Note the differences in the maximum stresses that are obtained in the tests of the different types of Blue. For example in the sample batch Blue under mid most of the maximum measured stresses are above the 1.0 MPa and maximum strains are around the $10 - 20\%$. Whereas the Thick blue schematic reconstruction show a different trajectory compared to the Blue Mid-colour line with maximum stresses below the 1.0 MPa and a maximum strain ranged from $15\% - 20\%$. Last the results of the thin blue samples are shown, here the maximum stresses that are found are even lower in the region of $0.5 - 0.75$ MPa, here again strains are between the $10\% - 20\%$.

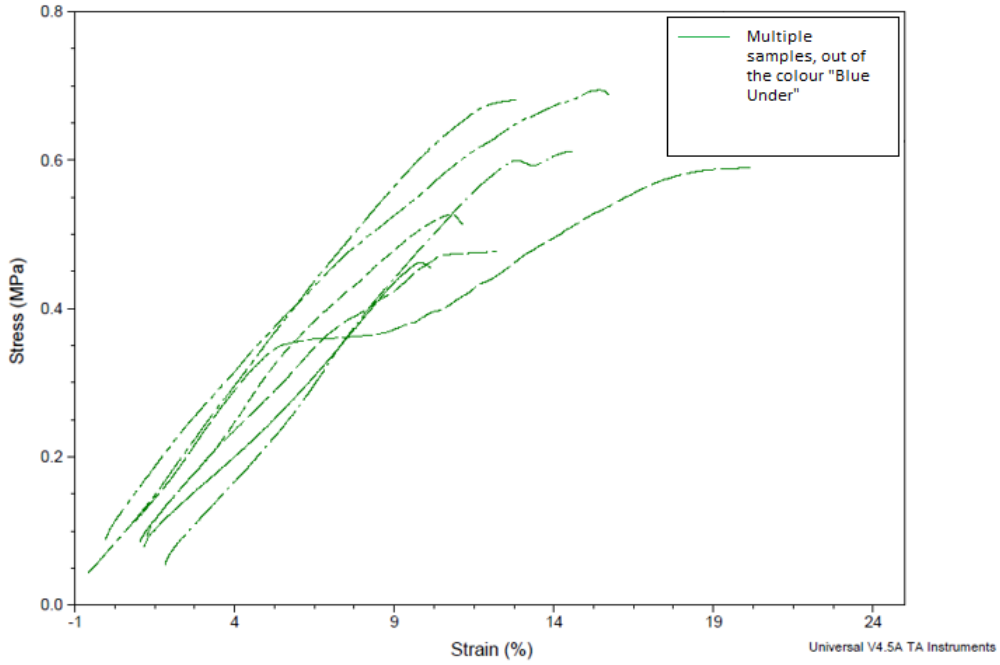

Figure 22: Stress-strain diagrams showing all obtained results of the tensile tests on ’Blue Under’ Schematic reconstruction.

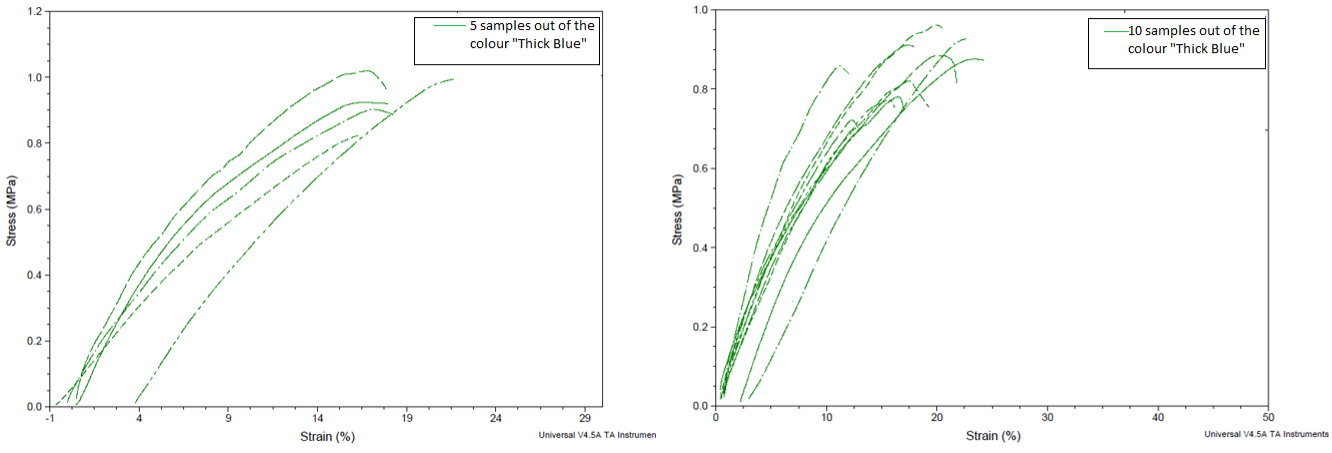

Figure 23: Stress-strain diagrams showing all obtained results of the tensile tests on ’Thick blue’ schematic reconstruction.

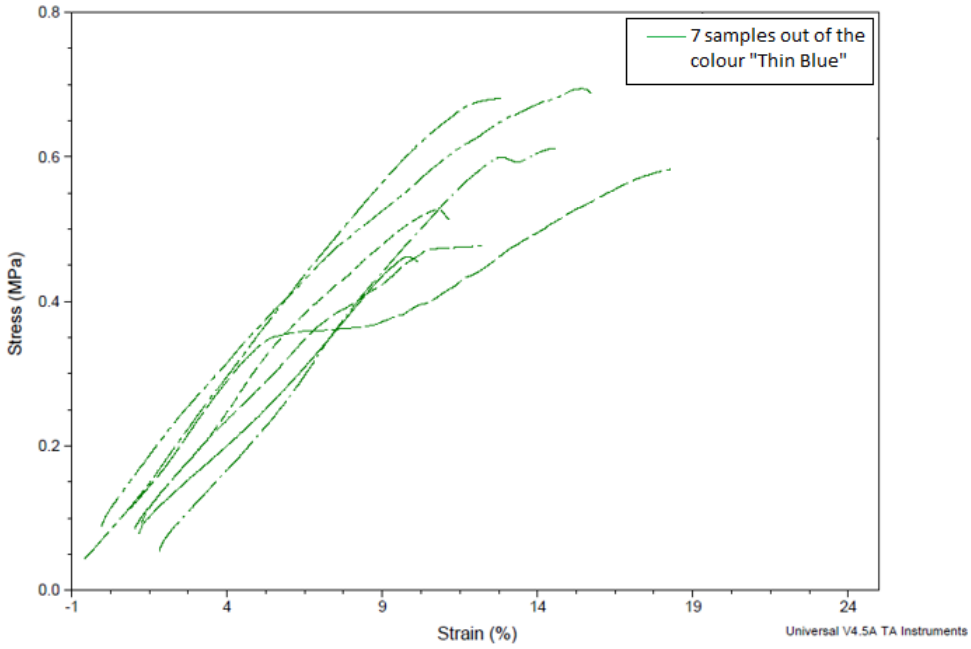

Figure 24: Stress-strain diagram showing all obtained results of the tensile tests on ’Thin blue’ schematic reconstruction.

Figure 25 shows the stress strain diagram of the Lips red schematic reconstructions with paint similar to the paint used for the lips of the *Girl*. Note that the the maximum stresses that are measured are around the $1,25$ MPa with strains around the 15% (note that outliers can be found with stresses up to $1,8$ MPa and lower than 1.0 MPa). Note that compared to the blue paint types higher ultimate tensile stresses and failure stresses are found.

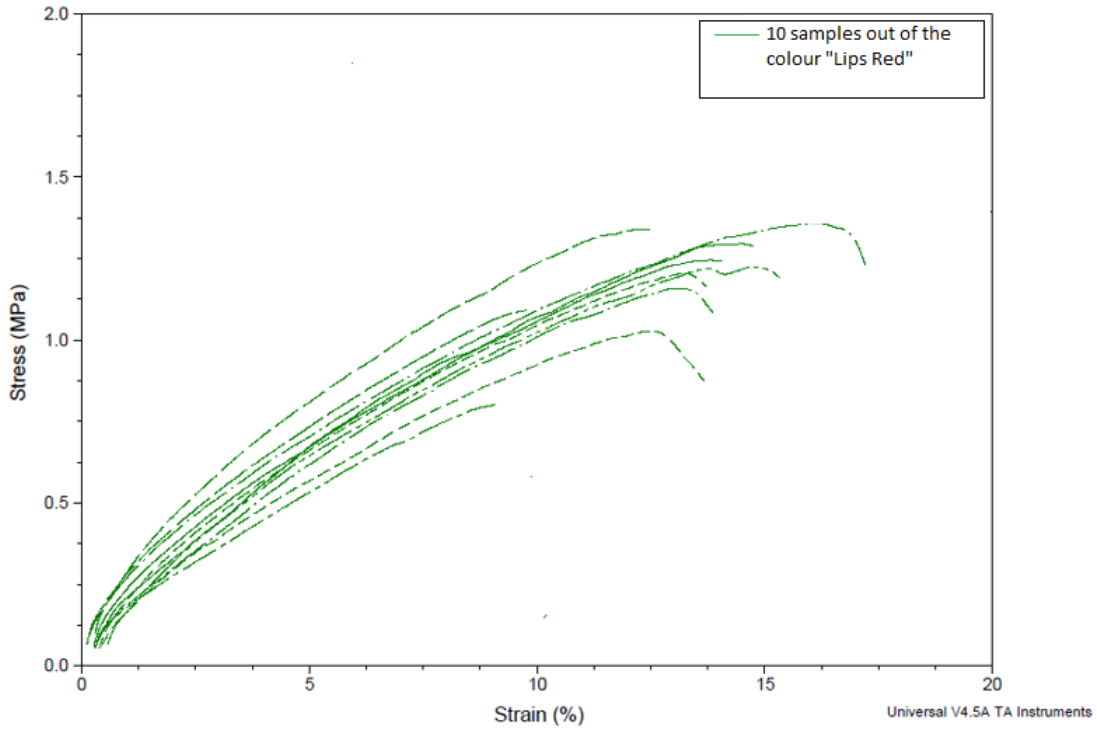

Figure 25: Stress-strain diagram showing all obtained results of the tensile tests on 'Lips Red'- schematic reconstruction.

The final two stress strain diagrams show the results of two ground layers, a brown under and a ground layer. As can be seen in the first figure, Figure 26, the resulting lines are steep, with high ultimate tensile and failure stresses ranging from 1.5 MPa up to 2.0 MPa and low strain values, almost all below 5% strain. Figure 27 shows the last stress strain curve obtained from tensile tests on the under layer brown sample batch. Contradictory to the Furthermore a side note has to be placed: the brown sample batch did not separate easily from the melinex base and subsequently not a lot of tests could be carried out.

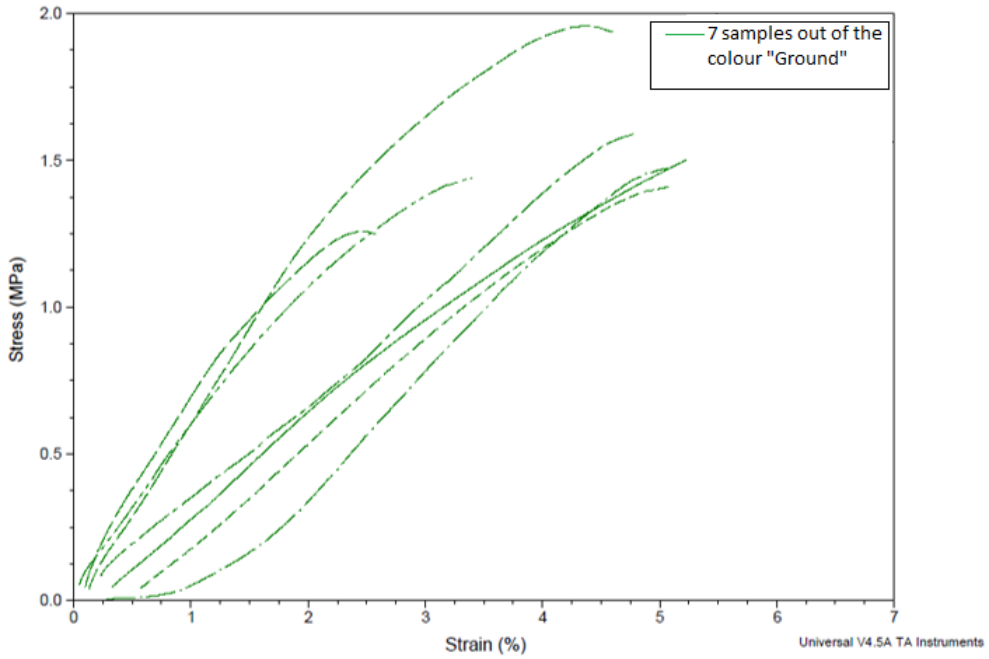

Figure 26: Stress-strain diagram showing all obtained results of the tensile tests on Ground layer specimen

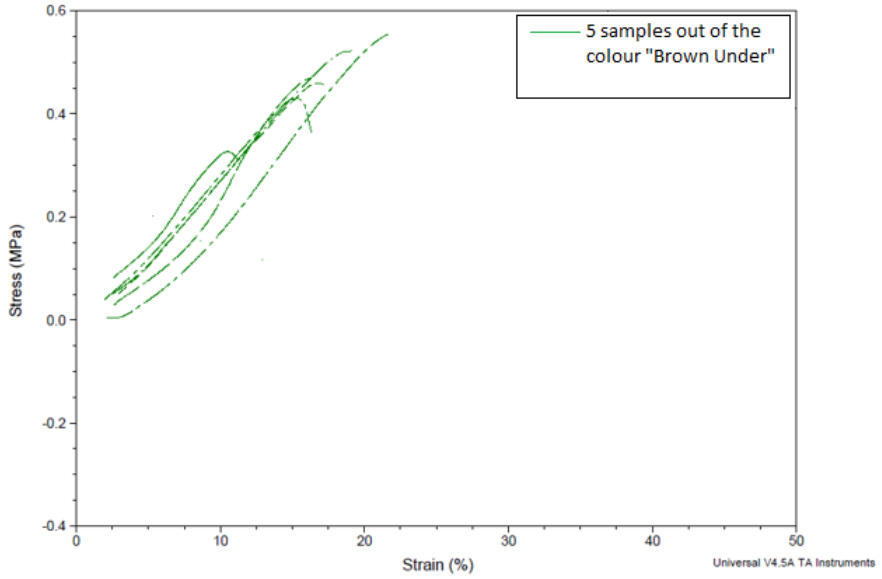

Figure 27: Stress-strain diagram showing all obtained results of the tensile tests on Brown under samples.

The following four figures, Figure 28 Figure 29 Figure 30 Figure 31, show box and whisper plots showing the averages and variations of the results obtained out of the tests conducted with the DMA. As can be seen the elastic modulus

of the Ground samples have a higher value than all the other samples, as shown in Figure 28. When the values of the colours (under) layers are inspected in Figure 29 and Figure 30 one can observe that the Lead white and Blue under have approximately the same values. Lips surface has values that are a bit higher than all the other colours and the Thick and Thin blue samples both have lower elastic moduli than the Blue under and Lead white samples. Furthermore as can be seen with the use of the whiskers that there is variation in the results. The last figure compares the three ground and under layers that have been tested. Here again one can observe that the elastic modulus of the Ground has a values approximately 3 to 4 times greater than the other two under layers.

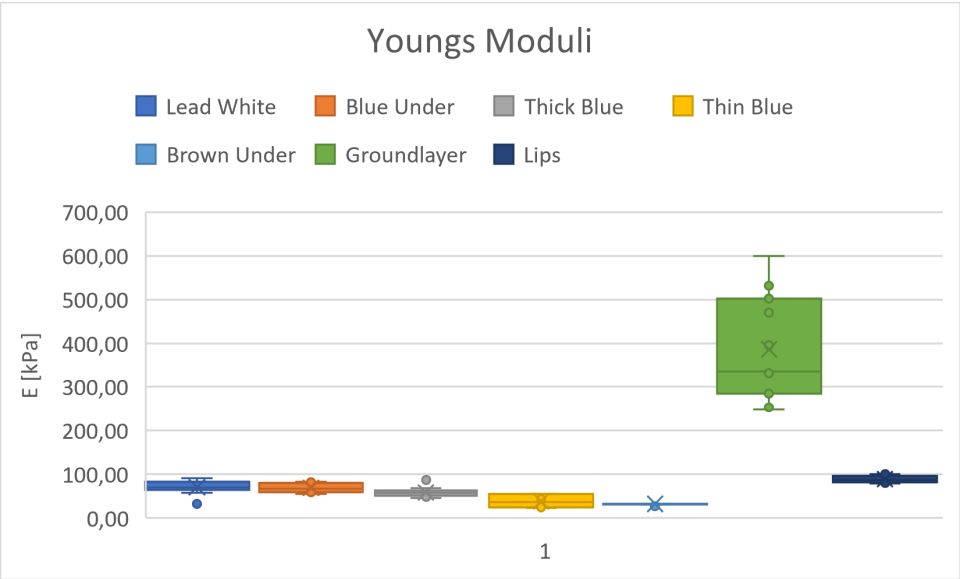

Figure 28: Box and whisker plot showing the Young's modulus and variation of each of the different types of tested schematic reconstructions in kPa. From left to right: Lead white, Blue under, Thick blue, Thin blue, Brown Under, Ground layer and Lips. Note the Young's modulus of the Ground layer which is approximately 4 to 5 times higher than other paint types.

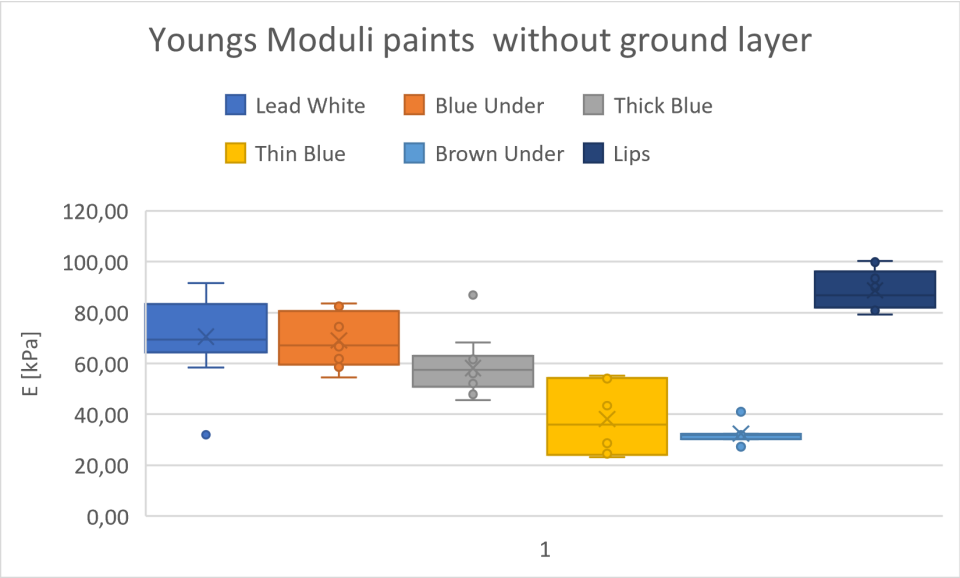

Figure 29: Box and whisker plot showing the Young's moduli and variation of the different types of tested paints in kPa. From left to right: Lead white, Blue under, Thick blue, Thin blue, Brown Under and lips. Note that Lead white has an average of around the 70 kPa and that most coloured paints have lower values except the red lips paint.

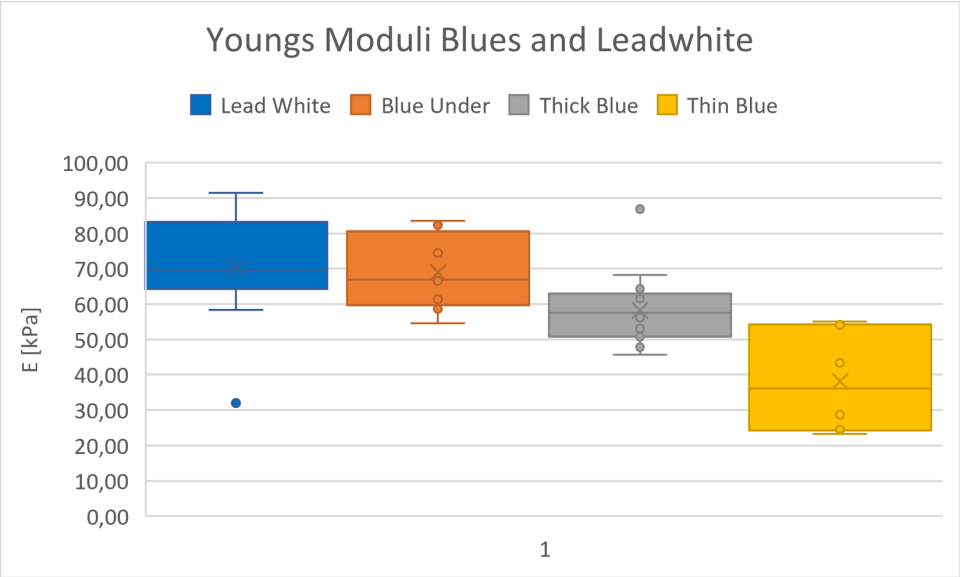

Figure 30: Box and whisker plot showing a zoomed in version of 4 types of paint, from left to right the Young's modulus and variation can be seen of each of the testes schematic reconstructions: Lead white, Blue under, Thick blue and Thin blue.

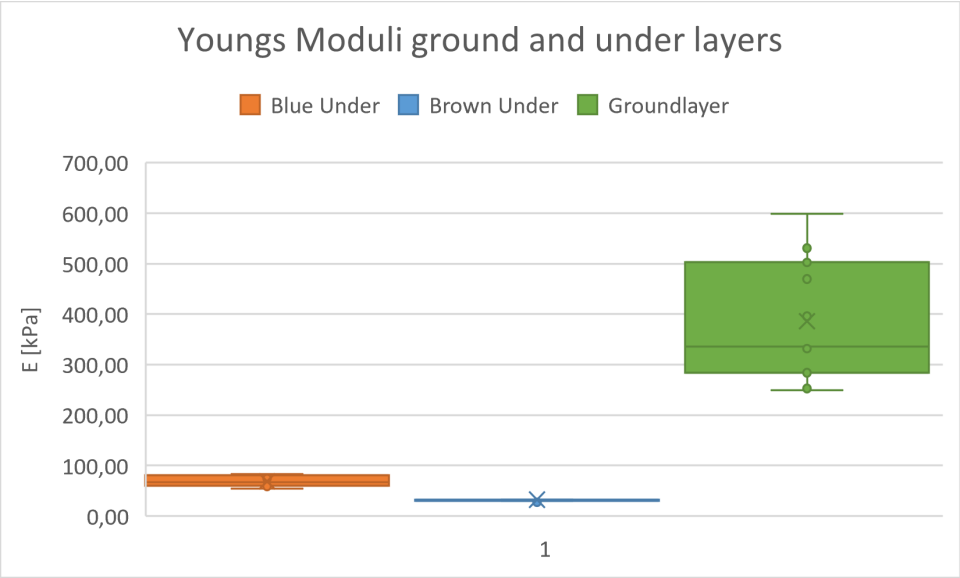

Figure 31: Box plot showing the Young's modulus and variation of each of the following tested schematic reconstructions: under and ground layers. From left to right the paint types Blue under Brown under and Ground layer can be seen. Note the big difference in value between the three types of paint.

The following two tables, Table 1 and Table 2, have been created with the obtained results and the use of the Equation 10 and Equation 11 . Table 1 shows the averages (μ) and the standard deviations (σ) of the found Young's Modulus of all the different tested schematic reconstructions. Because the raw data contained outliers, due to imperfections in the paint, the averages plus and minus 1 and 2 σ have been calculated. Assuming the obtained data can be represented within a normal distribution these values show the boundaries, and bandwidth, within which 68.26% and respectively 95.44% of the results can be found. Corrected data called "corrected $1 * \sigma$" and "corrected $2 * \sigma$" are a result of these calculated boundaries. Furthermore, with these values the newly calculated and corrected averages and standard deviations are given. Meaning that these are averages and standard deviations that are based on the values that lay within the previously described boundaries .

In the second table, Table 2, the mismatch between the Young's Modulus of two different layers has been calculated. This mismatch in stiffness has been calculated using the Young's modulus of each layer, calculations for both corrected and uncorrected values are shown. In order to calculate the stiffness mismatch two layers are chosen where the bottom layer is being called E_2 and the top layer E_1. The final table, Table 3, shows all the averages and standard deviations of the maximum found stresses. All the data points for the tables can be found in Appendix D.

Table 1: Results of tensile tests, averages and standard deviation values of Young's moduli of multiple paint types. Also the values of averages (μ) and standard deviations (σ) are shown when outliers are not taken out of the sample set based on standard deviation (σ). Full data set can be found in the appendices.

Young's Modulus [MPa]										
Colour	Uncorrected						Corrected 1*σ		Corrected 2*σ	
	μ	σ	μ+σ	μ-σ	μ+ 2*σ	μ- 2*σ	$\mu_{1\sigma}$	$\sigma_{1\sigma}$	$\mu_{2\sigma}$	$\sigma_{2\sigma}$
Lead White	7,05E-02	1,40E-02	8,45E-02	5,65E-02	9,85E-02	4,25E-02	7,08E-02	8,21E-03	7,33E-02	9,82E-03
Blue Under	6,90E-02	9,91E-03	7,89E-02	5,91E-02	8,88E-02	4,92E-02	6,79E-02	5,53E-03	-	-
Thick Blue	5,82E-02	9,90E-03	6,81E-02	4,83E-02	7,80E-02	3,84E-02	5,67E-02	4,82E-03	5,61E-02	6,46E-03
Thin Blue	3,76E-02	1,17E-02	4,93E-02	2,59E-02	6,11E-02	1,41E-02	3,60E-02	5,83E-03	-	-
Brown Under	3,24E-02	3,87E-03	3,62E-02	2,85E-02	4,01E-02	2,46E-02	3,17E-02	7,08E-04	-	-
Ground Layer	3,86E-01	1,16E-01	5,02E-01	2,70E-01	6,18E-01	1,54E-01	3,52E-01	6,36E-02	-	-
Lips	8,87E-02	7,61E-03	9,63E-02	8,11E-02	1,04E-01	7,35E-02	8,66E-02	5,67E-03	-	-

Table 2: Stiffness mismatches between multiple layer set are calculated based on uncorrected and corrected averages (μ) and standard deviations (σ). Full data set can be found in the appendices.

Young's Modulus Bottom layer / Toplayer (E_2/E_1) [-]			
Colour Combination	uncorrected		Corrected 1*σ
Ground layer / Lead White	5,47		4,97
Ground layer/ Thick Blue	6,64		6,21
Ground layer / Thin Blue	10,27		9,78
Ground Layer / Lips	4,35		4,06
Blue Under / Lead White	0,82		0,80
Blue Under / Thick Blue	1,19		1,20
Blue Under / Thin Blue	1,84		1,89
Brown Under / Lead White	0,46		0,45
Brown Under / Thick Blue	0,56		0,56
Brown Under / Thin Blue	0,86		0,88
Brown Under / Lips	0,36		0,37

Table 3: Results of tensile tests, averages (μ) and standard deviation(σ) of the maximum found stresses of different types of paint. Full data set can be found in the appendices.

Maximum Stresses [MPa]		
Colour	μ	σ
Lead White	1,09	0,30
Blue Under	1,11	0,17
Thick Blue	0,88	0,08
Thin Blue	0,54	0,13
Brown Under	0,45	0,07
Ground Layer	1,50	0,23
Lips	1,20	0,16

5.2 Failure mechanisms in Craquelure pattern

Figure 32, out of the literature study, shows the minimum crack channelling stress against the toughness ratios for different stiffness ratios. Whereas in the right part of Figure 33, also out of the literature study, shows the stiffness ratio verses the toughness ratio and the differences that can be expected whenever the moisture parameter changes. The left part in this figure shows the linear stress verses the toughness ratios, here also multiple stiffness ratios have been visualised in the graph. Giving an overview of the regions where the different failure mechanisms are active, based on the active stresses, stiffness and toughness mismatches and the moisture parameter α.

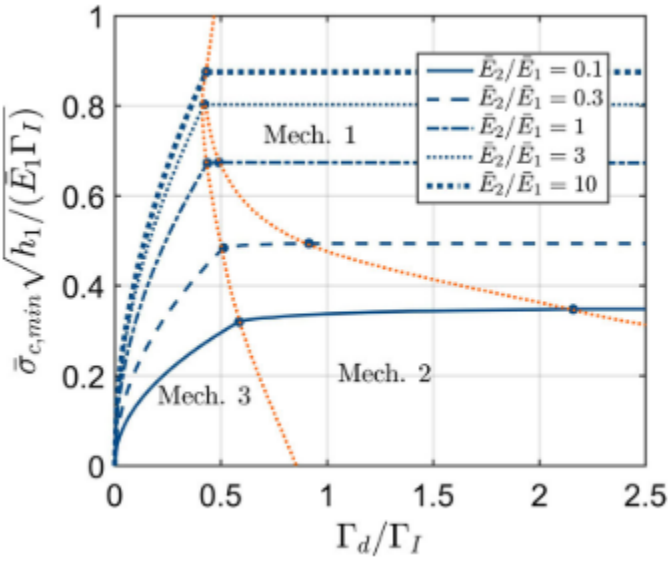

Figure 32: Failure map with 3 types of failure mechanisms, minimum crack channelling stress in the coating is depicted versus the toughness ratio, multiple stiffness ratios are shown. for constant moisture profile [7]

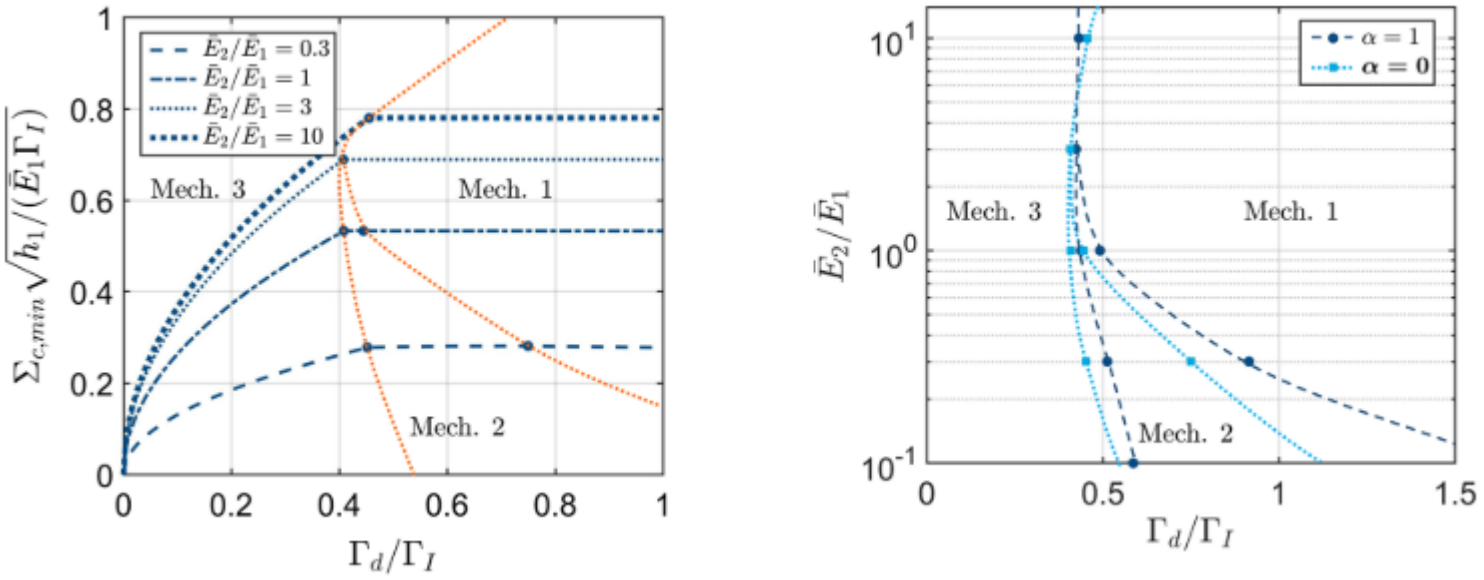

Figure 33: Left: Failure map shows three different types of failure modes for $\Sigma_{c,min}$ (linear part of stress profile) plotted against the toughness ratio at a $\alpha = 0$ value. Areas where failure mechanisms are active are distinguished from each other with the use of orange dotted lines. Right: Failure mechanism map, stiffness mismatch plotted against the toughness ratio. Two different failure mechanisms can be seen visualised in dark and light blue with different moisture parameters (respectively $\alpha = 1$ and $\alpha = 0$. [7]

Previously the stiffness mismatches have been calculated. These have been categorised in three types, Ground layer as base layer, the Blue under layer as base layer and the brown under as base layer. Both the uncorrected and corrected values show that the results of these three categories are:

1. Ground as base layer: uncorrected $4,4 \leq \mathrm{E}_2/\mathrm{E}_1 \leq 10,3$ and corrected $4,1 \leq \mathrm{E}_2/\mathrm{E}_1 \leq 9,8$
2. Blue Under as base layer: uncorrected $0,8 \leq \mathrm{E}_2/\mathrm{E}_1 \leq 1,8$ and corrected $0,8 \leq \mathrm{E}_2/\mathrm{E}_1 \leq 1,9$
3. Brown under as base layer: uncorrected $0,4 \leq \mathrm{E}_2/\mathrm{E}_1 \leq 0,9$ and corrected $0,4 \leq \mathrm{E}_2/\mathrm{E}_1 \leq 0,9$

When reviewing Figure 32, Figure 33 the following can be seen:

For Ground as base layer the following can be noted in the following figures:

1. Figure 32: Mechanism 2 is not present, for all toughness ratios.
2. Figure 33: Mechanism 2 is not present, for all toughness ratios and for all values of α. For all toughness ratios $\leq 0,4$ failure mode 3 will be dominant.

Secondly, Blue under as base layer the following can be noted in the following figures:

1. Figure 32: For toughness ratios $0,4 \leq \Gamma_2/\Gamma_1 \leq 0,6$ failure mechanism 2 can be found, for all other values mechanism 1 and 3 will be present.
2. Figure 33: Only for $\Gamma_2/\Gamma_1 \approx 0,5$ failure mechanism 2 can be found. For all smaller toughness ratios failure mode 3 will be dominant.

Lastly, brown under as base layer the following can be noted in the following figures:

1. Figure 32: For toughness ratios $0,4 \leq \Gamma_2/\Gamma_1 \leq 0,5$ failure mechanism 2 can be found, for all aother values mechanism 1 and 3 will be present.

2. Figure 33: Depending on the specific combination for between $0,4 \leq \Gamma_2/\Gamma_1 \leq 0,5$ and $0,5 \leq \Gamma_2/\Gamma_1 \leq 0,75$ failure mechanism 2 can be active. For smaller values failure mechanism 3 is active and values above this toughness ratio mechanism 1 is active.

As can be observed: both failure mechanisms 1 and 3 can be expected in the paint layers and failure mechanism 2 is present in lesser extent, depending on the (delamination) toughness. Furthermore, when one inspects different toughness ratios failure mode 1 merges into failure mode 3 and vice verse for the found elastic modulus ratios, often without the interference of failure mode 2 and sometimes with a small transition period with specific values of toughness ratios. Note that these results are based on newly made paint that has not been aged.

5.3 Topography

Figure 34 shows multiple pictures made with the program MountainsMap and literature (Figure 19, [12]). Showing part of the blue headscarf, 26 mm by 30 mm, where both the light and the darker, shadows, part of the headscarf can be seen, this part has already been visualised in f of Figure 10. As well as a topography chart visualising height differences of this area, dark blue indicate the deepest locations and red the highest. Both with a line across the figures, along this line a computer driven cross-section is made. Different sections of this line are shown in a graph in Figure 35, Figure 36 and Figure 37, where the topography of the painting along this line is shown in height profile figures. For more detailed figures showing the topography, cross-section and cracks see Appendix E.

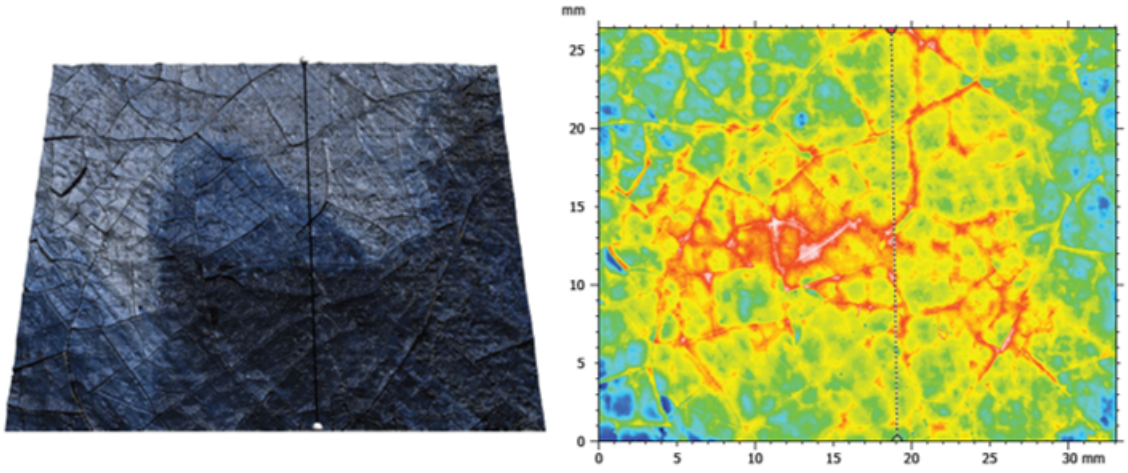

Figure 34: Left: zoomed in part of headscarf. Right: topography chart showing height differences. Differences in height and distance between points are given, dark blue indicate the deepest locations and red the highest. Made with the program MountainsMap and the use of Figure 19 [12].

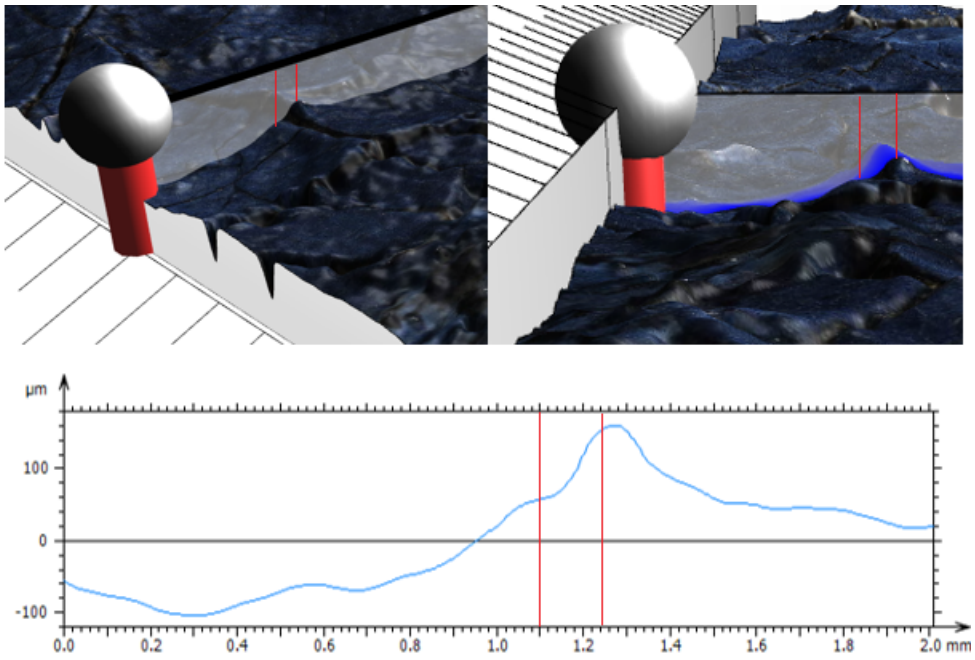

Figure 35: Part of Figure 34 showing a crack, between red lines, out of two different views, as well as the height profile of the crack. The crack is positioned just before the $1,2$ mm mark. Figure 19 [12].

Figure 35 shows the first part of the cross-section, visualised in three pictures. Two of which show focused pictures of a crack and the bottom shows the height profile of the cross-section (visualised as grey plane in the top pictures). Note that the visible crack is lower on the left side and higher on the right side, and that the line cuts the single crack perpendicular. In the bottom figure the height profile is visualised where the crack and both the left and right edges are between the 1.0 mm and 1.3 mm on the x-axis. The left edge of the crack has a height gain of around 100 μm.

In Figure 36 two different cracks can be found, note again that both cracks are positioned perpendicular to the grey plane that represents the cross-section. Again the height profile along this section of the cross-section is shown in the bottom picture. The crack on the left side is shown at 0.55 mm with the edges respectively at around 0.45 mm and 0.60 mm (see red lines) only two small hills can be seen, with a maximum of 40 μm in height. Another crack is shown at the other side of the figure, here a different profile can be seen, a small dimple representing the crack in the height profile at $2,45$ mm with both edges shown around $2,4$ mm and $2,55$ mm a maximum height gain of around 175 μm is measured.

The third and last Figure 37 depicts a more steeper crack in the lighter part of the blue headscarf where the tops of the edges at both sides are further apart, the crack is found just before the $1,1$ mm with edges around $0,9$ mm and $1,2$ mm, overall at the direct edges not a lot of height differences can be found. However at the side of this profile the height profile does drop

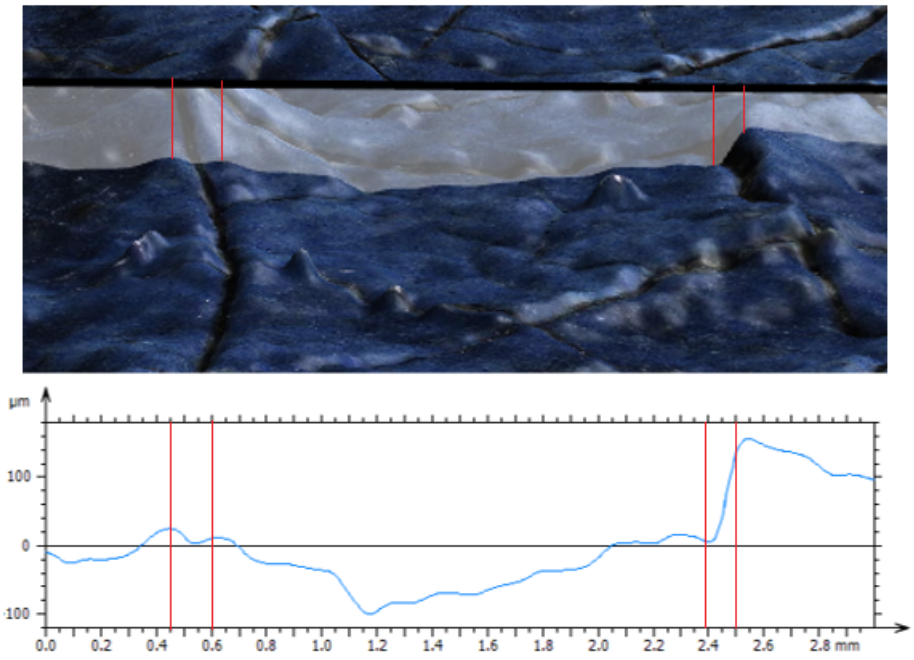

Figure 36: Two cracks can be found in the top figure, between red lines, note that the most left crack is relatively flat at the edges contrasting to this crack the left crack has a great height difference. Both the cracks, between red lines, can be found in the height profile figure at the bottom at $0,55$ mm and $2,45$ mm Figure 19 [12].

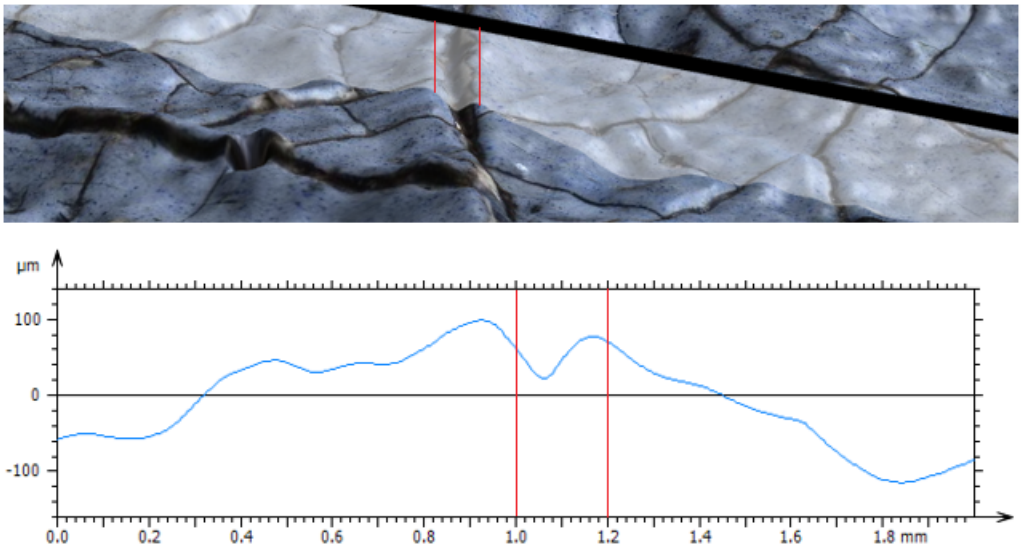

Figure 37: Zoomed in figure in the lighter part of the headscarf showing a crack, between red lines, with height difference within the crack and more horizontal difference between the (tops) of the edges as can be seen in the lower figure. The crack can be found at 1.1 mm Figure 19 [12].

6 Discussions and Recommendations

6.1 Preparation of Schematic Reconstructions

Girl with a Pearl Earring is a historical painting making it difficult to use for tests, because invasive and tests on the painting are prohibited. As a results schematic reconstructions have been used for the tensile tests, made by Mané Veldhuizen. Reproducing the paint out of a historic painting is difficult and the schematic reproductions do not fully represent the paint as it is in the painting. As can be read in the logbook of Mané Veldhuizen, the amounts of material used for producing the paint are not noted down in SI units. Moreover, paint colours are often mixed on 'feeling' and by comparing the colours with the original. However, the materials that are used for the schematic reconstructions are the materials that Johannes Vermeer would have used and therefore present a qualitatively, rather quantitatively accurate historical reconstruction.

Furthermore, the schematic reconstructions that are made are single layers of paint made using a draw down bar, a method for creating a single flat layer. However, also multilayered structures should have been made for the full use of the failure mechanism models as also the delamination toughness parameter is needed obtained out of a bilayer sample [6, 7]. This parameter is found with the use of a three or four point bending test on multilayered structures.

Another limitation includes the environmental conditions in which the samples were kept in the drying period before the tensile tests. The samples were handled taking instructions of Mané Veldhuizen into account and were kept in an interior environment with approximately constant parameters (approximately 20 degree Celsius and 50% relative humidity). However, these parameters were not exactly known and not the best for the purpose of drying paint. For further research it is recommended to ask the artist to weight all the materials used in the process of paint making and keep the samples in a controlled environment. This will result in a data set of mechanical properties with a higher reliability.

As a result, the schematic reconstructions that have been used for the tensile tests in order to find the mechanical properties of the paint in *Girl with a Pearl Earring* are not totally representing the real painting. Resulting in experimental results that are difficult to reproduce. However, the properties that are found should be close to the properties of the paint when the painting was recently painted.

6.2 Preparation and Results of Tensile Test

During the drying process of the schematic reconstructions both air pockets form and paint shrinks on the 'silicone-release melinex' both these effects create a rougher topography on the paint surface. As a result the paint is not completely homogeneous and the paint has to be visually inspected on imperfections before testing, imperfections are shown and marked in Figure 38. Both the visual inspection and further preparations, e.g. measuring of samples, are done by hand and are susceptible to human error. Furthermore, cracks can be formed in the order-scale of micro- or nano-meter while handling the samples during the preparation steps influencing the test results due to pre-stresses that form at the tip of a crack.

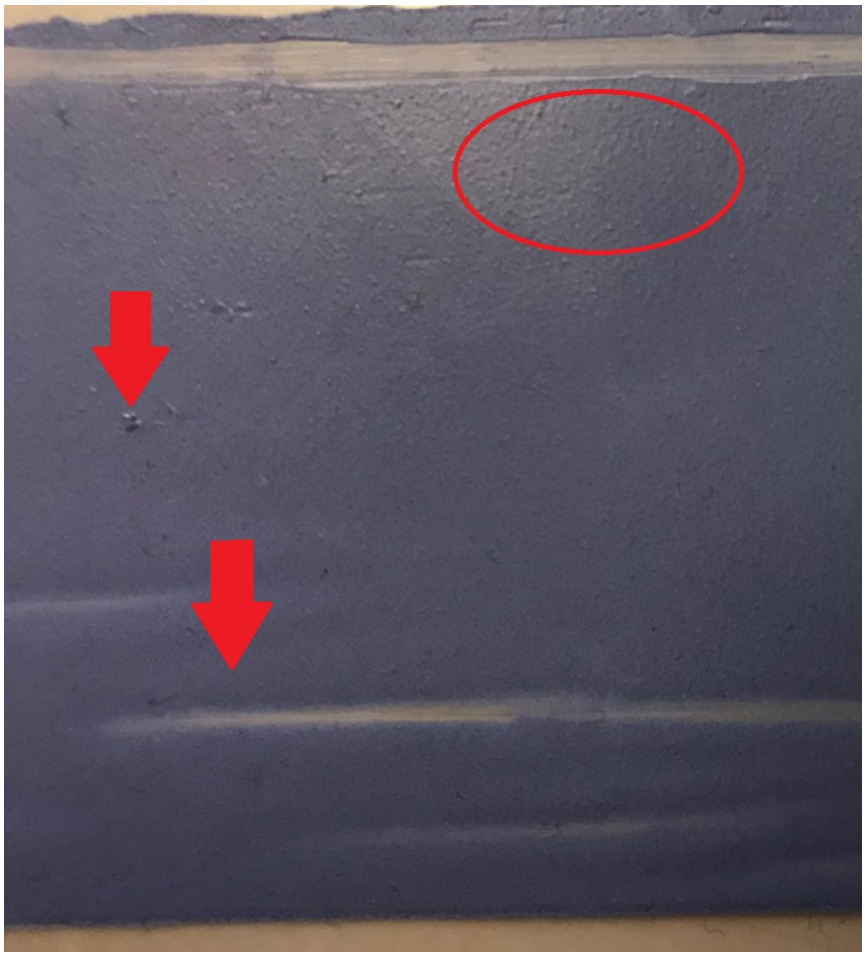

Figure 38: Imperfections visual in schematic reconstruction, within the red circle the surface is not totally flat, bumps can be seen. At both red arrows two different imperfections can be seen; an air bubble (at the top) and a whitish area whit a thinner layer of paint (at the lower arrow). See Appendix B for more examples of imperfections in the schematic reconstructions. Photo made in laboratory of TUDelft.

During the testing phase of the experimental samples, slip was detected whenever that paint samples in the clamps were closed with a force of 3 in-lb or less. When the screws, holding the clamps, are fastened with a force of 4lb the samples did not slip. However, the specific consequences of these forces on the sample are not known, as the samples are very thin and ductile there is an option that due to the forces the sample deformed creating stresses that interfere with the test results.

Figure 39 visualises the change in the elastic modulus of multiple types paint over time. This graph is constructed without taking parameters as (relative) humidity, temperature and environmental changes into account [13]. The green crosses visualise the changes in the Young's modulus of oil paint over a period of $10^{-2} - 10^{1}$ years ($0,01$ year $-$ 10 years old paint, logarithmic scale). Although a lot of variation in the stiffness distribution can be seen, the trend is that the paint becomes stiffer. However, the experimental results obtained have values of around 30 to 70 kPa, these found experimental results are not visualised in the graph as the vertical axis showing the Young's modulus starts at 10^{0} MPa (1000 kPa). However, the graph shows that oil paints of approximately 1 year old (10^{0}) have the lowest Young's

modulus, note that the schematic reconstructions have an age of a half year. Therefore, the found experimental values are not totally unusual.

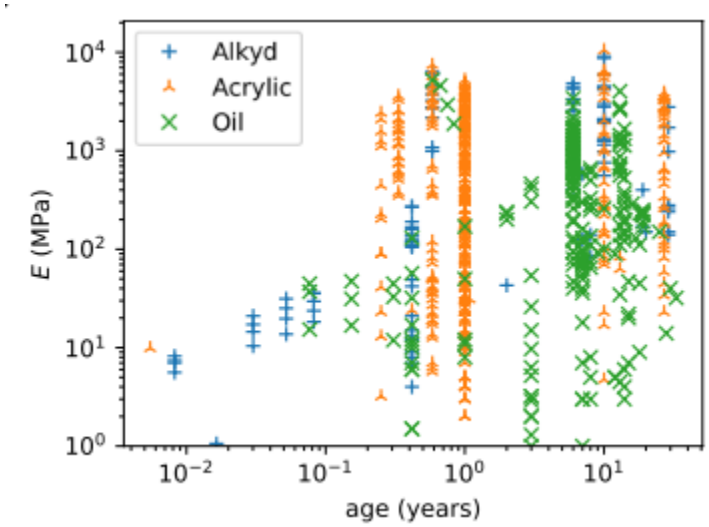

Figure 39: Graphical representation of the change in elastic modulus over time. Three types of paint are shown, Alkyd, Acrylic and oil. Note that the experimental values are in the order of kPa, 10^{-2} MPa, and thus not visualised in this graph. As can be seen, the Young's Modulus (E) of the oil paint has an upward trend over time [13].

6.3 Simplification of Models

Johannes Vermeer painted *Girl with a Pearl Earring* using a simple structure of preparatory and pictorial layers on top of each other, as can be seen in Figure 40 [3]. However, multiple preparatory and pictorial paint layers overlap and differ in thickness at multiple places. Therefore, the build up of *Girl with a Pearl Earring* is not as simple as assumed in the failure mechanism model that have been used, these models consist out of two separate layers on top of each other, as can be seen in Figure 41 [6, 7]. The cracks visualised with the use of MountainsMap software are out of these simply build-up area, and specifically chosen because of the simple build-up. However, even after these carefully chosen locations based on literature and previous research, the models that are used are simplifications and do not fully represent the paint, layer build-up and age of the original painting.

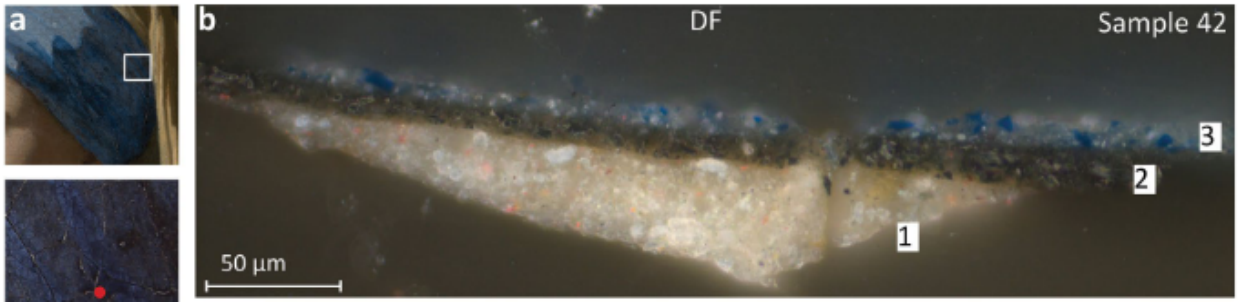

Figure 40: Cross-section of paint sample 42 from the painting *Girl with a Pearl Earring*, a shows the location of the paint sample both with a white square and a red dot. b Shows a light microscope (dark field) photo of the sample. 3 layers are identified, 1 ground $50\mu m$ 2 thin black under layer ($10\mu m$) and 3 thin blue surface layer [3].

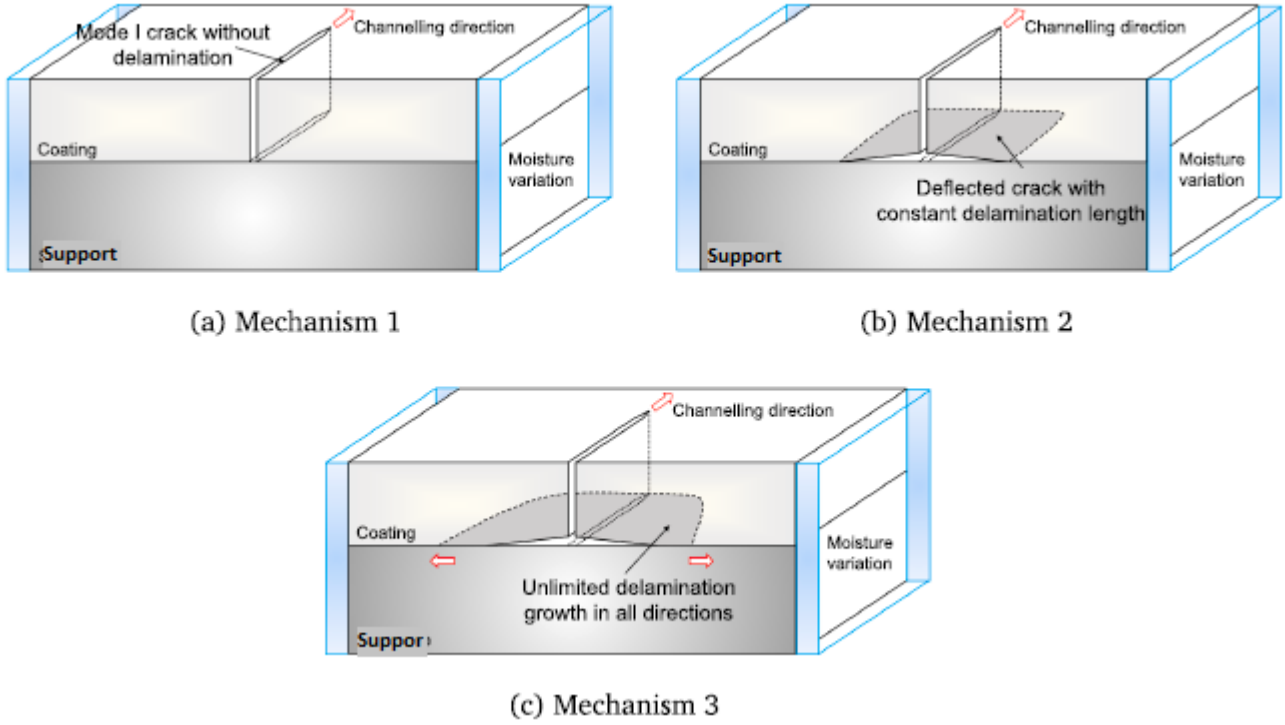

Figure 41: Three different types of cracks that can be found in a bilayer system. (a) Mechanism I: Perpendicular crack on the support (stable); (b) Mechanism II: Vertical crack with horizontal, stable and finite, crack (stable); (c) Mechanism III: Vertical crack with a horizontal infinite propagating crack (unstable, resulting in paint flaking) [6].

Furthermore, the conducted experiments only took preparatory and pictorial paint layers into account. Figure 42 shows that whenever the thickness ratio changes between 1 and 10 the areas where the failure mechanisms are active change. Showing that mechanism 3 becomes less dominant at lower stiffness and toughness mismatches. Therefore, it is recommended for further research to take the canvas and the lining methods into account even though this makes the model less simple.

Finally, as mentioned before only experimental results of the Young's modulus of the schematic reconstructions have been found. For full use of the failure mechanism models the (delamination) toughness should also be found with the use of multi layered samples. However, a value of 1 for the toughness mismatch is a conservative and safe estimate. Because the delamination toughness (Γ_d) is larger than the toughness mode I (Γ_I). Assuming $\Gamma_d/\Gamma_I = 1$ it is found that failure mechanism 3, total delamination, will never be present.

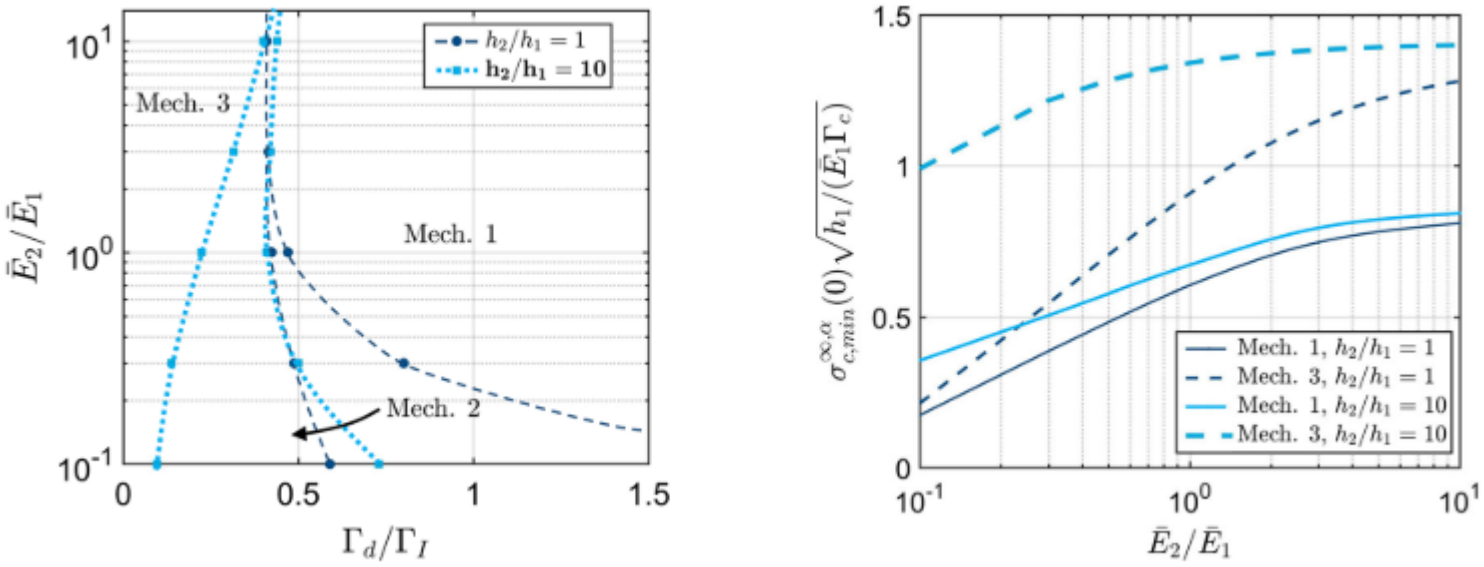

Figure 42: On the left the failure mechanisms for both a bilayer system of $h_2/h_1 = 1$ (dark blue) and $h_2/h_1 = 10$ (light blue) are shown, as a function of the elastic mismatch and the toughness mismatch (Γ_d/Γ_l). The graph on the right side, the critical cracking stress is visualised as a function of the stiffness mismatch. For both graphs $\beta_2/\beta_1 = 10$ and $D_2/D_1 = 1$ and $\alpha = 0.5$ [7].

7 Conclusion

In this thesis the formation of cracks and failure mechanisms in the paint layers found in historical paintings have been investigated, more specifically in the painting *Girl with a Pearl Earring*. In order to get a better insight in the degradation of historical paintings experimental results of reconstructed paint show, with the help of theoretical models, the failure mechanisms that are to be expected in *Girl with a Pearl Earring*. Literature research, observations made on the real painting and the results of the experimental values are compared in order to find the active failure mechanisms in the *Girl with a Pearl Earring* and together form a basis for a visual model showing the progression of the craquelure pattern over time.

7.1 What are the experimental mechanical properties of the paint used by Johannes Vermeer and how do these values relate to properties found in literature?

With the use of a Dynamic Mechanical Analyser the Young's modulus has been found of the schematic reconstructions. These single layered, made with historically correct materials reproduced paint samples have been made by Mané Veldhuizen. These tests have been executed on multiple different colours and paint types found in the painting *Girl with a Pearl Earring*; Lead White, Three types of blue (Thin blue, Thick blue, Blue under layer), Lips Surface (Red) and two types of ground (Ground, Brown under 2). Maximum stresses with values between $0,45$ MPa and $1,50$ MPa have been found (with standard deviation of $0,07$ MPa) and are shown in Table 3. And Young's modulus for the different colours between the $8,87$*10^{-2} MPa and $3,86$*10^{-1} MPa.

Analyses of the produced experimental data have shown that different paint colours, types of paint (pictorial layers and preparatory layers) and thicknesses in paint layers have a different elastic modulus, within the range $8,87$*10^{-2} MPa and $3,86$*10^{-1} MPa. Variations and outliers in the test data have been indicated with the use of standard deviations. Moreover, the stiffness mismatches between superimposed layers have been calculated, both based on test results and on data corrected for outliers and imperfections in the schematic reconstructions. Based on this data set and on the research on failure mechanisms an indication can be given on the types of crack that can be found in the painting. The annotation should be made that these observations are based on newly reconstructed paint layers and thus not directly comparable with the paint found in a historic painting.

The mechanical properties of paint change over time, the found experimental values belong to paint with an age of a few months. Literature research shows that paint of approximately 1 year old can be expected to have a Young's modulus of around 1 MPa to 10 MPa, which is a 10 - 100 times higher than the found experimental values. However, the Young's Modulus of paint do change over time, becoming higher over time. Therefore, the found values are expected to become higher over time and becoming more compliant to the found values in the literature.

7.2 How can the found mechanical properties of reconstructed paint samples be fitted in the failure mechanism model?

Figure 12, Figure 13 and Figure 11 (Figure 13 shown again below as Figure 43) show the multi layered structure illustrating the simple build-up and use of paint Johannes Vermeer used in *Girl with a Pearl Earring*. Previously conducted research shows that craquelure patterns can be predicted by calculating the differences in mechanical

properties of two superimposed layers and taking environmental conditions into consideration. The combination of these two show the possibility to model *Girl with a Pearl Earring* as a multilayered structure, simultaneously showing that three different types of craquelure can be active in the paint layers of a historical painting. Failure mode 1 shows only a vertical crack in the top layer. Whereas failure mode 2 and 3 also show a horizontal crack, note that mode 2 is stable and mode 3 is unstable, as shown in Figure 44. Stable meaning that the formation of the horizontal crack between superimposed layers is of finite length whereas unstable means that the crack is of infinite length and leads towards delamination.

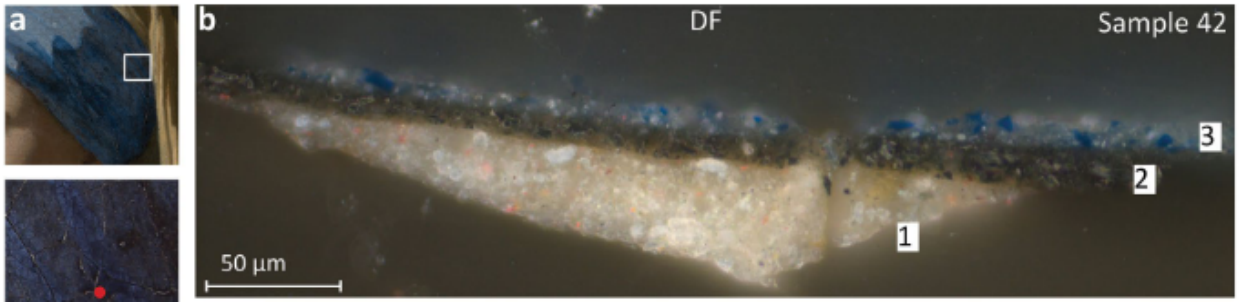

Figure 43: Cross-section of paint sample 42 from the painting *Girl with a Pearl Earring*, a shows the location of the paint sample both with a white square and a red dot. b Shows a light microscope (dark field) photo of the sample. 3 layers are identified, 1 ground $50\mu m$ 2 thin black under layer ($10\mu m$) and 3 thin blue surface layer [3].

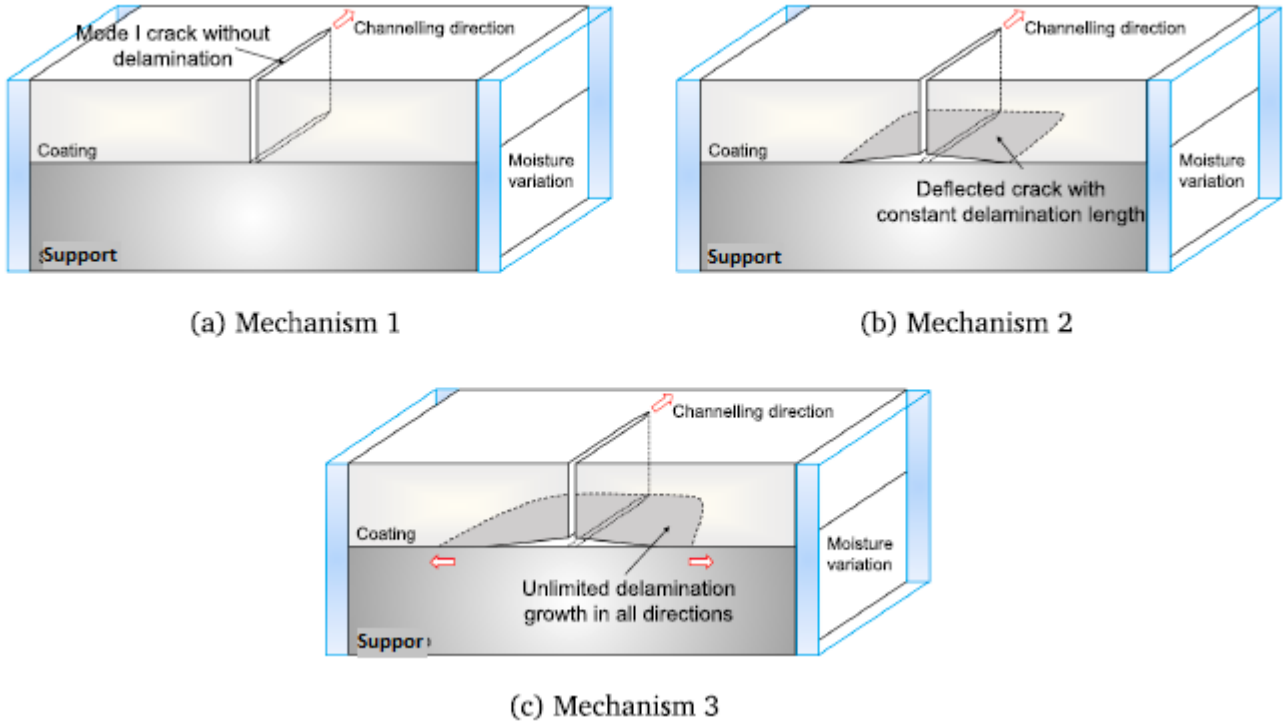

Figure 44: Three different types of cracks that can be found in a bilayer system. (a) Mechanism I: Perpendicular crack on the support (stable); (b) Mechanism II: Vertical crack with horizontal, stable and finite, crack (stable); (c) Mechanism III: Vertical crack with a horizontal infinite propagating crack (unstable, resulting in paint flaking) [6].

Based on the stiffness mismatches obtained out of the experimental results of the DMA tests on the reconstructed paint samples and together with the cross-section figures showing layer build-up used by Johannes Vermeer the active ranges of the failure mechanisms can be found with the use of the failure mechanism models. Based on these results, failure modes 1 and 3 are likely to be found, making painting susceptible for a failure mode where the paint comes loose and is able to delaminate, failure mechanism 2 is less present. Because failure mode 2 is mostly present for lower stiffness mismatches. Furthermore, the differences in Young's modulus increase the chance on starting the cupping process. However, when the assumed value of 1 for the toughness mismatch is used failure mechanism 3 will not be present and only failure mechanism 1 is found within the paint layers of the painting.

However, the X-ray photographs of the painting show multiple area's where the paint has come loose from the canvas, indicating failure mode 3, total delamination. Because of this extra research is needed in these area's as most of these areas do not, or in lesser extent, contain the most investigated blue paint types. Figure 45 shows the X-ray photo again of *Girl with a Pearl Earring* indicating that most of the loose fragments are in the bottom part of the painting in the yellow area and in the dark surroundings.

Figure 45: Left: Visible light photograph of *Girl with a Pearl Earring*. Right X-radiography photo of the same painting, visualising the wooden frame, canvas and nails. But, even more important, visualising black dots scattered over the painting. These black dots indicate the places where fragments of paint left the surface of the painting. In the middle a few bigger black spots can be seen, at the bottom an area of smaller dots. [11]

7.3 How do the theoretically described craquelure patterns and failure modes relate to the patterns observed in the *Girl with a Pearl Earring*

The zoomed in figure in Figure 37 (shown below again as Figure 46), and more in Appendix E, display detailed information on specific areas of *Girl with a Pearl Earring*. Here it can be seen that failure mechanisms 1 and 2 and the cupping process are more dominant than failure mechanism 3. The experimental results and the models show that

failure mechanisms 1 and 3 have a higher chance to be found, in combination with the X-ray photo that show the holes where the paint has come loose. One of the reasons for this mismatch could be the interaction of paint with the canvas, as Figure 42 shows the change in area at which mechanisms 2 is dominant subsequently making mechanisms 3 less dominant at lower stiffness ratios. Another parameter of influence is the moisture, however, as shown in Figure 9 the areas where the the failure mechanisms are active do not change significantly with changes in moisture parameter α. A third reason is the type of paint, most of the researched paint are blue types. Showing that more research on the toughness and properties of the canvas and interactions with the layers is necessary for further investigation on the failure mechanisms that are found in the pictorial layers of a historical painting.

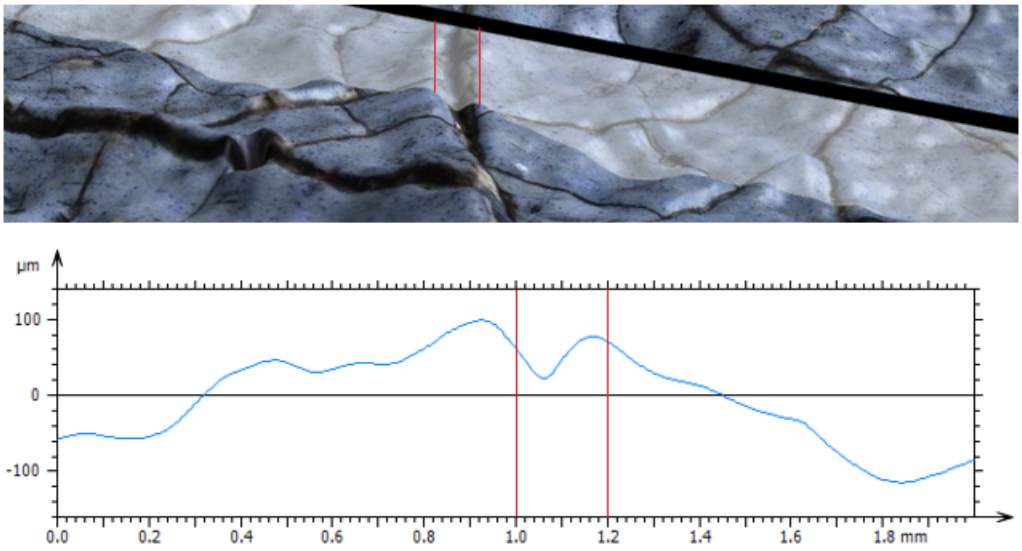

Figure 46: Zoomed in figure in the lighter part of the headscarf showing a crack, between red lines, with height difference within the crack and more horizontal difference between the (tops) of the edges as can be seen in the lower figure. The crack can be found at 1.1 mm Figure 19 [12].

Multiple different cracks, out of *Girl with a Pearl Earring*, are shown in the results section and in Appendix E. Showing different crack types; slightly lifted edges, edges that are relatively flat and lastly a type showing relatively more of a height differences with their surroundings around the edges. Previously presented results show that failure modes 1 and 3 were likely to be most present. However, as seen most of the edges around crack have slight height profiles indicating failure mode 2, with partial delamination. Moreover, these profiles found in the topography of the paint also indicate the cupping process which most likely happened due to lining processes executed in the past.

7.4 Outlook

Finally, a 2- or 3-Dimensional model of the *Girl with a Pearl Earring* can be made visualising the craquelure formation and propagation over time. Based on this research and minding some historically incorrect representations, the following should be taken into account. First, the cracks of the painting have to be fully identified and categorised with the use of the height profile maps. Thereafter, with the use of the mechanical properties of the different paint types and layer

build-ups and graphs of the failure mechanism model the origin for each crack has to be found and with the use of computer programs a visualisation of the formation of the craquelure can be made. Finally, extra tests have to be carried out in order to find the influence of a thicker canvas on the failure mechanisms as well as the experimental values of the delamination toughness have to be found.

References

[1] W. S. Elkhuizen, T. W. Callewaert, E. Leonhardt, A. Vandivere, Y. Song, S. C. Pont, J. M. Geraedts, and J. Dik, "Comparison of three 3D scanning techniques for paintings, as applied to Vermeer's 'Girl with a Pearl Earring'," *Heritage Science*, vol. 7, no. 1, pp. 1–22, 2019.

[2] W. S. T. Mayer and J. W, *The Science of Paintings*, vol. 12. 2001.

[3] A. van Loon, A. A. Gambardella, V. Gonzalez, M. Cotte, W. De Nolf, K. Keune, E. Leonhardt, S. de Groot, A. N. Proaño Gaibor, and A. Vandivere, "Out of the blue: Vermeer's use of ultramarine in Girl with a Pearl Earring," *Heritage Science*, vol. 8, no. 1, pp. 1–18, 2020.

[4] A. Vandivere, "Mauritshuis, girl with the blog," 2021.

[5] E. J. Hearn, *Mechanics of Materials 1; an introduction to the Mechanics of Elastic and Plastic deformation of solids and structural materials*. 1977.

[6] E. Bosco, A. S. Suiker, and N. A. Fleck, "Moisture-induced cracking in a flexural bilayer with application to historical paintings," *Theoretical and Applied Fracture Mechanics*, no. September, p. 102779, 2020.

[7] E. Bosco, A. S. Suiker, and N. A. Fleck, "Crack channelling mechanisms in brittle coating systems under moisture or temperature gradients," *International Journal of Fracture*, vol. 225, no. 1, pp. 1–30, 2020.

[8] W. Paul, D. Oliver, and P. Grütter, "Indentation-formed nanocontacts: An atomic-scale perspective," *Physical Chemistry Chemical Physics*, vol. 16, no. 18, pp. 8201–8222, 2014.

[9] TA Instruments, "DMA Q 800 Specifications," no. April, pp. 1–14, 2012.

[10] A. V. Loon, A. Vandivere, J. K. Delaney, K. A. Dooley, S. D. Meyer, F. Vanmeert, V. Gonzalez, K. Janssens, E. Leonhardt, R. Haswell, S. D. Groot, P. D. Imporzano, and G. R. Davies, "Beauty is skin deep : the skin tones of Vermeer ' s Girl with a Pearl Earring," *Heritage Science*, pp. 1–20, 2019.

[11] A. Vandivere, A. van Loon, K. A. Dooley, R. Haswell, R. G. Erdmann, E. Leonhardt, and J. K. Delaney, "Revealing the painterly technique beneath the surface of Vermeer's Girl with a Pearl Earring using macro- and microscale imaging," *Heritage Science*, vol. 7, no. 1, pp. 1–17, 2019.

[12] A. Vandivere, J. Wadum, and E. Leonhardt, "The Girl in the Spotlight: Vermeer at work, his materials and techniques in Girl with a Pearl Earring," *Heritage Science*, vol. 8, no. 1, pp. 1–10, 2020.

[13] G. dePolo, M. Walton, K. Keune, and K. R. Shull, "After the paint has dried: a review of testing techniques for studying the mechanical properties of artists' paint," *Heritage Science*, vol. 9, no. 1, pp. 1–24, 2021.

[14] A. Vandivere, J. Wadum, K. J. van den Berg, and A. van Loon, "From 'Vermeer Illuminated' to 'The Girl in the Spotlight': approaches and methodologies for the scientific (re-)examination of Vermeer's Girl with a Pearl Earring," *Heritage Science*, vol. 7, no. 1, pp. 1–14, 2019.

[15] N. Gallery, "National Gallery of Art The Camera Obscura and Painting in the Sixteenth and Seventeenth Centuries Author (s): JEAN-LUC DELSAUTE Source : Studies in the History of Art , Vol . 55 , Symposium Papers XXXIII : Vermeer Studies Published by : National Galler," vol. 55, no. 1998, pp. 110–123, 1998.

[16] F. Giorgiutti-Dauphiné and L. Pauchard, "Painting cracks: A way to investigate the pictorial matter," *Journal of Applied Physics*, vol. 120, no. 6, 2016.

[17] L. Bratasz, T. J. Paul, G. Trust, and R. Kozlowski, "Response of Wood Supports in Panel Paintings Subjected to Changing Climate Conditions Response of wood supports in panel paintings subjected to changing climate conditions B . Rachwał , Ł . Bratasz *, M . Łukomski , R . Kozłowski Jerzy Haber Institute of ," no. October, 2012.

[18] L. Bratasz, L. Krzemien, T. J. Paul, G. Trust, and R. Kozlowski, "Fatigue Damage of the Gesso Layer in Panel Paintings Subjected to Changing Climate Conditions Fatigue damage of the gesso layer in panel paintings subjected to changing climate conditions B . Rachwał , Ł . Bratasz , L . Krzemień , M . Łukomski * , R . Koz," no. December, 2012.

[19] M. F. Mecklenburg and C. S. Tumosa, "Mechanical Behavior of Paintings Subjected to Changes in Temperature and Relative Humidity," *Art in Transit: Studies in the Transport of Paintings*, pp. 173–216, 1991.

[20] J. D. J. van den Berg, K. J. van den Berg, and J. J. Boon, "Chemical changes in curing and ageing oil paints," *Triennial meeting (12th), Lyon, 29 August-3 September 1999: preprints*, vol. 1, no. January, pp. 248–253, 1999.

[21] D. Erhardt, C. S. Tumosa, and M. F. Mecklenburg, "Long-term chemical and physical processes in oil paint films," *Studies in Conservation*, vol. 50, no. 2, pp. 143–150, 2005.

[22] D. Erhardt, C. S. Tumosa, and M. F. Mecklenburg, "Applying science to the question of museum climate," *Museum microclimates: contributions to the Copenhagen conference, 19-23 November 2007*, pp. 11–18, 2007.

[23] S. v. d. L. L. Wadum J, Hoppenbrouwers R, *Vermeer illuminated. Conservation, restoration and research*. Wormer: V+K Publishing/Inmerc, 1994.

[24] e. Gaskell I, Jonker M, *Vermeer studies: studies in the history of art 55*. New Haven: National Gallery of Art Washington, 1988.

[25] C. Young and P. Ackroyd, "The mechanical behaviour and environmental response of paintings to three types of lining treatment," *National Gallery technical bulletin*, vol. 22, pp. 85–104, 2001.

[26] R. Hill, Joyce; Rebecca, *Conservation of Easel Paintings*. New York: Routledge, 2012.

[27] L. Krzemień, M. Łukomski, Bratasz, R. Kozłowski, M. F. Mecklenburg, L. Krzemien, Micha, Bratasz, R. Koz, and M. F. Mecklenburg, "Mechanism of craquelure pattern formation on panel paintings Mechanism of craquelure pattern formation on panel paintings," vol. 3630, 2016.

[28] S. Bucklow, "The Description of Craquelure Patterns Author (s): Spike Bucklow Published by : Taylor & Francis , Ltd . on behalf of the International Institute for Conservation of Historic and Artistic Works Stable URL : https://www.jstor.org/stable/1506709 REFERENCE," vol. 42, no. 3, pp. 129–140, 1997.

[29] R. A. Luimes, A. S. J. Suiker, A. J. M. Jorissen, P. H. J. C. V. Duin, and H. L. Schellen, "Hygro - mechanical response of oak wood cabinet door panels under relative humidity fluctuations," *Heritage Science*, pp. 1–23, 2018.

[30] W. B. Wei, *Art Conservation Mechanical Properties and Testing of Materials*. Singapore: Jenny Stanford Publishing Pte. Ltd., 1 ed., 2021.

A Literature, extra failure maps

A.0.1 Failure for bilayer system with a thick support

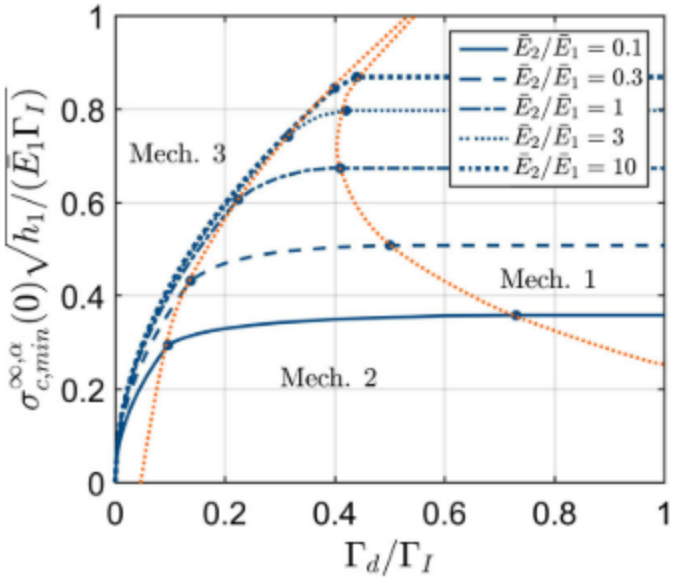

Figure 47: Failure mechanisms map for a bilayer system with a relatively thick support ($h_2/h_1 = 10$). Both the mismatch in coefficient of hygral expansion and ratio of the diffusion coefficients are respectively $\beta_2/\beta_1 = 10$ and $D_2/D_1 = 1$ and $\alpha = 0.5$. Minimum crack channelling stress $\sigma^{\infty,\alpha}_{c,min}(0)$ in the coating is plotted against the toughness ratio Γ_d/Γ_I. Multiple different stiffness mismatches are visualised with blue dotted lines in the graph, the orange dotted lines show the boundaries of the three different failure mechanisms. considering a broad selection of stiffness mismatches [7].

A relatively thick, $h_2/h_1 = 10$, support has been chosen and again the three types of failures are shown as can be seen in Figure 47. The minimum crack channelling stress σ is plotted against the toughness ratio and multiple types of stiffness mismatches are visualised through the dark blue lines.

Here for such thick supports the normalised failure stresses are mainly governed by the uniform part of the moisture content distribution. Furthermore for the hygral expansion value $\alpha = 0.5$ is used.

As can be seen the area where mechanisms two is active is becoming bigger and is becoming a more important failure mechanisms for situations with lower stiffness mismatches and thicker supports ($h_2/h_1 = 10$).

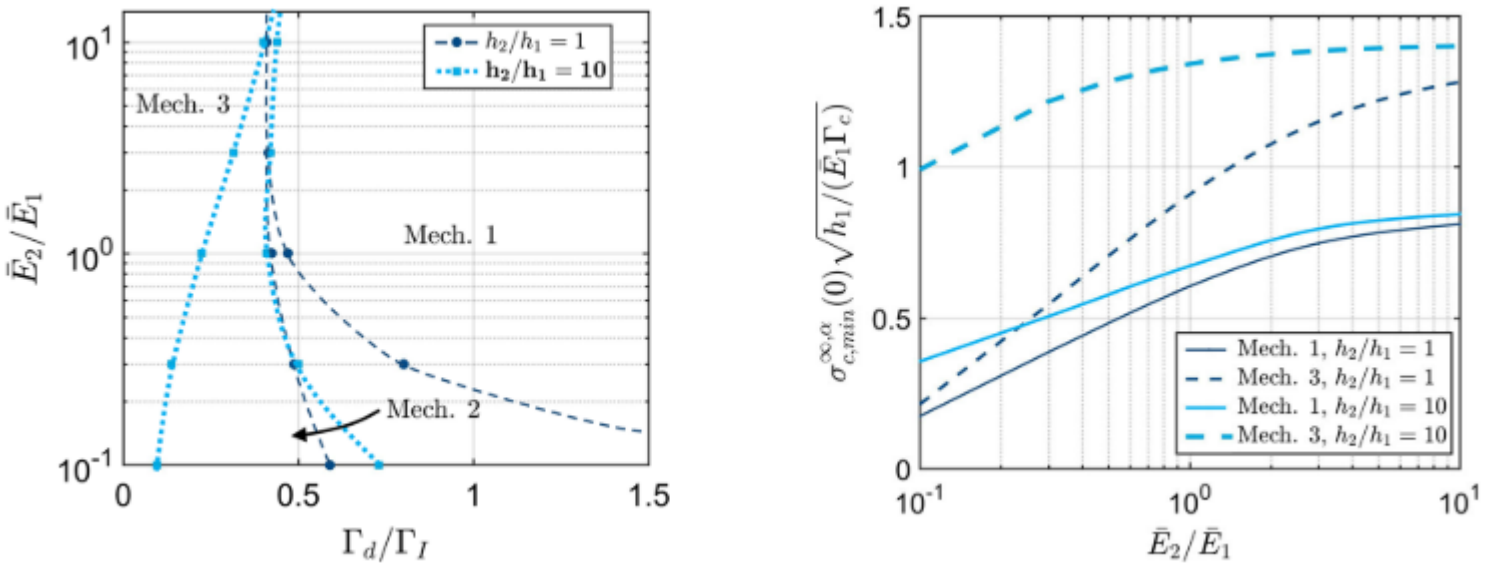

Figure 48: On the left the failure mechanisms for both a bilayer system of $h_2/h_1 = 1$ (dark blue) and $h_2/h_1 = 10$ (light blue) are shown, as a function of the elastic mismatch and the toughness mismatch (Γ_d/Γ_I). The graph on the right side, the critical cracking stress is visualised as a function of the stiffness mismatch. For both graphs $\beta_2/\beta_1 = 10$ and $D_2/D_1 = 1$ and $\alpha = 0.5$ [7].

Figure 48 shows another failure mechanism map explaining the different failure mechanisms in a graph where the Young's modulus mismatches is shown against the toughness ratio mismatch. Both the thickness ratio's of 1 and 10 are depicted, respectively with a dark or light blue line. Furthermore the hygral weighting factor $\alpha = 0.5$, hygral expansion mismatch $\beta_2/\beta_1 = 10$ and the diffusion coefficient mismatch $D_2/D_1 = 1$.

As can be seen when evaluating the toughness range Γ_d/Γ_l that mechanisms 2 is more active at lower values when the support becomes thicker (the light blue line becomes active instead of the dark blue line). Furthermore mechanisms 2 is less dominant or not present at all in the regions with a higher stiffness mismatch.

The total stress for crack channelling is visualised on the right side of Figure 48 (only visualised for mechanisms 1 and 3, at a weighting factor $\alpha = 0.5$) as a function of the stiffness mismatch, note that here the total stress is normalised. As shown the critical stress increases whenever with increasing stiffness mismatch. Furthermore, the critical stresses for the support with a smaller thickness mismatch (dark blue lines) are always lower than their equivalent stresses in bilayers with a higher thickness mismatch (light blue line).

B Schematic Reconstructions

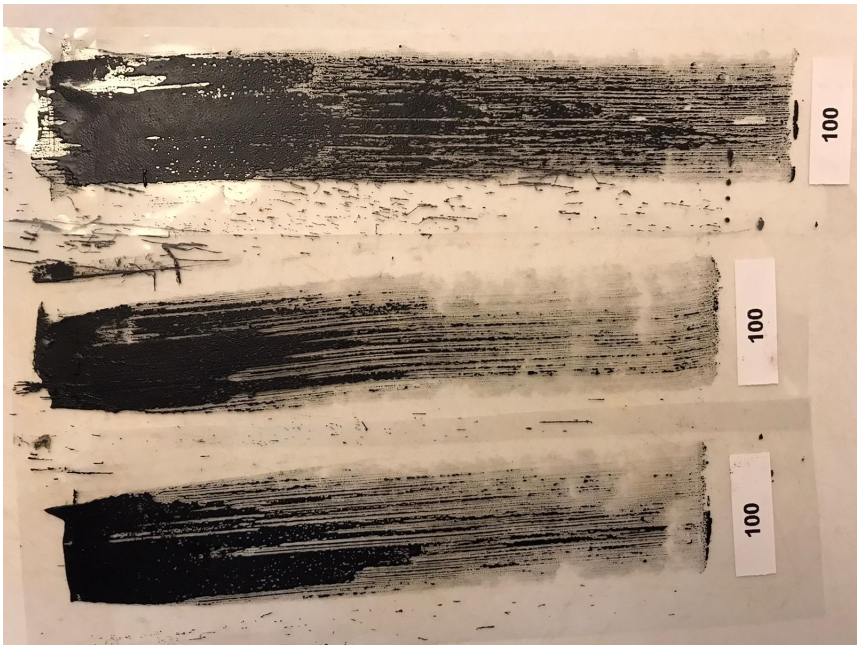

Figure 49: Three schematic reconstructions of the Black under layer, two thicknesses $50\mu m$ and $100\mu m$, all three became streaky after drying and are not usable for the tensile tests.

Figure 50: Three schematic reconstructions of the Brown under layer 1, two thicknesses $50\mu m$ and $100\mu m$, all three became streaky after drying and are not usable for the tensile tests.

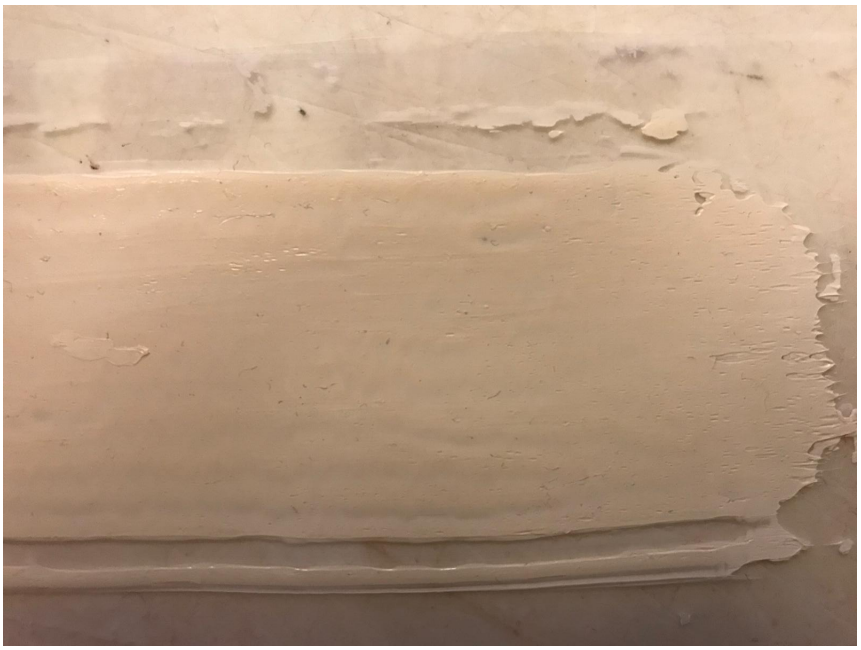

Figure 51: Imperfections visible in schematic reconstruction

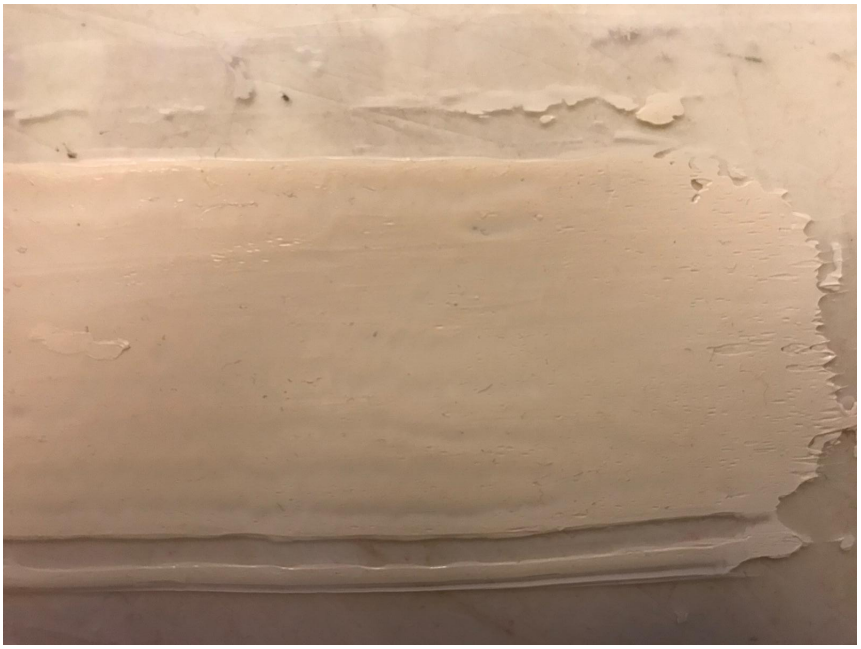

Figure 52: Imperfections visible in schematic reconstruction

Figure 53: Imperfections visible in schematic reconstruction

Figure 54: Imperfections visible in schematic reconstruction

C First Results Schematic Reconstructions

The first element with impact that should be noted is that not all colours could be separated form the melinex base layer compromising the amount of test that could be conducted. Furthermore the Brown under 1 and Black under layer

became streaky after drying and did not form a coherent layer, Figure 55, making the schematic reconstructions unusable for further testing (see Appendix B). Therefore, the following paint layers that have been testes in the following test are:

1. 'Lead white'
2. Three different types of blue; 'Thin blue layer shadows headscarf', 'Thick blue layer midtones headscarf' and 'Blue under layer midtones headscarf'
3. 'Lips surface'
4. Two types of ground; 'Ground' and 'Brown under 2'

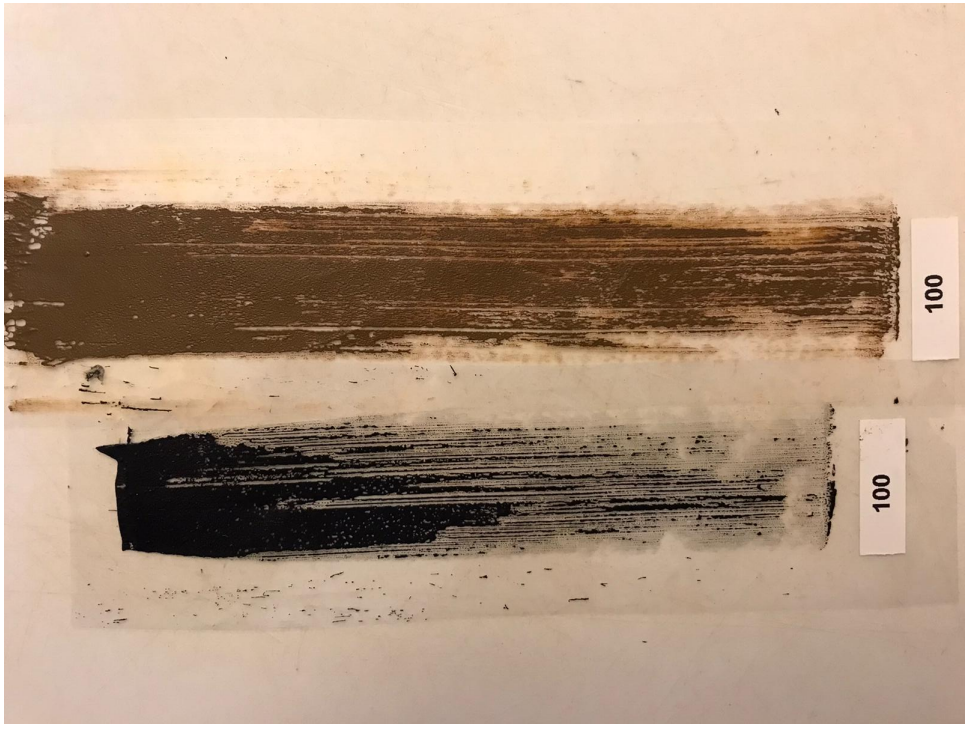

Figure 55: Two schematic reconstructions of the colours Brown under 1 and Black under that became streaky.

The first set of results consists out of four graphs of experimental tests that are shown, Figure 57; Figure 58; Figure 59; Figure 60. Each single graph shows three different tensile tests of a single colour, respectively Lips surface; Thick blue layer midtones headscarf; Ground layer; Lead white.

One of the first things visible in all four of the graphs is the steep sloped part at the end of the curve starting at different strain rates. The reason for this horizontal plateau in the graph (before the vertical part) is explicable, the paint strips are $100\mu m$ thick and have a low Young's modulus resulting in samples that are flexible and not stiff. Due to this the lower clamp slowly rises towards the upper clamp in the time period between the fastening of the specimen and the moment the test is being started. Depending on the dimensions of the sample and how far the clamp moved upwards a certain amount of time is needed to get the specimen in the starting position that is needed for the tensile test. These three positions before and during the test are shown in Figure 56 where, from left to right, the sample in the DMA is clamped in, the lower clamp has moved up and on the right the lower clamp has gone down again.

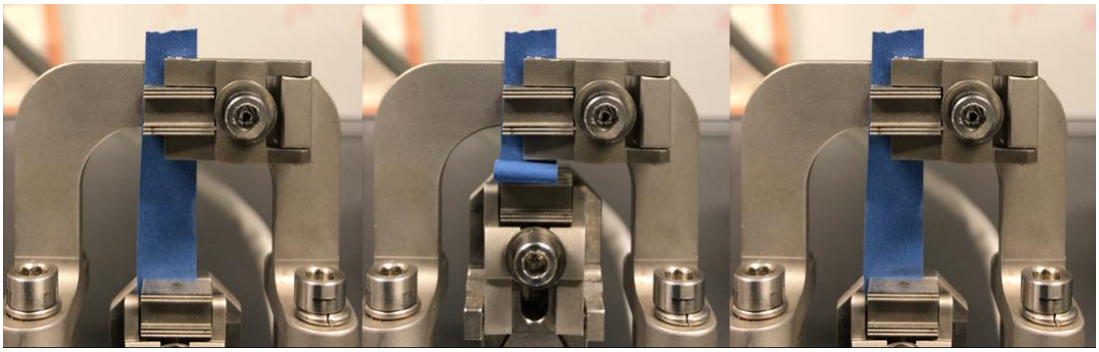

Figure 56: Three steps in tensile test; Left: moment the paint sample, out if a schematic reconstructions, is clamped in. Middle: lower clamps slowly moves upwards. Right: during test the lower clamp has gone fully down and sample is at full length for test.

Furthermore, values of both the gradient and the height of the graph are mentioned. The gradient of the line gives an insight into the Young's modulus as shown in Equation 12, this relation is true in the linear elastic part of the material [5]. And in combination with the height of the graph the toughness of the material can be calculated. The toughness being the ability of a material to resist a crack of propagating, the resistance to extension of a crack [5]. Meaning that the toughness equals the area beneath the graph until fracture. The height visualises the maximum stress that the specimens tolerate and are influenced by multiple factors such as clamping force, pre-stress and the presence of pre-cracks.

$$E = \frac{\sigma}{\epsilon} \tag{12}$$

Figure 57 shows the first three results of the Lips surface obtained out of the tensile test, the slope of the three tests are around the 6 MPa (6.741 MPa; 5.989 MPa; 5.066 MPa) meaning that the Young's modulus of the paint is around the 6 MPa. However, the toughness, which is the area marked out by the slope, will be different due to the changes in ultimate tensile stress. In Figure 58 three clearly separate lines are shown from a tensile test on Thick blue. The three tests that are shown here all have different ultimate tensile stresses (as can be seen in the variation in the heights). However, the values of the slopes are in the same region (1.696 MPa; 2.408 MPa; 2.897 Mpa). As with the Figure 57 the area underneath the triangular part of the graph changes due to the differences in height, therefor, the resulting toughness of each of the experimental tests will be different.

Figure 59 and Figure 60 both presents three initial tensile tests out of the specimen types Ground layer and Lead white respectively. Again the values that are shown in the figure represent both the gradient of each curve as well as the total heights, from start test up to the highest stress found. The mentioned remarks of the Lips Surface and Thick blue are also applicable on these paint samples.

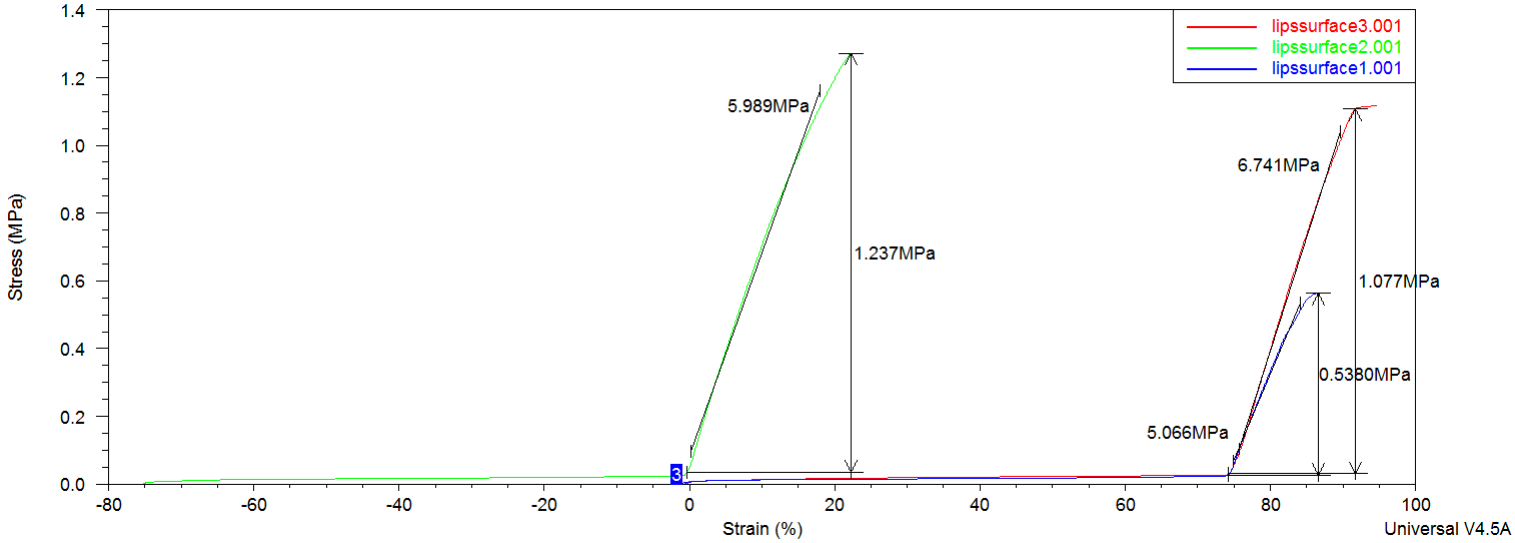

Figure 57: Three experimental tensile tests of the Lips Surface specimen, three tensile tests are shown in different colours. With the use of the TA Analysis programme values belonging to the slopes and total heights of the slope are visualised. Results found in laboratory of TUDelft with the use of DMA and accompanying software.

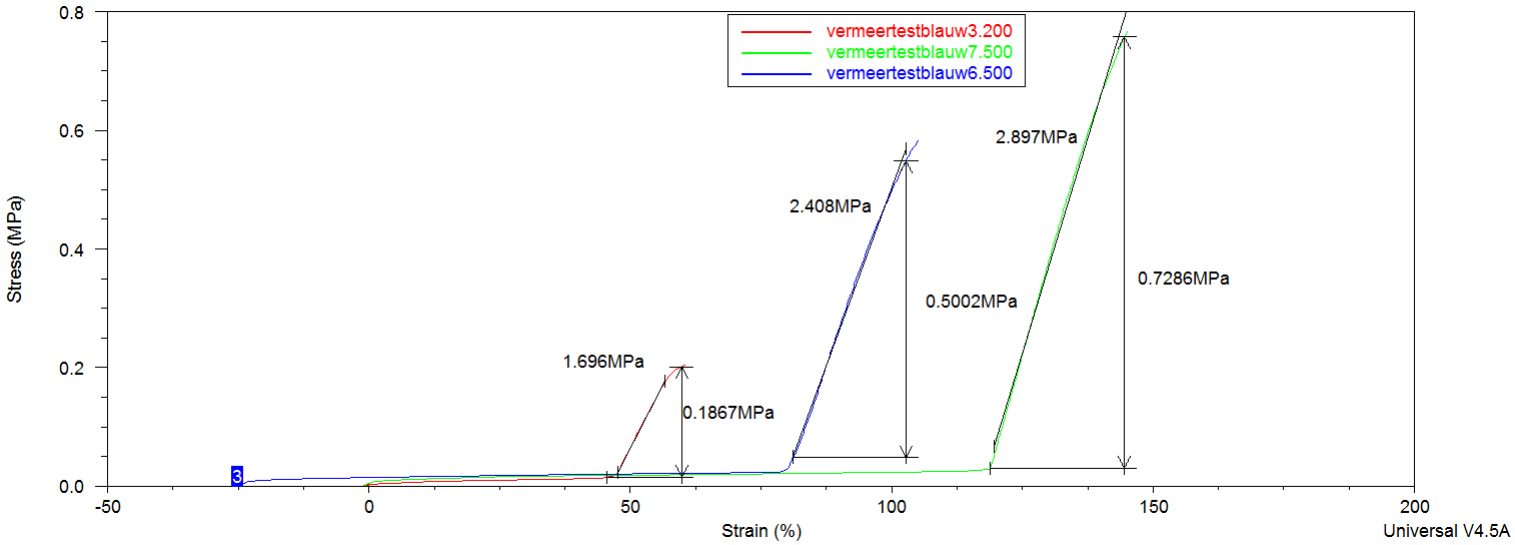

Figure 58: Three experimental tensile tests of the Thick blue specimen are shown, different named tests are visualised with different colours. Differences in height as well as the slop of the steep part are shown, values are calculated with the help of TA Analysis programme. Results found in laboratory of TUDelft with the use of DMA and accompanying software.

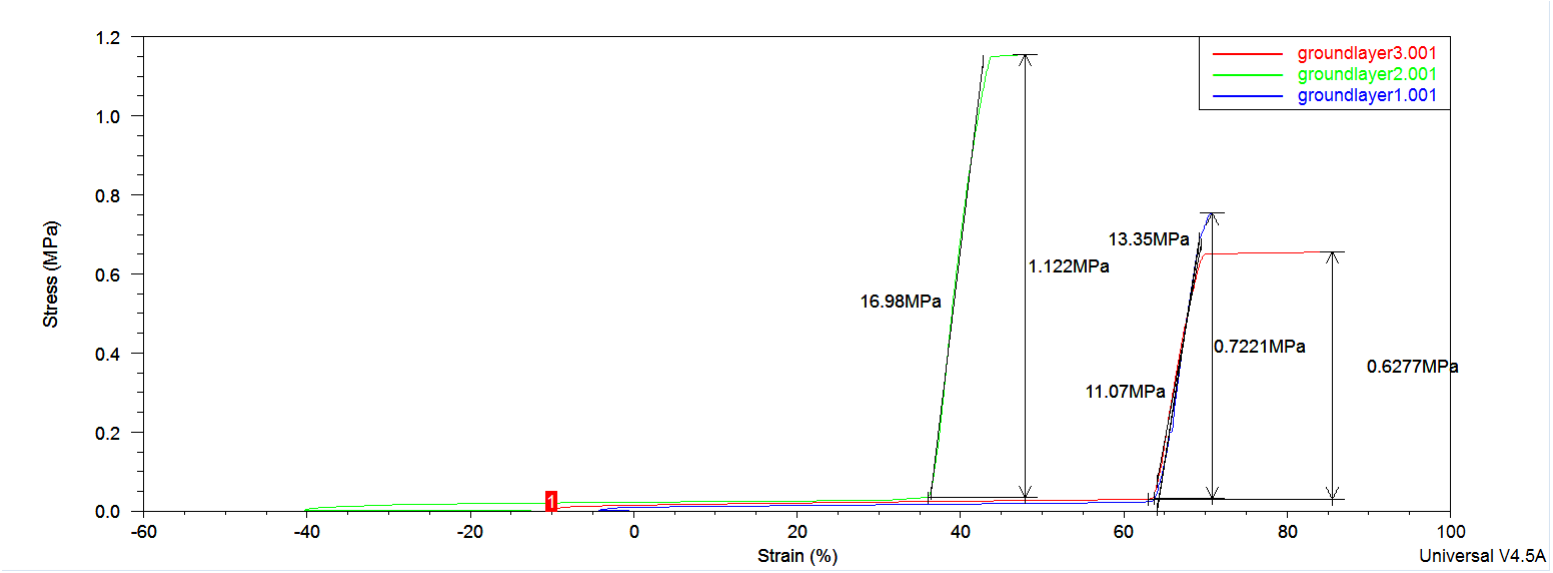

Figure 59: Three experimental tensile tests of the Ground layer specimen are visualised, different named tests are visualised with different colours. Differences in height as well as the slop of the steep part are shown. Results found in laboratory of TUDelft with the use of DMA and accompanying software.

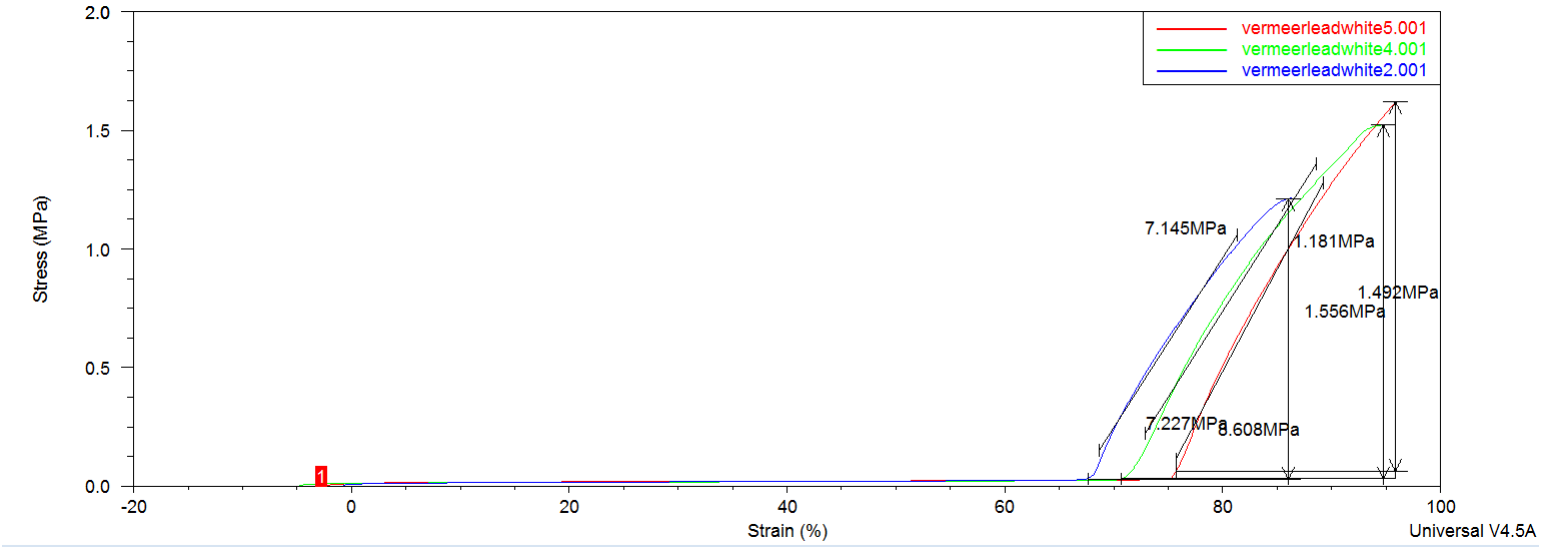

Figure 60: Three experimental tensile tests of the Lead white paint specimen, different named tests are visualised with different colours. Differences in height as well as the slop of the steep part are shown. Results found in laboratory of TUDelft with the use of DMA and accompanying software.

D Raw Data Tensile Tests

D.1 Excel data

Table 4: Table showing the raw data collected from the tensile test, data of Lead white samples are shown.

STIFFNESS Lead White												
	tijd 1 (1)	length (6)	stress (7)	strain (8)	tijd 2	length (2)	stress (2)	strain (2)		E (N/m)	E (kPa)	
mn	3,874667	17,28	0,20	219,99	7,0416600	19,95	1,34	255,59		31984,07	31,98	
mo	2,997334	4,05	0,20	19,67	6,2643340	6,15	1,28	35,35		69449,18	69,45	
mp	0,194667	11,82	0,21	1,27	1,9946670	13,63	1,08	12,91		74552,55	74,55	
mq	12,336670	16,59	0,10	9,31	24,4710000	17,59	0,40	14,25		60746,07	60,75	
mr	3,602167	10,17	0,08	22,97	6,6358320	12,59	1,41	40,23		76644,82	76,64	
ms	0,025667	7,65	0,06	0,03	2,0091670	9,64	1,29	17,98		68618,78	68,62	
mt	0,147500	9,38	0,18	1,15	1,1476670	10,38	1,02	8,87		108174,80	108,17	
mu	0,419500	9,51	0,20	1,47	2,1196670	11,35	1,09	15,41		64328,32	64,33	
mw	0,521660	12,77	0,20	1,54	1,9718340	14,45	0,80	11,83		58319,08	58,32	
mx	0,040000	12,03	0,03	0,10	1,4233300	13,43	0,80	8,55		91476,43	91,48	
na	0,135333	7,44	0,33	0,82	0,8020000	8,11	0,91	4,98		140078,13	140,08	
ne	0,748500	11,40	0,22	4,14	1,6818340	12,44	0,80	11,05		83755,04	83,76	
nf	1,316167	10,19	0,04	0,41	2,7330000	11,61	0,88	10,44		83250,28	83,25	
ng	3,989667	14,42	0,18	10,14	8,4049900	16,79	1,03	23,31		64390,23	64,39	
nh	0,498500	10,90	0,20	4,36	1,9153340	12,35	0,99	14,30		79163,96	79,16	
ni	0,408500	7,15	0,21	3,50	1,2751660	8,05	0,90	11,65		84897,79	84,90	
nj	0,527167	10,27	0,10	1,27	1,6938330	11,26	0,61	8,88		66121,77	66,12	
nk	0,028167	10,26	0,03	0,19	0,7098334	10,96	0,57	0,56		1492933,09	1492,93	
								AVE		70513,23		
								stdev		14002,47		
								AVE+1sig		84515,70		
								AVE-1sig		56510,75		
								AVE+2sig		98518,17		
								AVE-2sig		42508,28		
							gecorrigeerd			70778,34		
							1 sigma			8212,43		
							gecorrigie AVE			73265,31		
							2 sigma stdev			9821,65		

Table 5: Table showing the raw data collected from the tensile test, data of Thick blue samples are shown.

STIFFNESS Thick blue										
	tijd 1 (1)	length (6)	stress (7)	strain (8)	tijd 2	length	stress	strain		E (N/m)	E (kPa)
mm	0,027333	15,10	0,01	0,46	2,377500	17,33	0,81	12,17		68166,36	68,17
mp	4,319166	15,57	0,08	0,57	14,151660	17,95	0,71	12,62		52109,26	52,11
mq	0,089333	13,99	0,03	0,11	2,405000	16,34	0,80	13,24		58382,05	58,38
mu	0,014833	13,90	0,01	3,79	5,163500	16,03	0,79	15,85		64264,17	64,26
mv	0,043167	16,45	0,06	0,59	3,108334	19,54	1,01	15,73		62938,49	62,94
mw	0,248667	15,11	0,05	2,65	3,065500	17,99	0,77	17,73		47822,74	47,82
mx	0,045333	8,76	0,05	0,65	1,728833	10,46	0,84	14,42		57479,86	57,48
my	0,211000	16,02	0,02	3,07	5,144667	19,10	0,81	18,63		50762,87	50,76
mz	0,117166	12,90	0,10	1,35	1,600666	14,39	0,63	10,39		58201,53	58,20
na	0,320500	14,18	0,18	2,55	2,754000	16,62	0,80	16,24		45636,18	45,64
nb	0,250330	12,34	0,20	2,24	1,467000	13,56	0,62	9,62		56132,99	56,13
nc	0,336833	11,90	0,20	2,33	1,586834	13,18	0,70	10,42		61586,62	61,59
nd	0,308000	13,58	0,21	2,22	1,691500	14,98	0,62	10,67		48902,23	48,90
ne	0,324334	10,74	0,20	3,02	1,607834	12,03	0,69	12,09		53115,00	53,11
nf	0,233000	13,01	0,22	2,05	1,083166	13,86	0,67	7,31		86911,98	86,91
						THICK			AVE	58160,82	58,16
									STDEV	9897,66	9,90
									AVE+1sig	68058,48	
									AVE-1sig	48263,16	
									AVE+2sig	77956,14	
									AVE-2sig	38365,51	
						gecorigeerd			AVE	56715,92	
						1sigma			STDEV	4824,25	
						gecorigeerd			AVE	56107,17	
						2 sigma			STDEV	6457,45	

Table 6: Table showing the raw data collected from the tensile test, data of Thin blue samples are shown.

STIFFNESS Thin Blue												
	tijd 1 (1)	length (6)	stress (7)	strain (8)	tijd 2	length	stress	strain	E (N/m	)	E (kPa)	
mn	0,058500	13,62	0,10	1,51	1,69200	15,26	0,39	11,38	28689,89		28,69	
mo	0,388000	16,58	0,20	3,25	2,00483	18,23	0,40	11,84	23236,64		23,24	
mp	0,651332	18,05	0,21	4,94	1,80150	19,20	0,50	10,31	55135,21		55,14	
mr	0,363833	19,37	0,20	1,69	2,23067	21,24	0,58	10,50	43405,81		43,41	
ms	2,830166	13,90	0,48	13,28	3,29683	14,35	0,55	16,21	24499,82		24,50	
mt	2,467660	13,03	0,19	2,22	5,25117	14,27	0,60	9,82	54046,69		54,05	
mu	faulty measures											
mv	0,045333	10,00	0,09	1,00	0,61200	10,57	0,23	5,20	32176,18		32,18	
mw	0,696833	8,13	0,16	2,44	1,68033	8,94	0,42	8,97	39618,74		39,62	
						thin						
									AVE		37601,12	
									STDEV		11739,30	
									AVE+1 sig		49340,42	
									AVE-2sig		25861,83	
									AVE+2sig		61079,72	
									AVE-2sig		14122,53	
						gecorigeerd 1sig			AVE		35972,66	
									STDEV		5830,90	

Table 7: Table showing the raw data collected from the tensile test, data of Blue under samples are shown.

STIFFNESS Blue under															
	tijd 1 (1)		length (6)		stress (7)	strain (8)	tijd 2	length (2)		stress (2)	strain (2)		E (N/m	)	E (kPa)
mm	3,605500		14,09		0,41	6,92	6,4390000	15,84		1,09	17,10		66578,53		66,58
mo	0,120000		15,11		0,20	0,99	2,7701660	17,78		1,01	15,70		54606,97		54,61
mp	1,536167		12,58		0,14	1,01	5,9683340	14,86		1,33	15,16		83650,31		83,65
mq	0,850000		12,41		0,23	1,03	3,0335000	14,35		1,24	13,26		82342,81		82,34
mr	0,765000		13,96		0,60	4,59	1,9151660	15,13		1,02	11,52		61370,01		61,37
ms	0,203167		14,23		0,35	1,57	1,3348340	15,37		0,84	8,06		74491,53		74,49
mt	0,271334		17,34		0,27	2,10	3,1698340	20,26		1,21	15,94		67420,47		67,42
mu	0,850167		14,19		0,68	5,07	2,1170000	15,46		1,11	12,36		59041,94		59,04
mv	0,105333		12,68		0,17	0,87	1,8053300	14,39		1,03	11,26		82495,60		82,50
mw	0,266333		13,04		0,36	2,02	2,3998340	15,18		1,17	15,04		61865,71		61,87
mx	0,124833		16,63		0,06	0,12	3,0066600	18,61		0,77	9,64		75561,29		75,56
my	0,285000		11,85		0,36	2,18	1,9517160	13,52		1,00	13,10		58622,68		58,62
									BUM			AVE	69003,99		
												STDEV	9914,15		
				gecorigeerde								AVE+1sig	78918,14		
												AVE+-1Sig	59089,84		
					op 1sigma							AVE	67881,26		
												STDEV	5525,26		
										op 2 sigma		AVE	-		
												STDEV			

Table 8: Table showing the raw data collected from the tensile test, data of Lips (red) samples are shown.

STIFFNESS Lips surface											
	tijd 1 (1)	length (6)	stress (7)	strain (8)	tijd 2	length	stress	strain		E (N/m)	E (kPa)
mm	0,067167	13,71	0,19	0,88	1,45067	15,11	1,08	10,21		94966,69	94,97
mn	0,124167	12,92	0,19	1,18	1,60766	14,41	0,94	10,25		82478,84	82,48
mo	0,130333	12,64	0,20	1,10	1,66383	14,18	1,04	10,52		89924,49	89,92
mp	0,103167	12,61	0,20	1,18	1,51817	14,03	1,03	10,05		93447,66	93,45
mq	0,131833	12,29	0,28	0,99	1,26533	13,43	1,00	8,16		100359,31	100,36
mr	0,115333	10,23	0,19	1,14	1,08200	11,20	0,76	8,11		80821,75	80,82
ms	0,180833	10,82	0,39	1,55	1,39767	12,04	1,24	10,07		99873,97	99,87
mt	0,296000	11,90	0,39	2,25	1,59600	13,20	1,12	10,90		83655,90	83,66
mu	0,352667	13,93	0,40	2,42	1,81933	15,39	1,10	10,91		82529,76	82,53
mv	0,325500	12,13	0,42	2,11	1,97567	13,78	1,22	12,18		79212,83	79,21
						LIPS		AVE		88727,12	
								STDEV		7605,20	
								AVE+1sig		96332,32	
								AVE-1sig		81121,92	
								AVE+2sig		103937,53	
								AVE-sig		73516,71	
							gecorigee AVE			86602,31	
							1sig stdev			5666,10	

Table 9: Table showing the raw data collected from the tensile test, data of Brown Under samples are shown.

STIFFNESS Brown Under												
	tijd 1 (1)	length (6)	stress (7)	strain (8)	tijd 2	length	stress	strain		E (N/m	)	E (kPa)
mn	0,31567	12,87	0,11	4,74	1,66583	14,23	0,37	13,26		30301,17		30,30
mo	0,15883	9,00	0,11	3,86	1,04217	9,92	0,31	11,18		27266,55		27,27
mp	0,36933	14,28	0,10	5,00	2,13617	16,03	0,43	15,28		31792,01		31,79
mq	0,69550	12,30	0,09	4,31	3,11233	14,10	0,46	16,08		31879,54		31,88
mr	0,35800	13,93	0,09	4,02	1,77483	15,35	0,36	12,34		32108,02		32,11
ms	0,79250	12,35	0,13	7,22	2,07600	13,62	0,44	14,88		40961,15		40,96
mt	0,85183	11,35	0,04	5,02	3,70217	13,52	0,51	19,59		32288,84		32,29
							brown	AVE				32371,04
								STDEV				3868,98
								AVE+1sig				36240,02
								AVE-1sig				28502,06
								AVE+2sgi				40109,00
								AVE-2sig				24633,08
								gecor 1 sig				31673,92
								stdev				708,13

Table 10: Table showing the raw data collected from the tensile test, data of Ground samples are shown.

STIFFNESS Ground layer												
	tijd 1 (1)	length (6)	stress (7)	strain (8)	tijd 2	length	stress	strain		E(N/m)	E (kPa)	
mm	1,94633	14,90	0,41	7,82	3,296500	15,40	1,16		10,81	253089,31	253,09	
mn	1,14333	15,95	0,28	1,00	3,193500	16,83	1,56		5,51	284085,31	284,09	
mp	4,99033	14,93	0,20	16,15	9,207501	15,27	0,75		18,01	294906,01	294,91	
mr	0,85100	12,86	0,18	1,01	2,684500	13,39	1,26		4,22	335875,04	335,88	
ms	3,42100	10,99	0,45	2,00	6,254668	11,59	1,48		6,14	248896,33	248,90	
mt	0,13217	10,42	0,39	0,58	0,248833	10,53	0,86		1,38	598982,50	598,98	
mu	0,91867	9,76	0,20	1,63	2,368667	10,14	1,31		4,44	395429,64	395,43	
mv	0,16833	14,64	0,17	0,23	0,635000	14,98	1,10		2,07	502611,96	502,61	
mw	0,05417	17,15	0,23	0,28	0,420833	17,52	1,18		2,06	531128,51	531,13	
mx	0,61583	14,53	0,18	0,46	2,132500	15,01	1,05		3,07	331725,19	331,73	
my	0,18783	17,06	0,56	0,94	0,738000	17,62	1,85		3,67	469784,37	469,78	
							ground	AVE			386046,74	
								STDEV			115890,45	
								AVE+1sig			501937,19	
								AVE-1 sig			270156,30	
								AVE+2sig			617827,64	
								AVE-2sig			154265,85	
								gecor1sig		AVE	351967,59	
										STDEV	63642,88	

D.2 Graphical data

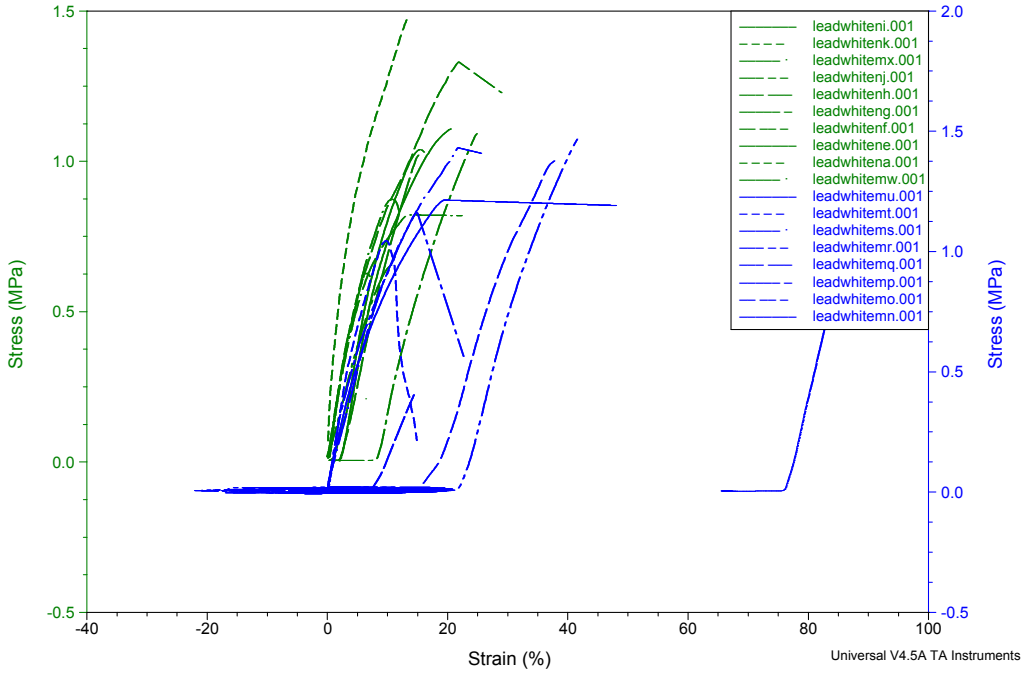

Figure 61: Graph showing stress strain model of Lead white samples, data obtained with use of DMA, TUDelft.

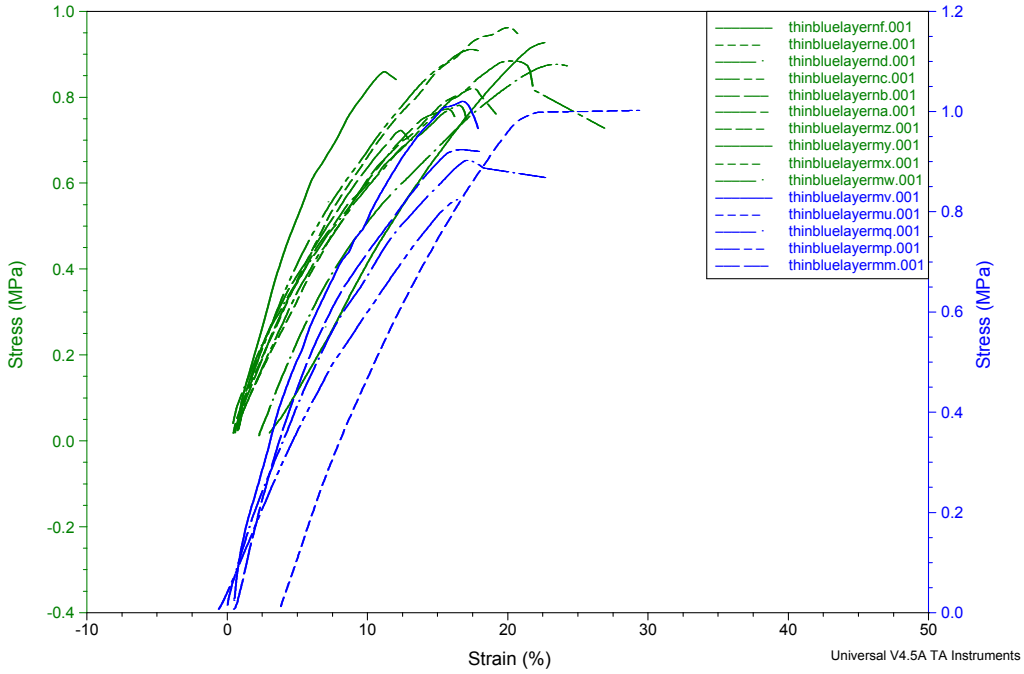

Figure 62: Graph showing stress strain model of Thick Blue samples, data obtained with use of DMA, TUDelft. Note that the legend edscribes: 'Thinbluelayerxx', this should be 'thickbluelayerxx'.

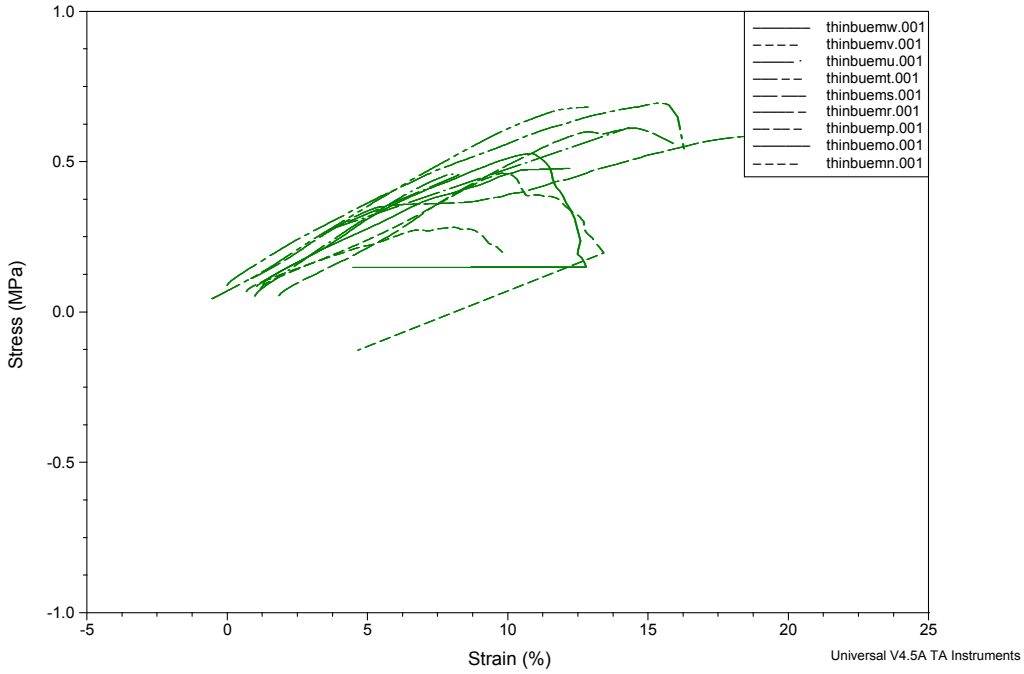

Figure 63: Graph showing stress strain model of Thin blue samples, data obtained with use of DMA, TUDelft.

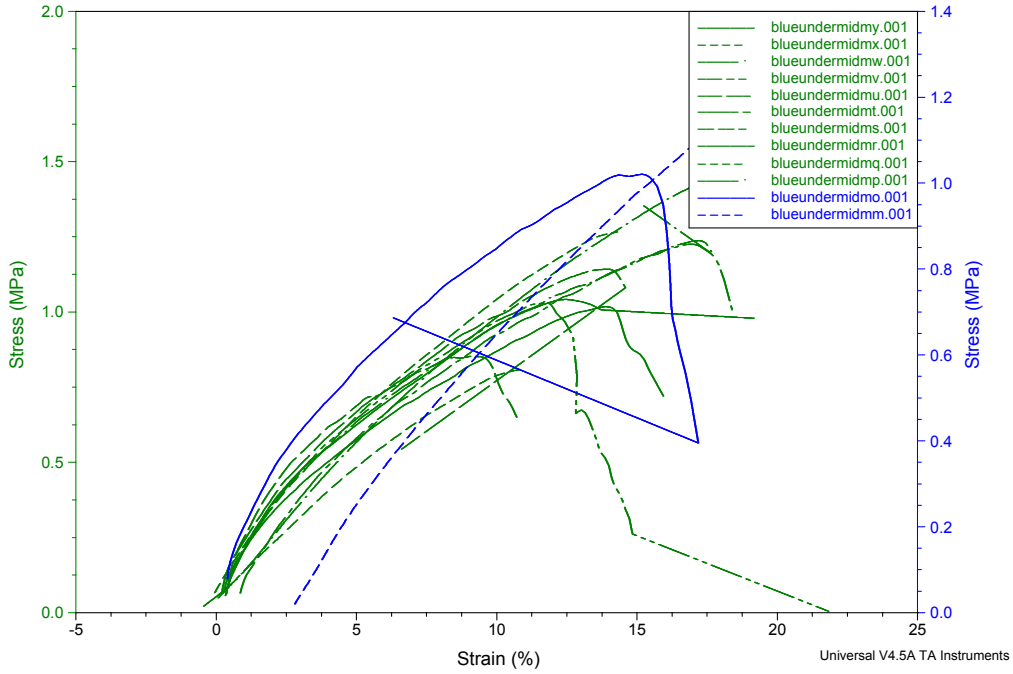

Figure 64: Graph showing stress strain model of nlue Under samples, data obtained with use of DMA, TUDelft.

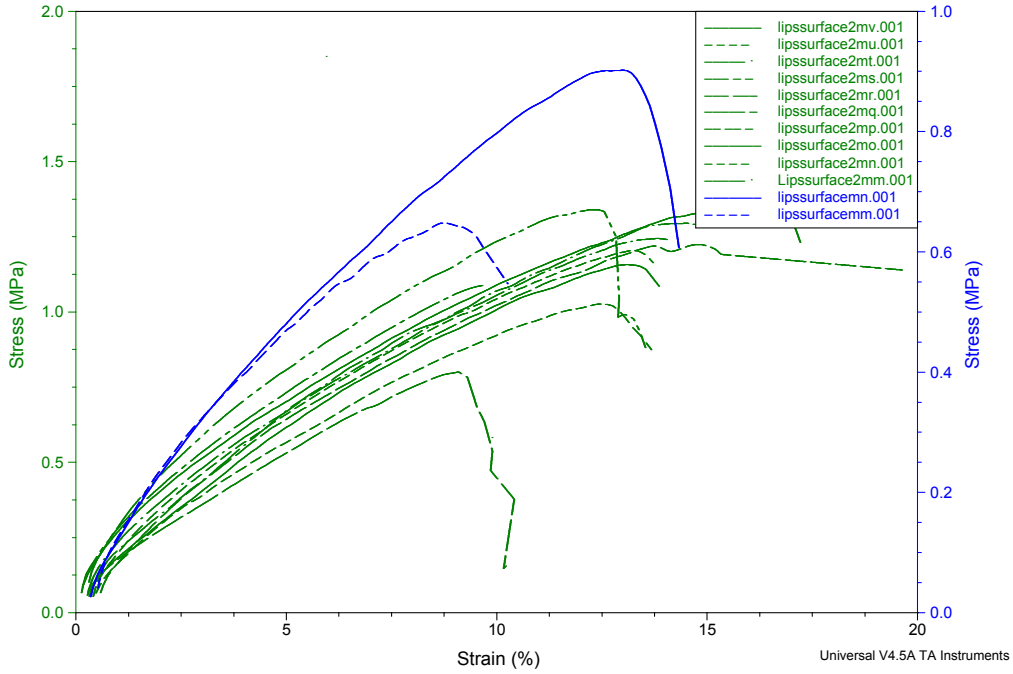

Figure 65: Graph showing stress strain model of Lips samples, data obtained with use of DMA, TUDelft.

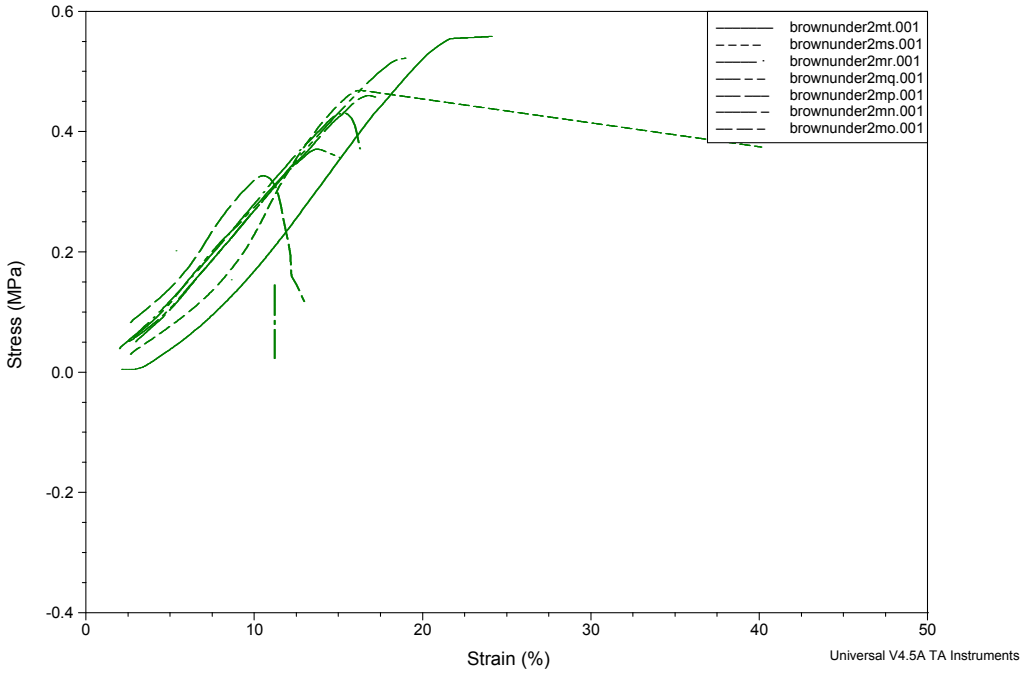

Figure 66: Graph showing stress strain model of Brown under samples, data obtained with use of DMA, TUDelft.

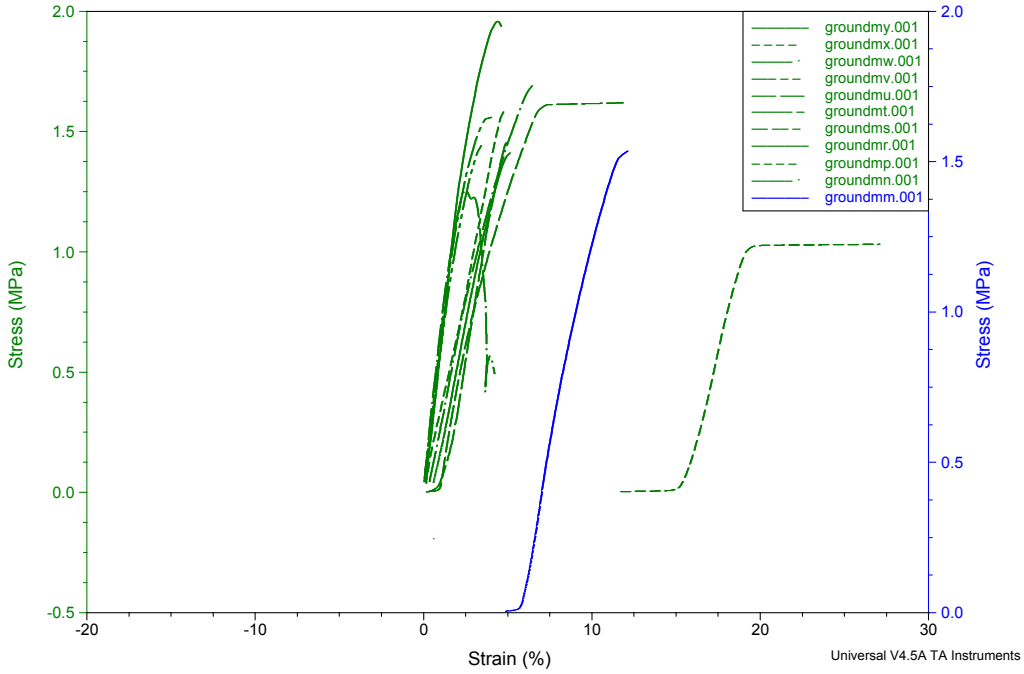

Figure 67: Graph showing stress strain model of Ground samples, data obtained with use of DMA, TUDelft.

E Crack Details

E.1 Crack 1

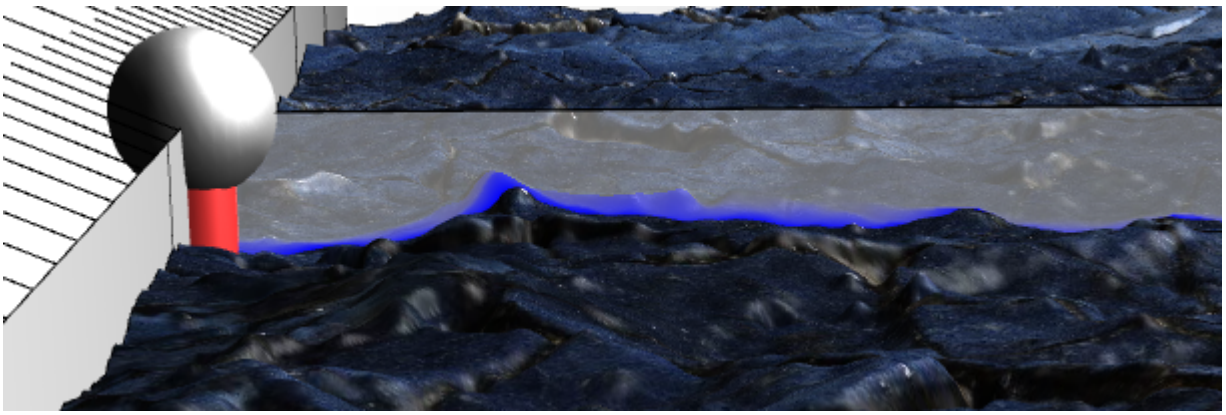

Figure 68: Headscarf detail, crack 1

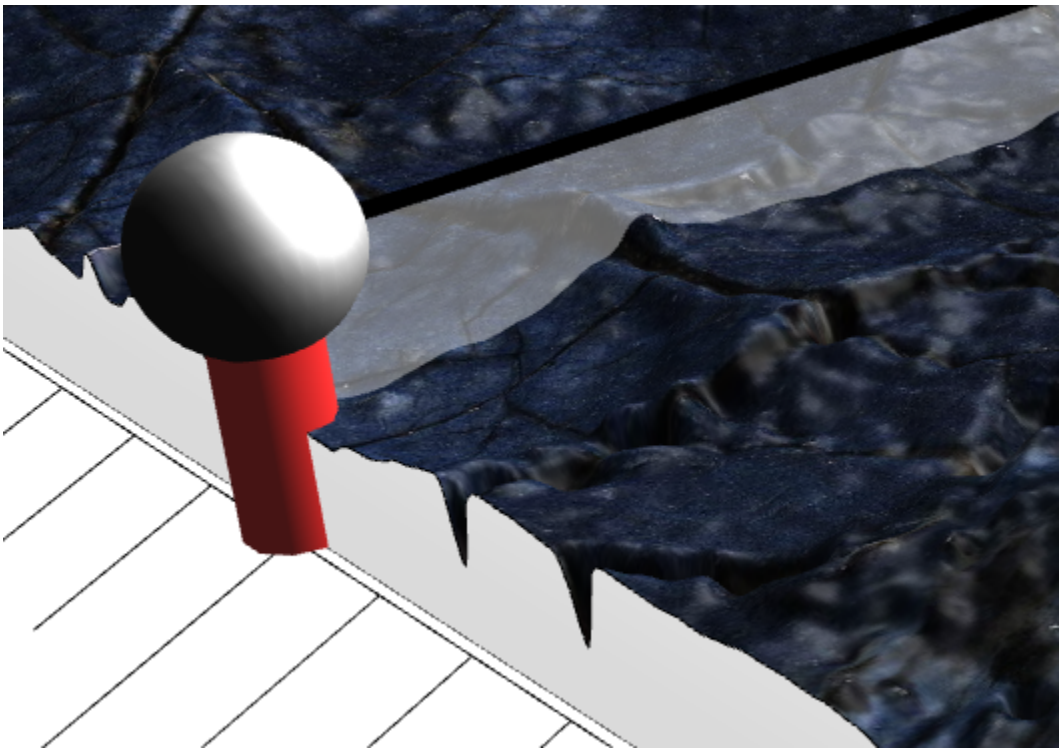

Figure 69: Headscarf detail, crack 1

E.2 Crack 2 and 3

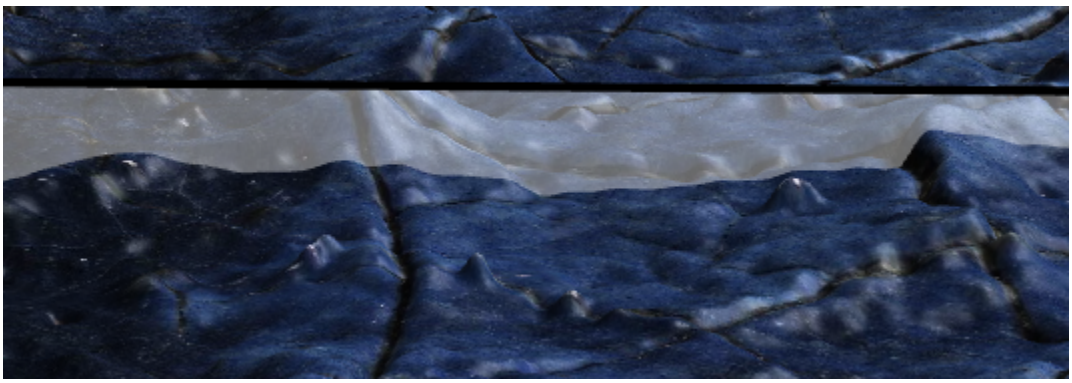

Figure 70: Headscarf detail, crack 2 and 3

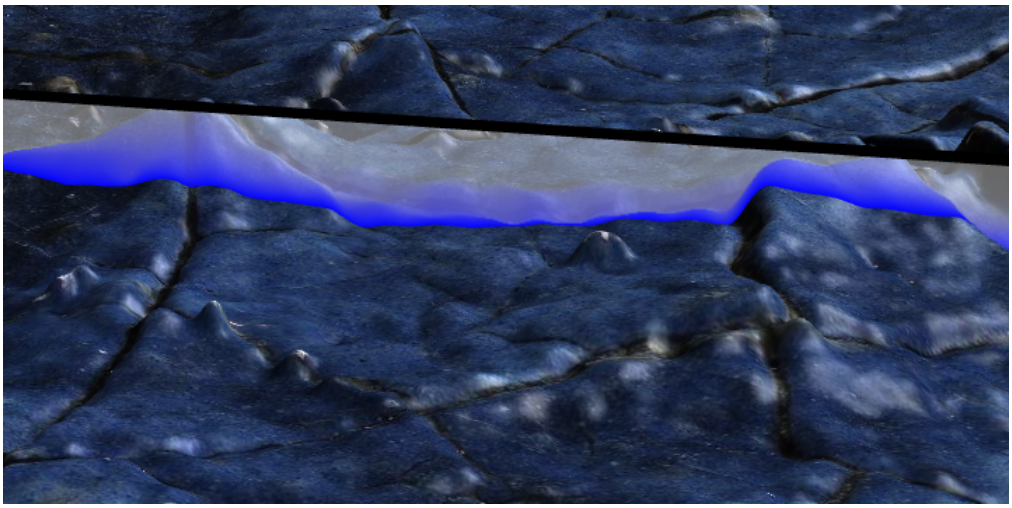

Figure 71: Headscarf detail, crack 2 and 3

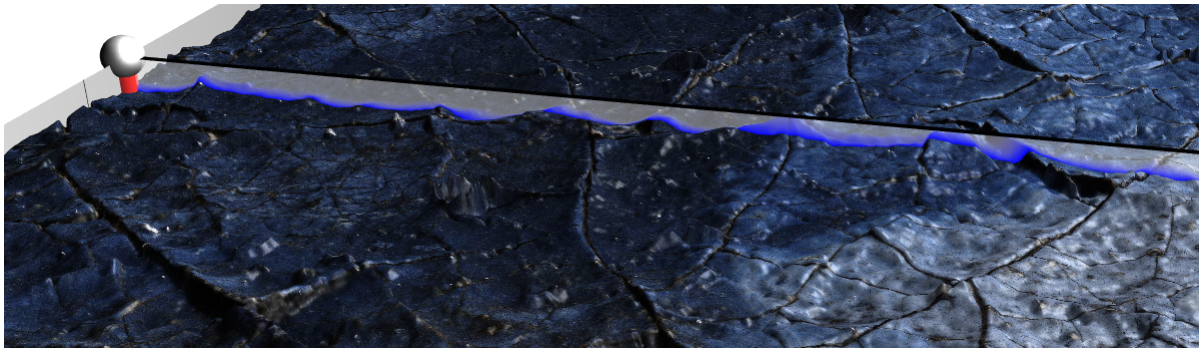

Figure 72: Headscarf detail, crack 2 and 3

E.3 Crack 4

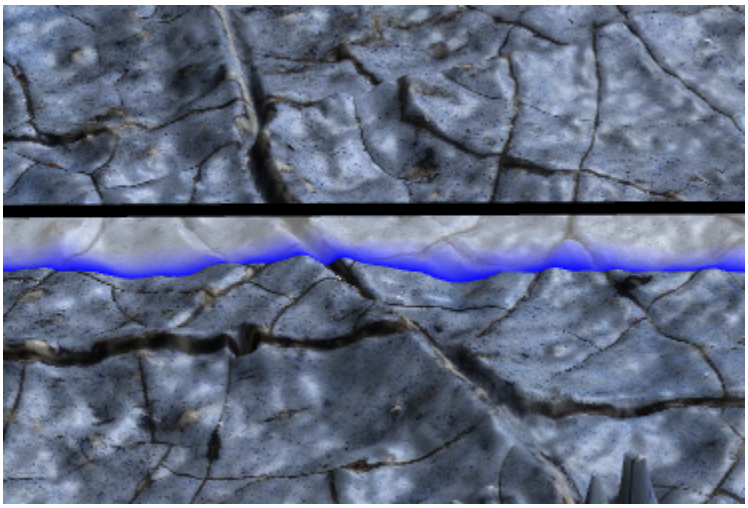

Figure 73: Headscarf detail, crack 4

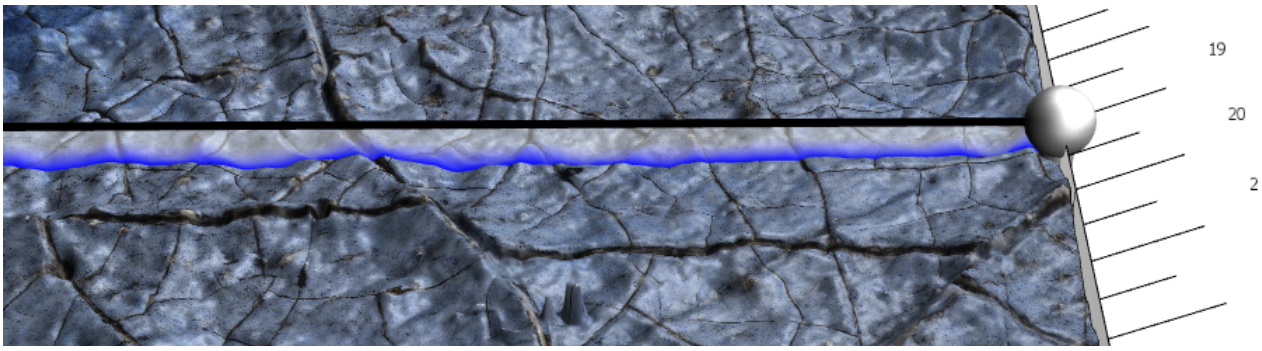

Figure 74: Headscarf detail, crack 4

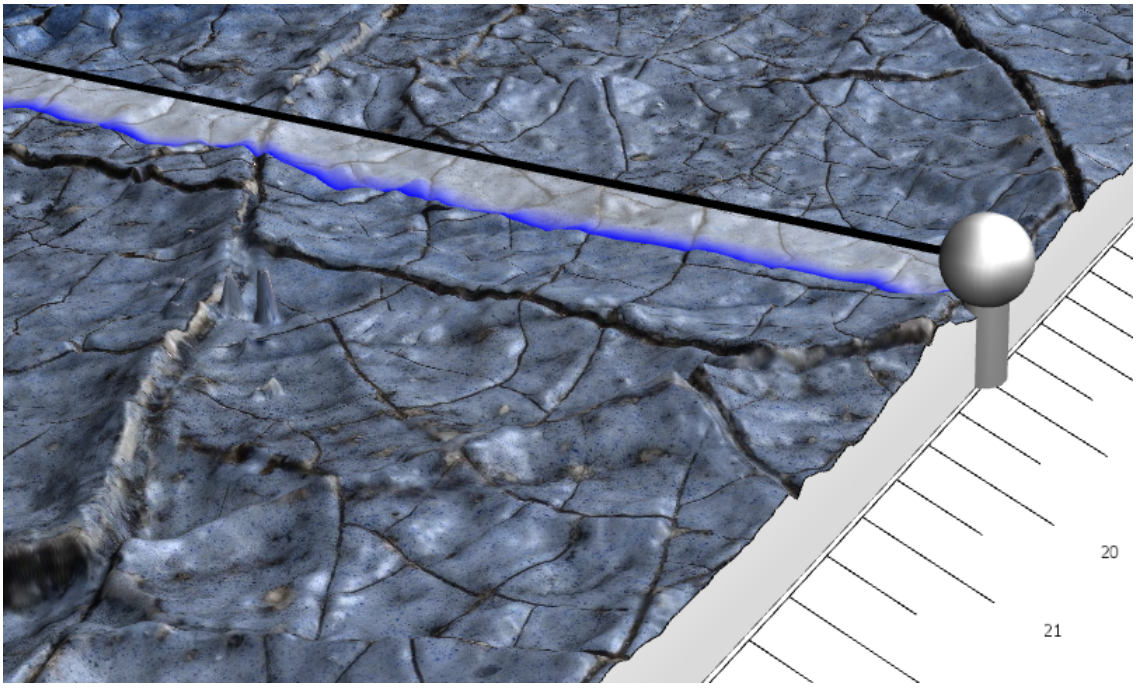

Figure 75: Headscarf detail, crack 4

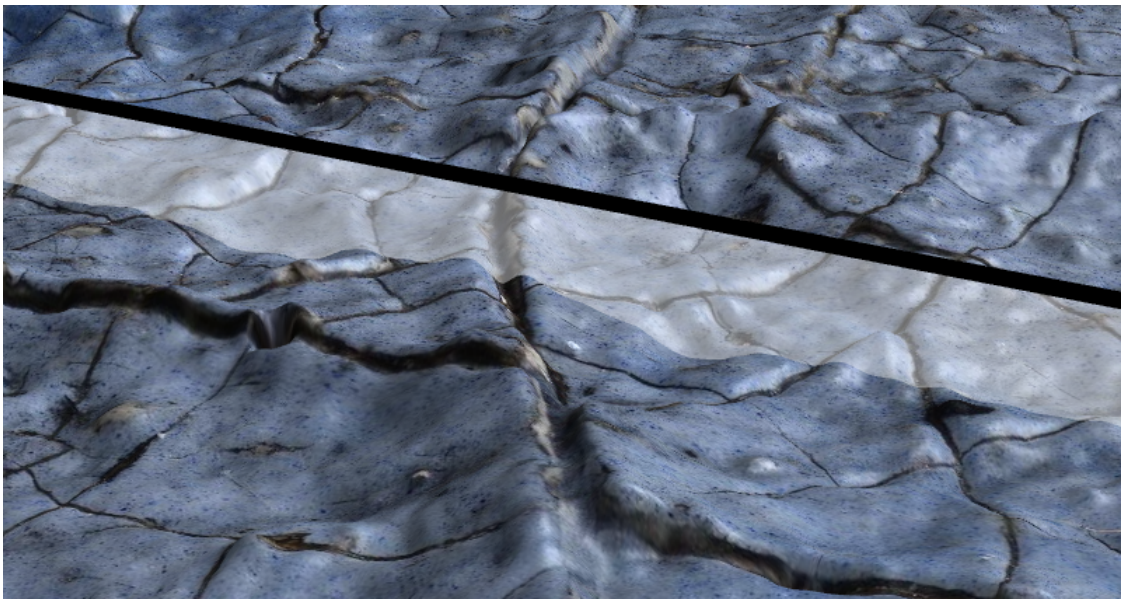

Figure 76: Headscarf detail, crack 4

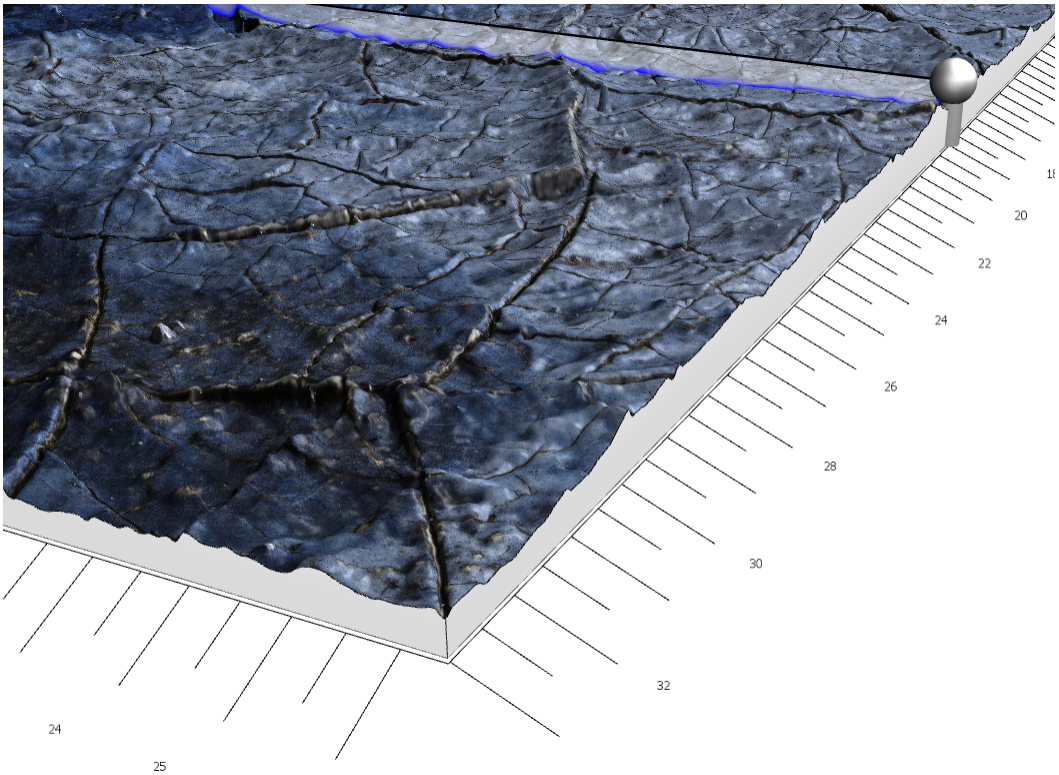

Figure 77: Headscarf detail, crack 4

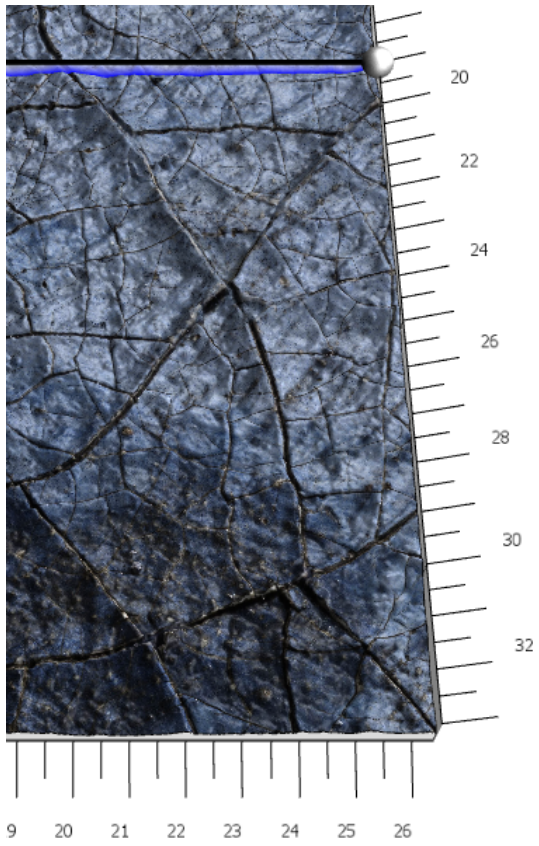

Figure 78: Headscarf detail, crack 4

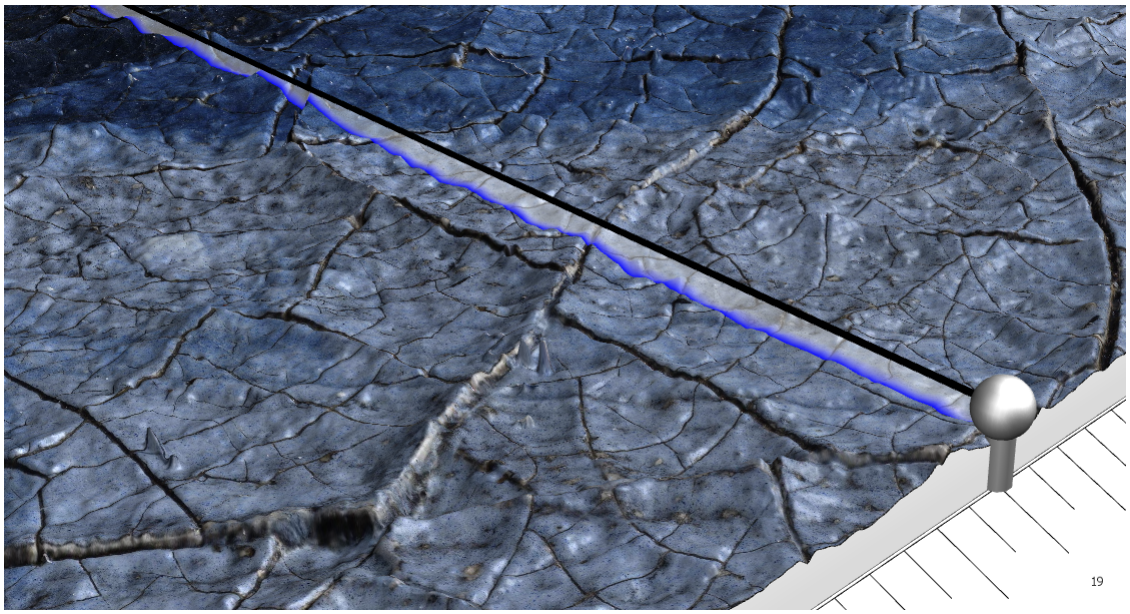

Figure 79: Headscarf detail, crack 4